DOKUZ EYLÜL UNIVERSITY

GRADUATE SCHOOL OF NATURAL AND APPLIED SCIENCES

PERFORMANCE ANALYSIS AND OPTIMIZATION OF INTEGRATED FUEL CELL-BATTERY SYSTEMS FOR MARINE APPLICATIONS

by

Süleyman Aykut KORKMAZ

May, 2023

İZMİR

PERFORMANCE ANALYSIS AND OPTIMIZATION OF INTEGRATED FUEL CELL-BATTERY SYSTEMS FOR MARINE APPLICATIONS

A Thesis Submitted to the

Graduate School of Natural and Applied Sciences of Dokuz Eylül University

In Partial Fulfillment of the Requirements for the Degree of Doctor of

Philosophy in Marine Engineering, Marine Transportation Systems Engineering Program

by

Süleyman Aykut KORKMAZ

May, 2023

İZMİR

Ph.D. THESIS EXAMINATION RESULT FORM

We have read the thesis entitled **"PERFORMANCE ANALYSIS AND OPTIMIZATION OF INTEGRATED FUEL CELL-BATTERY SYSTEMS FOR MARINE APPLICATIONS"** completed by **SÜLEYMAN AYKUT KORKMAZ** under supervision of **ASST. PROF. DR. K. EMRAH ERGİNER** and we certify that in our opinion it is fully adequate, in scope and in quality, as a thesis for the degree of Doctor of Philosophy.

…….

Asst. Prof. Dr. K. Emrah ERGİNER

Supervisor

……..	……...
Asst. Prof. Dr. Mustafa NURAN	Prof. Dr. Can Özgür ÇOLPAN
Thesis Committee Member	Thesis Committee Member
……..	……...
Prof. Dr. Önder KIZILKAN	Assoc. Prof. Dr. Ceyhun YILMAZ
Examining Committee Member	Examining Committee Member

Prof. Dr. Okan FISTIKOĞLU
Director
Graduate School of Natural and Applied Sciences

ACKNOWLEDGMENT

The author would like to express deep gratitude to the thesis advisor Asst. Prof. Dr. K. Emrah ERGİNER for his invaluable supervision, advice, encouragement, support, and insight through the research process.

Also, the author would like to express the deepest appreciation to Prof. Dr. Can Özgür ÇOLPAN, who has been a tremendous mentor to me during my graduate studies. I have benefited from his boundless experience and guidance in my academic life. In addition, I would like to acknowledge the valuable support and help of Asst. Prof. Dr. Mustafa NURAN.

The author thanks his special research fellows Olgun KONUR, Onur YÜKSEL, Sera Ayten ÇETİNKAYA, and Anıl ERDOĞAN for their valuable contributions to the published articles, conference papers, and to this study, as well.

Last, but definitely not least, the author gratefully thanks his wife Jamal ESENKANOVA for her understanding and supportive talks. Without her support and motivation, I would not have completed this thesis.

And finally, the author thanks his self-sacrificing mother Elif KORKMAZ, and lovely sisters F. Binnur KAYA and L. Zinnur YAPRAK for always supporting and believing in me. The author would like to remember his deceased father Necati KORKMAZ, who passed away on 8th June 2020. The author very much wishes he could see him now he has completed his Ph.D.!

The author would like to thank Dokuz Eylul University's Scientific Research Projects for providing funding to his research with the project number [2020.KB.MLT.012].

Süleyman Aykut KORKMAZ

PERFORMANCE ANALYSIS AND OPTIMIZATION OF INTEGRATED FUEL CELL-BATTERY SYSTEMS FOR MARINE APPLICATIONS

ABSTRACT

The shipping industry has been under pressure to reduce its environmental footprint due to increasingly stringent regulations. The “Green Ship" concept, which focuses on zero or low exhaust gas emission propulsion systems, has gained attention in the maritime community. To achieve the objectives, two case-studies are presented in this thesis. In the first case-study, the environmental and economic impacts of using fuel-cell and battery-based hybrid configurations are investigated. Phosphoric acid and molten carbonate fuel cell systems can take the place of the diesel generators on a large tanker to supply the vessel’s total electricity demand. Environmental and economic analyses of the utilization of the specified fuel-cell systems with batteries on a large commercial tanker vessel are provided. The results show that the carbon dioxide emissions could be reduced by up to forty-nine-point seventy-five percent, and the lowest electricity production cost is found at zero point one eight one USD per kilowatt hour for current fuel prices with utilization of molten carbonate fuel cells and lithium nickel manganese cobalt oxide battery cells. In the second case-study, the operating parameters of a semi-empirical mathematical model of a proton-exchange membrane fuel-cell (PEMFC) are extracted and compared using various metaheuristic algorithms (MHAs). In this regard, sum-squared error (SSE) is employed as the objective function to find values of seven unknown modeling parameters. As a case study, parameter extraction is carried out utilizing the MHAs for a commercial PEMFC. Three different multi-attribute decision-making methods are used to rank the MHAs. The results showed that MFA had the lowest SSE and shortest run-time, while Grey Wolf Optimizer achieved the highest objective function efficiency.

Keywords: Battery, fuel cell, marine, mathematical modeling, metaheuristic algorithms, multi-attribute decision making, optimization.

DENİZCİLİK UYGULAMALARI İÇİN ENTEGRE YAKIT PİLİ-BATARYA SİSTEMLERİNİN PERFORMANS ANALİZİ VE OPTİMİZASYONU

ÖZ

Deniz taşımacılığı sektörü, giderek daha sıkı düzenlemelere tabi olduğundan, çevresel ayak izini azaltma baskısı altındadır. "Yeşil gemi" konsepti, sıfır veya düşük egzoz gazı emisyonlu tahrik sistemlerine odaklanarak denizcilik camiasında dikkat çekmektedir. İstenilen amaca ulaşabilmek amacıyla bu tez yakıt pili sistemleri içeren iki vaka çalışmasını incelemektedir. İlk vaka çalışmasında, yakıt hücresi ve batarya tabanlı hibrit konfigürasyonların çevresel ve ekonomik etkileri incelenmektedir. Fosforik asit ve erimiş karbonatlı yakıt hücresi sistemleri, bir kimyasal tanker üzerinde dizel jeneratörlerin yerini alcak şekilde geminin toplam elektrik talebini karşılamaktadır. Belirtilen yakıt hücresi sistemlerinin bataryalarla birlikte ticari bir tanker gemisinde kullanımının çevresel ve ekonomik analizleri gerçekleştirilmektedir. Sonuçlar, karbon dioksit emisyonlarının yüzde kırk dokuz virgül yetmiş beşe kadar azaltılabileceğini ve erişimiş karbonatlı yakıt hücreleri ve lityum nikel manganez kobalt oksit batarya hücrelerinin kullanımıyla güncel yakıt fiyatları için en düşük elektrik üretim maliyetinin kilovat saat başına binde yüz seksen bir Amerikan doları olduğunu göstermektedir. İkinci vaka çalışmasında, bir proton-değişim membranlı yakıt hücresinin (PEMFC) yarı-ampirik matematiksel modelinin operasyon parametreleri çeşitli meta-sezgisel algoritmalar (MSA) kullanılarak çıkarılıp karşılaştırılmıştır. Bu bağlamda, yedi bilinmeyen modelleme parametresinin değerlerini bulmak için toplam kare hatası (TKH) amaç fonksiyonu olarak kullanılmaktadır. Vaka çalışması olarak, bir ticari PEMFC için MSA'lar kullanılarak parametre çıkarımı gerçekleştirilmiştir. MSA'ları sıralamak için üç farklı çok kriterli karar verme yöntemi kullanılmıştır. Sonuçlar, *Moth Flame Algoritma*sı'nın en düşük TKH ve en kısa çalışma süresine sahip olduğunu, *Grey Wolf Optimizer*'ın ise en yüksek amaç fonksiyonu verimliliğini elde ettiğini göstermiştir.

Anahtar Kelimeler: Batarya, yakıt pili, denizcilik, matematiksel modelleme, meta-sezgisel algoritmalar, çok kriterli karar verme yöntemleri, optimizasyon.

CONTENTS

Page

Ph. D. THESIS EXAMINATION RESULT FORM……..…….....……ii
ACKNOWLEDGEMENTS……..…….…….…….....…iii
ABSTRACT……..…….…….…….....…iv
ÖZ……..…….…….……..…….....…...v
LIST OF FIGURES……..…….…….……..…….....….ix
LIST OF TABLES……..…….…….……..…..…….....xi

CHAPTER 1 - INTRODUCTION.....1

1.1 Motivation of the Thesis 4
1.2 Objective of the Thesis.....5
1.3 Thesis Outline.....5

CHAPTER 2 - BACKGROUND AND LITERATURE REVIEW 7

2.1 Renewable Energy Sources and Technologies 8
2.2 Hydrogen Energy and Fuel Cells 9
2.2.1 Hydrogen Energy.....9
2.2.1.1 Hydrogen Production.....10
2.2.1.2 Hydrogen Storage Methods 14
2.2.2 Fuel Cell Technology 17

CHAPTER 3 - EXTRACTING SEMI-EMPIRICAL MODEL PARAMETERS FOR A COMMERCIAL PEMFC FOR MARINE VESSELS USING MHAS AND MULTI-ATTRIBUTE DECISION-MAKING METHODS 20

3.1 Literature Review.....20
3.1.1 Literature Review on Marine Vessels Utilizing Fuel Cell.....20
3.1.2 Literature Review on Modeling of PEMFCs.....23

3.1.3 Literature Review on Metaheuristic Algorithm for Parameter Extraction of PEMFCs 26
3.2 Mathematical Modeling 33
3.2.1 0D Semi-empirical Electrochemistry Model of PEMFC Stack 33
3.2.2 Metaheuristic Optimization Algorithms for PEMFC Stack Parameter Extraction 36
3.2.2.1 Fitness Function Definition and Parameter Settings for MHAs 36
3.2.2.2 Genetic Algorithm (GA) 38
3.2.2.3 Differential Evolution (DE) 38
3.2.2.4 Salp Swarm Algorithm 39
3.2.2.5 Moth-Flame Algorithm (MFA) 40
3.2.2.6 Whale Optimization Algorithm (WOA) 41
3.2.2.7 Sine Cosine Algorithm (SCA) 43
3.2.2.8 Cuckoo Search Algorithm (CS) 44
3.2.2.9 JAYA 45
3.2.2.10 Grey Wolf Optimizer (GWO) 45
3.2.3 Multi-attribute Decision-Making Methods (MADM) 47
3.2.3.1 Technique for Order of Preference by Similarity to Ideal Solution 47
3.2.3.2 Multi-Objective Optimization on the Basis of Raito Analysis 49
3.2.3.3 Preference Ranking Organization Method for Enrichment of Evaluations 50
3.3 Results and Discussion 51
3.3.1 PEMFC Model Validation Results 51
3.3.2 Metaheuristic Algorithms and MADM Methods Results 54

CHAPTER 4 - ENVIRONMENTAL AND ECONOMIC ANALYSES OF FUEL CELL AND BATTERY-BASED HYBRID SYSTEMS UTILIZED AS AUXILIARY POWER UNITS ON A CHEMICAL TANKER VESSEL 62

4.1 Literature Survey on Marine Transport Applications.....62
4.2 System Description.....66
4.3 Modeling of Fuel Cell and Battery Configuration 72
4.3.1 Mathematical Modeling of the Hybrid Power Plants 72
4.3.2 Environmental Analysis of Hybrid System 76
4.3.3 Economic Analysis of Hybrid System.....77
4.4 Results and Discussion 79
4.4.1 Mathematical Modeling Results of the Fuel Cell/Battery Hybrid System on Chemical Tanker Vessel.....79
4.4.2 Environmental Analysis of the Hybrid System.....81
4.4.3 Economic Analysis of Hybrid System.....84

CHAPTER 5 - CONCLUSIONS 88

REFERENCES 94

LIST OF FIGURES

Page

Figure 2.1 Classification of energy resources and technologies 8
Figure 2.2 Classification of hydrogen production 10
Figure 2.3 The schematic of the compressed hydrogen storage and its subsystems ..15
Figure 2.4 The pressure–capacity diagram according to the absorption and desorption processes 16
Figure 2.5 Schematic diagram of a fuel cell with its main components 18
Figure 3.1 Schematic of the operation of a PEMFC.....24
Figure 3.2 Classification of Fuel Cell Modeling 25
Figure 3.3 The number of related papers on the Web of Science for MHAs used in PEMFC parameter extraction.....28
Figure 3.4 The comparison of the polarization curves of the 250 W PEMFC using the E-CGA as in this study and HGA as in the study of Mo et al. (2006): (a) and (b) for identification and (c) and (d) for validation.....53
Figure 3.5 Polarization curve of H-1000XP.....54
Figure 3.6 Polarization curves when estimated parameters of (a) MFA, (b) DE, (c) JAYA, (d) CS, (e) IWOA, (f) GWO were used 57
Figure 3.7 Convergence curves of each algorithm's best solutions 58
Figure 3.8 Distribution of the lowest error obtained by the algorithms in each run ..58
Figure 3.9 Convergence curve of MFA 59
Figure 3.10 Convergence curve of GWO 59
Figure 3.11 Convergence curve of CS.....60
Figure 3.12 Convergence curve of JAYA.....60
Figure 4.1 Utilization hours of the plant according to operation modes 67
Figure 4.2 FC/battery hybrid electricity distribution system scheme.....70
Figure 4.3 Ship power distribution system model algorithm scheme 73
Figure 4.4 State-based EMS algorithm scheme 74
Figure 4.5 Fuel consumptions on different operation modes and total fuel consumption of the proposed combined systems and D/G plant 80

Figure 4.6 CO_2 production on different operation modes and total fuel consumption from the fuel cell/battery hybrid systems and D/G plant according to operation modes.....82
Figure 4.7 The production of (a) NO_x, (b) N_2O, (c) VOC, (d) CO, (e) SO_x, (f) PM emissions from plants for different operation modes 84
Figure 4.8 SoH curves of batteries were (a) utilized (b) not utilized during the navigation.....85
Figure 4.9 LEC values obtained for each configuration mode.....86
Figure 4.10 Electricity production costs of utilizing fuel cell/battery hybrid configurations and D/Gs onboard 87

LIST OF TABLES

Page

Table 2.1 Fuel cell types and main specifications 19
Table 3.1 Parameter setting of the algorithms 37
Table 3.2 The main parameters of the PEMFCs 52
Table 3.3 Ranges taken for the parameters' estimation 52
Table 3.4 Results of parameters for 250 W FC in Range 2 53
Table 3.5 Results of the statistical comparison 55
Table 3.6 The rank of each algorithm determined by selected MADM methods 55
Table 3.7 The estimated parameters by the algorithms 56
Table 4.1 Specifications of the marine diesel generators and electrical load 67
Table 4.2 Technical specifications of the commercial PAFC 68
Table 4.3 Technical specifications of the commercial MCFC 69
Table 4.4 Proposed system configurations 70
Table 4.5 Selected battery cells for system configurations 71
Table 4.6 EF of diesel fuels (g emission/ g fuel) 77
Table 4.7 Bunker prices for diesel fuels and LNG 79
Table 4.8 Optimum batteries and charge-discharge hours 79
Table 4.9 The emission reduction potential of the proposed system configurations compared to conventional diesel generators 82
Table 4.10 Weights, volumes, costs, and battery lifespans of the system configurations 86

CHAPTER 1
INTRODUCTION

The driving force behind the increase in maritime transport is the growth in world trade volume. According to the data gathered by the World Trade Organization (WTO), the volume and value of world trade have increased by 400 times and 274 times in 2020 compared to 1950, respectively (World Trade Organization [WTO], 2022). A significant percentage of the increasing world's trade by volume is realized by seaborne trade. In 2020, approximately 89% of the cargo in the world was transported by maritime transportation (Ministry of Transport and Infrastructure [MTI], 2021). During the transportation of the goods, the propulsion unit of the maritime fleet is still mainly provided by internal combustion engines (ICEs) are the main contributor to global warming and greenhouse gas emissions by using fossil-based fuels such as Heavy Fuel Oil (HFO) and Marine Diesel Oil (MDO). The need to close the door of fossil fuel usage in energy demand is not only due to the possibility of depletion of these fuels soon, but also because the environmental effects can cause irreversible damage.

The reduction in emission production by increasing energy efficiency has been among the most important subjects for shipowners (Kaya & Erginer, 2021) in the last two decades. International Maritime Organization (IMO) has also supported the reduction in greenhouse gas (GHG) emission production based on maritime transportation with new regulations and mandatory measures for ships, which were first initiated with the adoption of MARPOL Annex VI - Prevention of Air Pollution from Ships in 1997. SEEMP (Ship Energy Efficiency Management Plan) and EEDI (Energy Efficiency Design Index) amendments were entered into force on 1 January 2013 that gave progressive CO_2 emission reduction goals to ships by using energy efficiency-increasing techniques and emission reduction technologies. Technological advances have accelerated the achievement of these goals in the maritime industry. However, it was reported that the effect of seaborne GHG emissions on global anthropogenic CO_2 emissions increased from 2.76% (962 million t) in 2012 to 2.89% (1,056 million t) in 2018 (International Maritime Organization [IMO], 2020). IMO

took after the United Nation's (UN) sustainable development goal 13 (climate action) by adopting the initial strategy on the reduction of GHG emissions from ships. The strategy aims at reducing the total annual ship based GHG emissions by at least 50% by 2050 compared to 2008 (IMO, 2018).

The IMO has conducted four GHG studies on emitted emissions from ships in the year 2000 (IMO, 2000), 2009 (IMO, 2009), 2014 (IMO, 2014), and 2020 (IMO, 2020). Initially, IMO focused on reducing NO_x and SO_x emissions due to international shipping activities, as demonstrated in Annex VI of the MARPOL Convention, which is the first and main regulation that emphasized air pollution prevention requirements from ships adopted in 1997. The Energy Efficiency Design Index (EEDI) and the Ship Energy Efficiency Management Plan (SEEMP) were the first regulations to minimize carbon dioxide-based airborne emissions from ships, and these were established in Annex VI in 2011 and went into force in 2013. For different ship types and size segments, EEDI is a technical measure that specifies a minimum energy efficiency level expressed in grams of CO_2 per ship's capacity mile for new ships to promote the adoption of more energy-efficient equipment and engines, while the Ship Energy Efficiency Management Plan (SEEMP) is a low-cost operational approach by applying energy efficiency measures that creates a framework for enhancing the energy efficiency of new or existing marine vessels over 400 GT (IMO, 2022). The IMO introduced the Energy Efficiency Existing Indicator (EEXI) and Carbon Intensity Indicator (CII) to minimize ship GHG emissions by making additional amendments to Annex VI on the MEPC76 (Marine Environment Protection Committee 76) session in June 2021. EEXI is a metric connected to a ship's technological design. Ships must acquire EEXI approval just once throughout their lifespan, by the first periodical survey taking place no later than in 2023 (Det Norske Veritas [DNV], n.d.). CII is a marine vessel grading system based on in-service/operational efficiency (Lloyd Register [LR], n.d.). EEXI and CII will come into effect in January 2023, so the carbon taxation market is expected to be active in recent years based on airborne pollution caused by shipping activities. Market taxation prices for bunker fuels are expected to exceed $100 per ton (Gerretsen, 2022).

One of the suggested solutions for decreasing emissions from ships is the implementation of hybrid fuel cell systems, which has compelled shipping companies to create innovative technologies and adopt alternative fuels to mitigate the environmental consequences of their vessels. Shipping companies began by implementing emission reduction measures recommended in SEEMP recommendations, which are simple to implement and need low initial investment. However, the acceptance of EEXI has resulted in the implementation of energy-efficient equipment on all ships to fulfill the emission reduction objective of a 40% reduction from 2008 levels by 2030.

Hybrid fuel cell systems are one of the recommended technologies in the guidelines for reducing emissions from seaborne trade by generating energy from a range of fuels such as hydrogen, ammonia, methanol, liquefied natural gas (LNG), and others, which have also many advantages according to the other power systems such as high modularity, high efficiency, low air emissions, and reduced noise emissions, no moving parts, and fewer maintenance needs (Markowski & Pielecha, 2019). Commercially available fuel cell technologies are proton-exchange membrane fuel cells (PEMFC), alkaline fuel cells (AFC), direct methanol fuel cells (DMFC), phosphoric acid fuel cells (PAFC), molten carbonate fuel cells (MCFC), and solid oxide fuel cell (SOFC). Today, PEMFC has become the preferred fuel cell type among fuel cells due to its technological maturity and high electrical efficiency (Sohani et al., 2020). The fact that it has a shorter start-up time compared to fuel cells operating at high temperatures, especially SOFC and MCFC, made it possible to use it in the field of transportation (Department of Energy [DoE], n.d.-a). These features have enabled research and development studies and projects to be considerably higher than other fuel cells (van Biert, Godjevac, Visser, & Aravind, 2016) on the usage of PEMFC to power small ferries, yachts, and boats that usually navigate in coastal areas (Coppola, Micoli, & Turco, 2020).

1.1 Motivation of the Thesis

The shipping industry is a significant contributor to global greenhouse gas emissions, and there is a growing need to reduce its environmental impact. Fuel cell technology is a promising alternative to traditional combustion engines in the maritime sector, offering high efficiency and low emissions. However, there are several challenges to the implementation of fuel cell systems in different types of vessels, including the development of accurate mathematical models, the selection of appropriate fuel cell types, and the consideration of both environmental and economic factors.

This thesis aims to address some of these challenges by presenting two case studies focused on the application of fuel cell technology in small and large marine vessels. The first case study focuses on the development of a semi-empirical model of a PEMFC to be used in a small boat. Metaheuristic algorithms are used to extract the model's parameters, and multi-criteria decision methods are applied to determine the most suitable algorithm for the given application. The second case study considers the environmental and economic implications of using fuel cells in a large tanker vessel. Specifically, phosphoric acid fuel cells and molten carbonate fuel cells are evaluated in a hybrid configuration with batteries, and the results are analyzed in terms of both environmental impact and economic viability.

By conducting these case studies, this thesis contributes to the development of more efficient and environmentally friendly marine propulsion systems. The results of this research will provide valuable insights for engineers, designers, and policymakers interested in promoting sustainable shipping practices.

1.2 Objective of the Thesis

The objectives of the thesis were:

- To develop a semi-empirical model of a PEMFC that can accurately predict its performance.

- To evaluate the performance of several metaheuristic algorithms in extracting the parameters of the PEMFC model using multi-criteria decision methods.

- To integrate a battery model with a state of health sub-system to consider the aging effect of the batteries and predict the future fuel cell and emissions using the outputs of the mathematical model.

- To analyze the addition of a battery pack to the system using various charging strategies, and select the optimum energy storage configuration, charge-discharge rates, and the number of parallel sets by considering battery price, weight, and fuel-saving ratios.

- To assess the emission reduction (ER) of the proposed strategies for the current and future time range and evaluate the economic performance of the proposed configurations.

1.3 Thesis Outline

The following chapter provides a background and literature review of hydrogen and fuel cell technologies. It covers renewable energy sources and technologies, hydrogen energy, hydrogen production and storage methods, and fuel cell technology.

The third chapter presents a case study of utilizing PEMFC for a small fishing boat. This chapter includes a literature review of marine vessels utilizing fuel cells, modeling of PEMFCs, and metaheuristic algorithm for parameter extraction of

PEMFCs. It also presents the mathematical modeling of the PEMFC stack, metaheuristic optimization algorithms, and multi-attribute decision-making methods. The chapter concludes with the results and discussions of the PEMFC model validation and metaheuristic algorithms with Multi Attribute Decision Making (MADM methods ranking the metaheuristic optimization algorithms according to SSE, run-time, and best objective function efficiency performance metrics.

The fourth chapter presents an environmental and economic analysis of fuel cell and battery-based hybrid systems utilized as auxiliary power units on a chemical tanker vessel. This chapter includes a literature survey on marine transport applications, system description, and modeling of the fuel cell and battery hybrid configuration. It also includes mathematical modeling of the hybrid power plants, environmental analysis of the hybrid system, and economic analysis of the hybrid system. The chapter concludes with the results and discussion of the environmental and economic analysis of the hybrid system.

The last chapter provides a summary of the research findings, conclusions, and recommendations for future research. The chapter also includes a discussion of the contributions of the research to the field of fuel cell technology and maritime applications.

CHAPTER 2
BACKGROUND AND LITERATURE REVIEW

Internal combustion engines have dominated the world's power demand since they were invented in the 19th century. Although electric motor and battery technologies emerged almost half a century earlier than internal combustion engines, the technical maturity of internal combustion engines has reached earlier. The breakthrough for technological advances in the field of renewable energy technologies came with increased incentives following the 1973 oil crisis. These incentives resulted in the invention of solar cell technologies (National Renewable Energy Laboratory [NREL], n.d.) and the implementation of large wind farm projects in subsequent years (Nixon, 2008).

Global climate changes have been acting as another series of breakthrough events in the field of green energy production. It has been shown that the share of fossil fuels in the world's energy mix reduces every passing year (Ritchie, Roser, & Rosado, 2022). Renewable energy sources have proven themselves to replace the position of fossil fuels in the energy mix in the near future. However, renewable energy sources have been struggling to solve some challenges, e.g., energy transportation, area requirement, technical maturity, lack of incentives, and cost. Hydrogen can take part in effectively transporting renewable energy by utilizing its high gravimetric energy density. Although the production process of hydrogen can be carried out with fossil fuel sources, the reducing cost trend of green hydrogen production with renewable energy sources has increased the interest of the world, starting from the developed countries, in hydrogen technologies. In addition, the future cost of hydrogen fuel supply is projected to be below the current electricity costs supplied from grids in European countries (Zhou & Searle, 2022).

This chapter introduces a brief introduction to renewable energy sources and technologies that can be utilized for hydrogen production. Then, the production, storage, and utilization methods of hydrogen are discussed. A comprehensive literature

survey is also conducted that presents the fuel cell utilization in marine transportation and modeling studies of PEM fuel cells.

2.1 Renewable Energy Sources and Technologies

Energy sources could be classified into two main categories: non-renewable sources and renewable sources (Artkın, 2018; Raza et al., 2016). Energy obtained from natural sources that are renewed more quickly than is used up is referred to as renewable energy. Every renewable energy source requires its technology to transform the source of energy into a form of energy that can be used by humans or machines so, these can provide electricity or fuels, such as hydrogen, that are similar to the ones currently produced from fossil fuels.

Today, many countries use a mixture of renewable and non-renewable energy sources in their energy supply due to energy security and reliability concerns. New technologies that use renewable energy sources can produce electricity at a lower environmental impact than can be produced from fossil fuels and nuclear energy. Examples of renewable energy sources include wind energy, solar energy, hydropower, biomass, geothermal energy, and marine/ocean (wave, current, and tide) energy. A more detailed classification of energy sources is depicted in Figure 2.1.

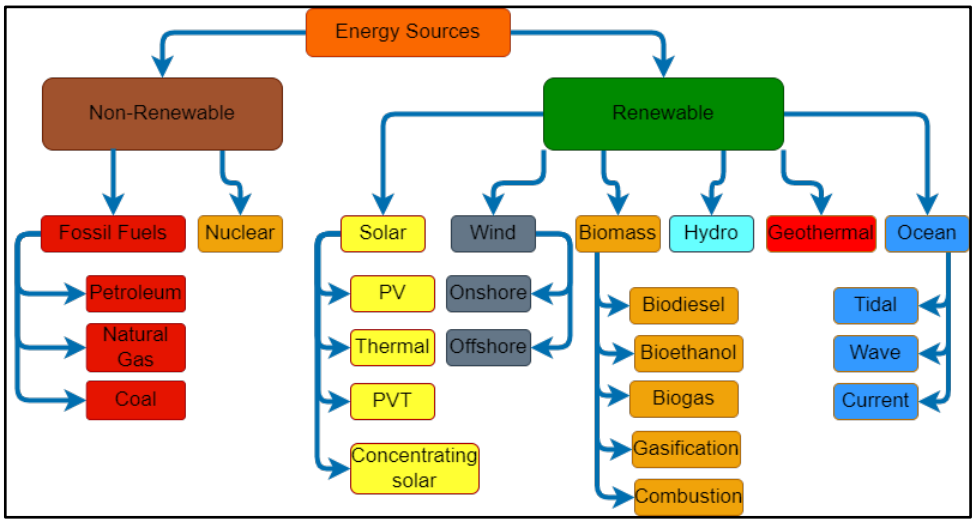

Figure 2.1 Classification of energy resources and technologies (Adapted by the author from (Artkın, 2018; Ghosal, 2022; Raza et al., 2016))

Systems that generate electrical power and/or heat using renewable energy sources are called "renewable energy technologies." Photovoltaic solar panels, thermal solar panels, photovoltaic-thermal (PVT) panels, wind turbines, geothermal power plants, hydroelectric power plants, biomass-based power systems, and ocean/marine energy-based power systems are accepted in this area (Kaltschmitt, Streicher, & Wiese, 2007). Integration of these technologies into the existing energy infrastructure will be essential in the process of moving toward sustainable development in terms of environmentally sustainable, climate-friendly, and cost-competitive shortly.

2.2 Hydrogen Energy and Fuel Cells

Green hydrogen, an energy carrier based on green and renewable sources, offers possibilities for sustainable transportation in the future. A diversified, growing number of countries are looking at the potential of employing renewable energies, including green hydrogen, for power generation and mobility. The use of green hydrogen as an energy carrier in fuel cell systems is a promising alternative due to its ability to convert chemical energy to electrical energy efficiently among competitors and provide emission-free applications.

2.2.1 Hydrogen Energy

The hydrogen atom is the lightest and most abundant type of atom in nature. Thus, provides a high gravimetric energy density of 120 Mj/kg which is 3 times that of hydrocarbon fuels, such as gasoline has energy density of 44 Mj/kg (Ramirez-Vidal, Sdanghi, Celzard, & Fierro, 2022). Hydrogen thus has the highest potential to replace liquid fuels in terms of energy content and gravimetric energy density. In addition, hydrogen is an extremely clean and renewable energy carrier for two reasons: First, and most importantly, it can be utilized to store energy generated by wind and solar power; second because it is a clean source of energy being non-polluting in terms of particulate matter emissions.

2.2.1.1 Hydrogen Production

Hydrogen can be produced from a variety of feedstocks. Hydrogen production processes could be classified by source as fossil fuels and renewable sources. The process of obtaining hydrogen from fossil fuels is divided into 2 main categories as hydrocarbon reforming and hydrocarbon pyrolysis. Hydrogen production obtained from renewable resources is divided into two; biomass processes and water splitting (Nikolaidis & Poullikkas, 2017). A more detailed classification is shown in Figure 2.2.

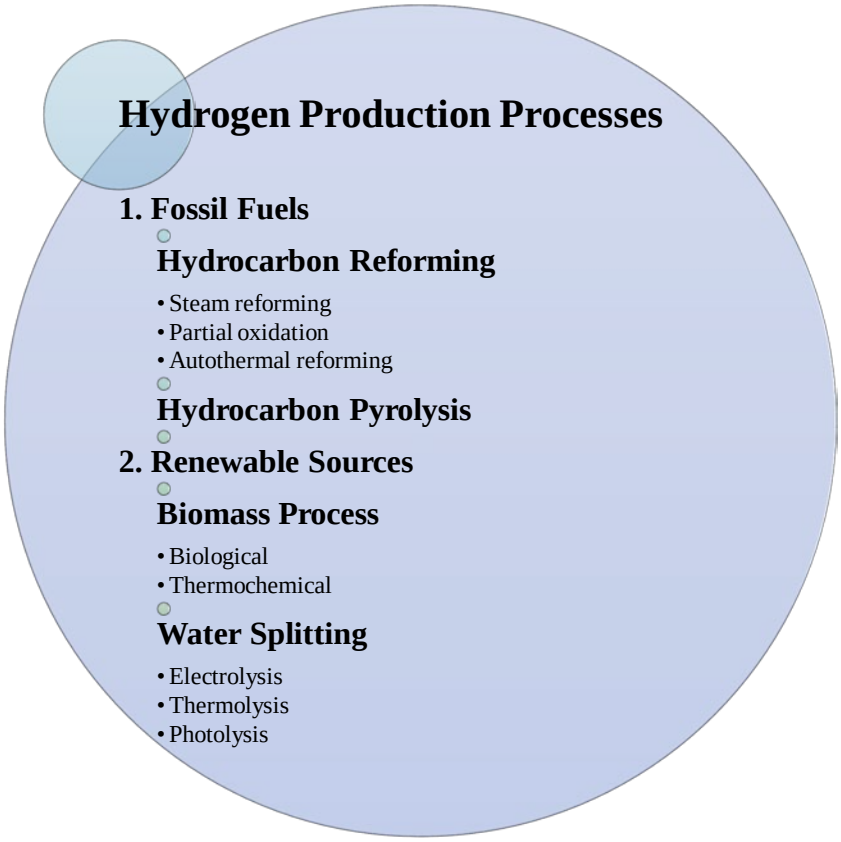

Figure 2.2 Classification of hydrogen production (Adapted by the author from (Nikoliadis & Poullikkas, 2017))

The method called "steam reforming" which is used to obtain hydrogen from hydrocarbon fuels, is carried out endothermically by sending steam onto the hydrocarbon fuel, and the main equations through the process are shown in Equations 2.1 – 2.3: (Nikolaidis & Poullikkas, 2017)

Reformer: $C_nH_m + nH_2O \rightarrow nCO + \left(n + \frac{1}{2}m\right)H_2$ (2.1)

WGS reactor: $CO + H_2O \rightarrow CO_2 + H_2$ (2.2)

Methanation reaction: $CO + 3H_2 \rightarrow CH_4 + H_2O$ (2.3)

The other basic method is the partial oxidation method, in which oxygen is sent to the hydrocarbon fuel as a reactant and the reaction takes place exothermically the main equation of the process is shown in Equations 2.4 – 2.7: (Nikolaidis & Poullikkas, 2017)

Reformer: $C_nH_m + \frac{1}{2}nO_2 \rightarrow nCO + \frac{1}{2}mH_2$ (catalytic) (2.4)

$C_nH_m + nH_2O \rightarrow nCO + \left(n + \frac{1}{2}m\right)H_2$ (non–catalytic) (2.5)

WGS reactor: $CO + H_2O \rightarrow CO_2 + H_2$ (2.6)

Methanation reaction: $CO + 3H_2 \rightarrow CH_4 + H_2O$ (2.7)

The method by which these two methods are combined is called the "autothermal method". This process aims to increase the amount of hydrogen production by using the heat released in partial oxidation in the steam reforming process. The reaction equation is shown in Equation 2.8: (Nikolaidis & Poullikkas, 2017)

$$C_nH_m + \frac{1}{2}nH_2O + \frac{1}{4}nO_2 \rightarrow nCO + \left(\frac{1}{2}n + \frac{1}{2}m\right)H_2 \quad (2.8)$$

Another method used to obtain hydrogen from hydrocarbon fuels is the pyrolysis method, which is based on the thermal decomposition of the fuel itself. The general reaction is given: (Nikolaidis & Poullikkas, 2017)

$$C_nH_m \rightarrow nC + \frac{1}{2}mH_2 \quad (2.9)$$

The utilization of fossil fuel-based hydrogen production methods, despite their convenience and cost-effectiveness, is deemed unsustainable in the long-term due to their reliance on finite energy sources. To address this concern, there has been an increasing focus on exploring alternative and renewable sources of hydrogen production, including water splitting and biomass, to ensure sustainable energy production.

Biomass is made from wood, aquatic plants, crops, and various waste resources (municipal solid waste, animal waste, wood waste, food processing waste, industrial waste, and biological waste) (Demirbaş, 2001). There are two basic methods for producing hydrogen from biomass and one of them is the thermochemical process. It is known that this method can provide hydrogen production at higher stoichiometric ratios, much faster than biological methods, by pyrolysis and gasification methods (Fremaux, Beheshti, Ghassemi, & Shahsavan-Markadeh, 2015). The hydrogen production equations by the pyrolysis method and gasification method are shown in Equations 2.9-2.11 and 2.13-2.14, respectively: (Nikolaidis & Poullikkas, 2017)

$$Pyrolysis\ of\ biomass \rightarrow H_2 + CO + CO_2 + hydrocarbon\ gases + tar + char \quad (2.10)$$

$$C_nH_m + nH_2O \rightarrow nCO + (n + 1/2\,m)H_2 \quad (2.11)$$

$$CO + H_2O \rightarrow CO_2 + H_2 \quad (2.12)$$

$$Biomass + Air \rightarrow H_2 + CO + N_2 + CH_4 + other\ CHs + tar + H_2O + char \quad (2.13)$$

$$Biomass + Steam \rightarrow H_2 + CO + CO_2 + CH_4 + other\ CHs + tar + char \quad (2.14)$$

The other method of producing hydrogen from biomass is called a biological process. The main approaches to producing hydrogen from biological wastes are photo- and dark fermentations, direct and indirect bio-photolysis, and multi-stage or sequential dark photo-fermentation. These methods are environmentally friendly and

contribute to the sustainable development of hydrogen production by requiring less energy (Nikolaidis & Poullikkas, 2017).

In addition to biomass-based methods, several water-splitting technologies can produce hydrogen from renewable sources such as solar and wind energy. One of the most commonly used methods is electrolysis, which involves using an electric current to split water into hydrogen and oxygen. The reaction can be represented by the following Equation 2.15 (Liu, Xu, Yang, & Jiang, 2020).

$$2H_2O + electrical\ energy \rightarrow 2H_2 + O_2 \quad (2.15)$$

Electrolysis can be powered by renewable sources such as solar, wind, or hydropower, making it a promising method for sustainable hydrogen production.

Another method is photolysis, which uses solar energy to split water molecules into hydrogen and oxygen. In this process, a semiconductor material is used to absorb sunlight and generate an electric current, which is used to split water. The reaction can be represented by the following equation 2.16 (Walter et al., 2010).

$$2H_2O + photons \rightarrow 2H_2 + O_2 \quad (2.16)$$

Photolysis has the advantage of being powered directly by sunlight and can potentially have high conversion efficiencies, making it an attractive option for renewable hydrogen production (Walter et al., 2010).

Thermolysis is another water-splitting method that involves using heat to split water into hydrogen and oxygen. This process can be powered by concentrated solar energy or nuclear energy. The reaction can be represented by the following equation 2.17 (Boretti, 2022).

$$2H_2O + heat\ energy \rightarrow 2H_2 + O_2 \quad (2.17)$$

Thermolysis has the potential for high efficiency and low environmental impact, but it requires high temperatures and may involve the use of corrosive chemicals (Boretti, 2022).

All of these methods for producing hydrogen from renewable sources, whether it be through electrolysis, photolysis, or thermolysis, offer environmentally friendly and sustainable approaches to hydrogen production. These methods require less energy and produce fewer emissions, which contributes to the sustainable development of hydrogen production (Hota, Das, & Maiti, 2023).

2.2.1.2 Hydrogen Storage Methods

Hydrogen storage is an important technology driving the advancement of hydrogen and fuel cell technologies including stationary power, portable power, and transportation applications. There are several methods found in the literature including compressed hydrogen storage, metal hydrides, liquid hydrogen storage, cryo-compressed hydrogen storage, and chemical hydride storage.

Compressed hydrogen storage is a widely-used technology that involves the physical storage of hydrogen gas in high-pressure tanks. One of the primary benefits of using a compressed hydrogen storage system is the ability to rapidly refuel vehicles in as little as 3-5 minutes (Stetson, McWhorter, & Ahn, 2015). However, this technology also has some limitations, particularly when used in portable applications where the volumetric capacity of commercial tanks is low, even at high pressures (Langmi, Engelbrecht, Modisha, & Bessarabov, 2022). A major disadvantage of compressed hydrogen storage is the low volumetric density of the tanks, even at pressures greater than 70 MPa. This limits the amount of hydrogen that can be stored in the tanks, particularly for portable applications. Additionally, safety concerns are associated with storing hydrogen at such high pressures. These issues must be taken into consideration when designing and implementing compressed hydrogen storage systems. Figure 2.3 presents a schematic of the compressed hydrogen storage system. Further research is needed to address the limitations of compressed hydrogen storage,

particularly with regard to increasing the volumetric capacity of the tanks and improving safety measures.

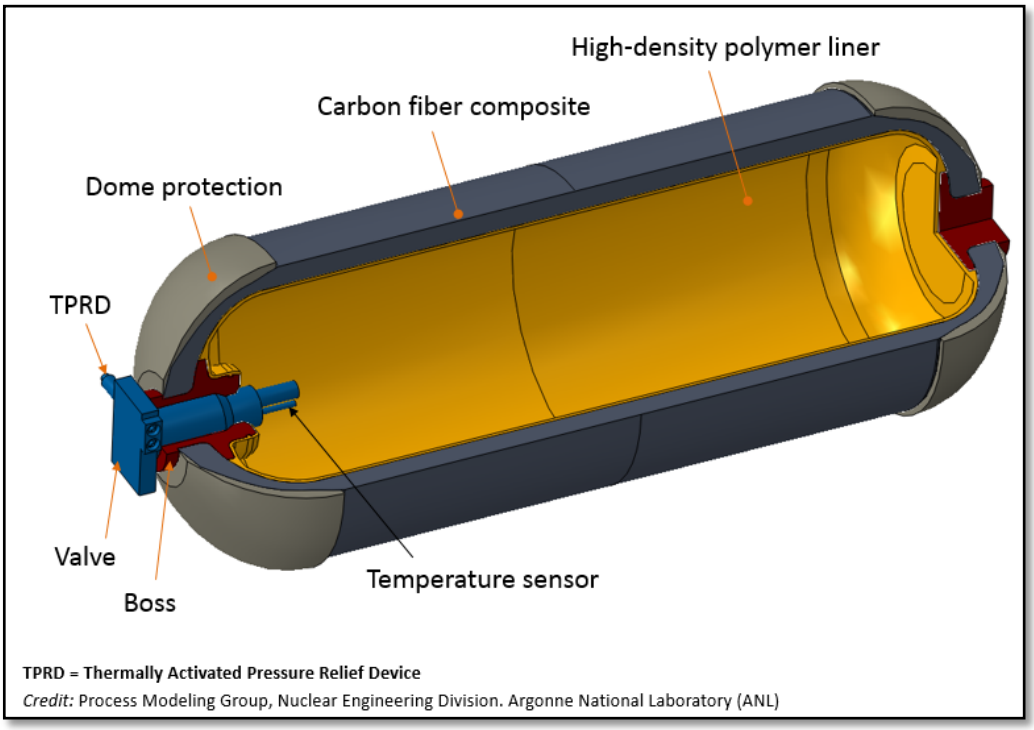

Figure 2.3. The schematic of the compressed hydrogen storage and its subsystems (DoE, n.d.-b)

Metal hydrides, referred to as MH_x, have been identified as a promising class of materials for hydrogen storage due to their versatile range of potential applications. These applications include but are not limited to hydrogen fuel cell technology, hydrogen production via electrolysis, hydrogen purification and separation, and thermal energy storage systems. Research in this field has primarily focused on complex hydrides composed of ionic alkali or alkaline earth metals and complex anions containing centric atoms such as transition or main group metals or metalloids, such as Fe, Ni, B, Al, or N, that are covalently bonded to hydrogen. These complex metal hydrides have demonstrated potential as a practical hydrogen storage option, with minimal energy requirements for hydrogen uptake and release.DoE, n.d.-c). The performance of a metal hydride tank mainly includes the parameters. These are capacity, releasing time, recharging time, and cycle life. The process of metal hydride formation is exothermic and involves the release of heat. Upon the formation of metal hydride, hydrogen can be liberated through the application of sufficient heat. Figure

2.4 illustrates the storage capacity of hydrogen in relation to pressure, with metal hydride and adsorbent storage being the only methods of storage that do not rely on chemical absorption in a liquid state. It should be noted that hydrogen is stored through chemical absorption in a liquid state in all other storage methods. Aromatic molecules with carbon–carbon double bonds are the most useful substances for liquid chemical hydrogen storage. As an example, methylcyclohexane (C_7H_{14}) releases three H_2 molecules when heated and occurs toluene (C_7H_8) (Berry, Martinez-Frias, Espinosa-Loza, & Aceves, 2004).

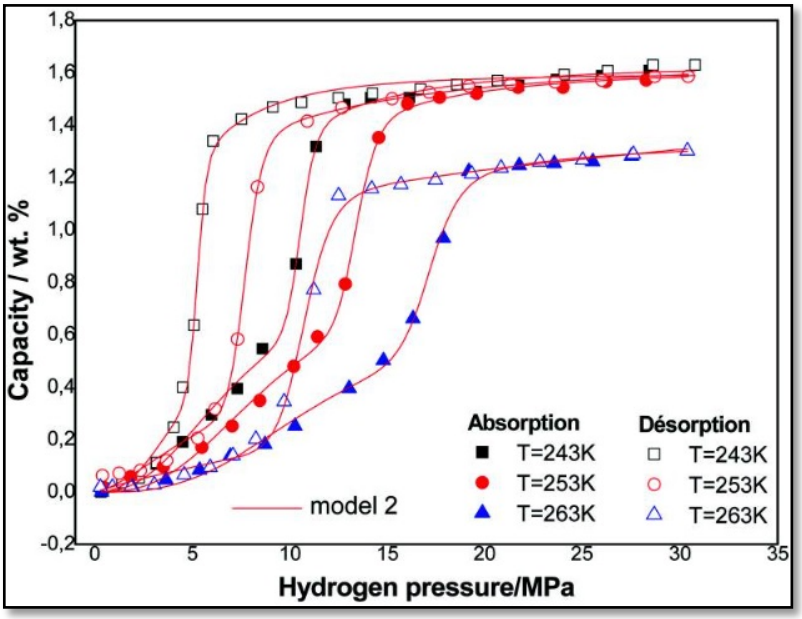

Figure 2.4. The pressure–capacity diagram according to the absorption and desorption processes (Aouaini, Bouazizi, Almoneef, Al-Ghamdi, & Lamine, 2021)

Cryo-compressed hydrogen and liquid hydrogen (LH_2) storages are alternative methods where hydrogen cools down and is liquidized at −253°C (ca. 20 K) and also compressed into tanks that can be pressurized to approximately 250–350 atm (El-Eskandarany, 2020). Therefore, the liquid hydrogen size requires larger tanks reaching about 3 times larger than the currently used gasoline tank. Production of liquid hydrogen requires the liquefiers use that employ different principles of cooling. There are several techniques that liquid-state hydrogen production. These are the Linde-Hampson liquefiers, the Linde dual-pressure liquefiers, the Claude liquefiers, the Kapitza liquefiers, and the Hey-landt liquefiers (Veziroglu, Sherif, & Barbir, 2005).

2.2.2 Fuel Cell Technology

A fuel cell is a system that converts some of the chemical energy stored in a suitable fuel directly into (direct current) electrical energy and heat through an oxidizer as a result of a series of electrochemical reactions with high efficiency and low environmental impact (Grove, 1839).

In 1838, Christian Friedrich Schönbein laid out the theoretical foundations of fuel cell technology (Andújar & Segura, 2009). At the same time, William Robert Grove, who worked independently of Christian F. Schönbein, produced the first fuel cell, which he called a "gas voltaic battery", using materials similar to today's phosphoric acid fuel cell (PAFC). As a result of a series of experiments, he was able to produce hydrogen and oxygen on a platinum catalyst layer using a dilute sulfuric acid solution and explained that an electric current was produced by passing the released electrons through an external circuit (Grove, 1839). In addition, he observed that there was a continuous current between the electrodes in the containers that he was sealing and that the water level in the container increased as long as this current continued (Grove, 1843).

A single cell consists of two catalyst layers, an anode, and a cathode, separated by an electrolyte and two current collectors (end plates) involving fuel and airflow channels are located in the anode and cathode catalyst layer sides, respectively, and the main components of the fuel cell as shown in Figure 2.5.

Fuel cells generate a continuous supply of power by utilizing the feed of fuel and air through electrochemical reactions that occur at the catalyst layer. This concept was first introduced by (Grove, 1843). Within the fuel cell, ions are transported from one electrode to another through the electrolyte, while electrons travel through an external circuit to produce electricity. Although a single cell is capable of generating power, the output is typically insufficient. To produce a substantial amount of power, multiple single cells are connected in series through a process known as "stacking." This

stacking process is generally accomplished through the use of bipolar plates, which provide channels for the flow of oxidant and fuel throughout the stack.

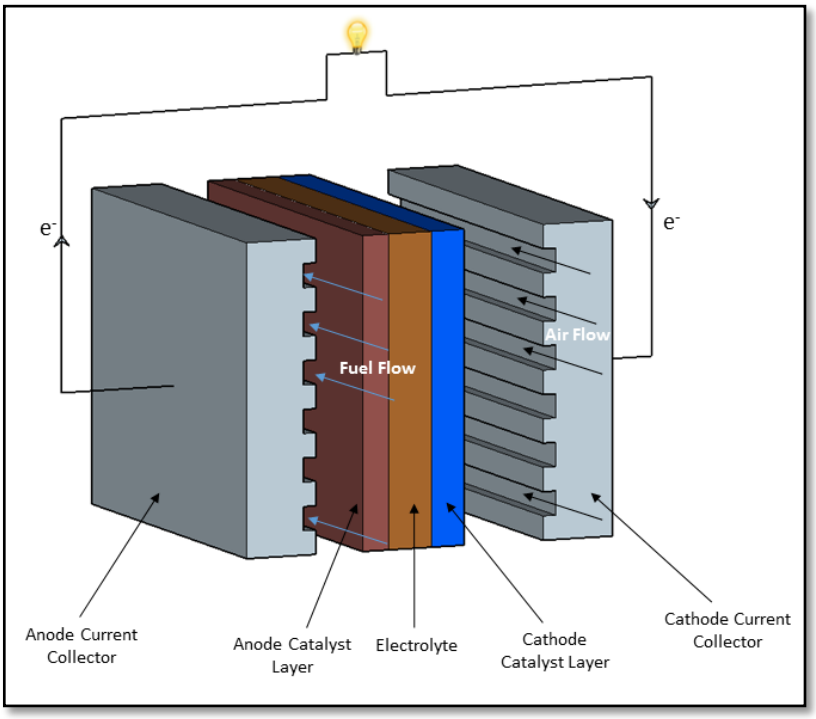

Figure 2.5 Schematic diagram of a fuel cell with its main components

Fuel cells are classified by considering many different features. In particular, the type of fuel used in the classifications, the type of electrolyte used in the fuel cell, operating temperatures, and use in stationary or mobile applications were considered. The fuel cell terminology that is widely used and most accepted is determined by the type of electrolyte used and shown in Table 2.1. In addition, the most commonly used fuel cell types today are (Mench, 2008) polymer electrolyte membrane fuel cells (PEMFC), direct methanol fuel cells (DMFC), solid oxide fuel cells (SOFC), molten carbonate fuel cells (MCFC), alkaline fuel cell (AFC), and phosphoric acid fuel cells (PAFC). Each kind has its pros and cons. PEMFCs are popular for mobile applications because of their lower operating temperatures, quick start-up times, and high efficiency compared to other types of fuel cells. DMFCs are also popular for mobile applications due to their high-power density and efficient conversion of methanol fuel. These two are also classified as "low-temperature fuel cells" due to their low operating temperatures. On the other hand, SOFCs and MCFCs are categorized as "high-

temperature fuel cells" because of their higher operating temperatures and are mainly used in stationary applications. SOFCs and MCFCs are both considered to be more energy efficient than PEMFCs and DMFCs because of their high-temperature operation that could be utilized; however, their increased temperatures require more expensive construction materials. PAFCs are also categorized as high-temperature fuel cells; however, their operating temperatures are slightly lower than those of SOFCs and MCFCs, and PAFCs use hydrocarbon fuels, such as natural gas and propane.

Table 2.1. Fuel cell types and main specifications (Mench, 2008)

Type of FC	**Electrolyte Material**	**Mobile Ion**	**Operating Temperature**
PEMFC	Flexible solid per-fluorosulfonic acid polymer	OH^-	30 – 100 ºC
DMFC	Polymer electrolyte membrane	H^+	<100 ºC
AFC	Potassium hydroxide solution	H^+	50 – 200 ºC
PAFC	A phosphoric acid solution in a porous silicon carbide matrix	H^+	~220 ºC
MCFC	Lithium/ Potassium carbonates in a porous matrix	$(CO_3)^{2-}$	~650 ºC
SOFC	Yttria (Y_2O_2 stabilized zirconia (ZrO_2)	O^{2-}	500 ºC – 1000 ºC

CHAPTER 3
EXTRACTING SEMI-EMPIRICAL MODEL PARAMETERS FOR A COMMERCIAL PEMFC FOR MARINE VESSELS USING MHAS AND MULTI-ATTRIBUTE DECISION-MAKING METHODS

Fuel cell vehicles' low environmental impacts, current technological advancements, and commercial manufacturing have opened the path to their employment in a variety of areas. The usage of fuel cell technology in marine transport has increased as the IMO's environmental regulations have been tightened.

In this chapter, operating parameters of a semi-empirical mathematical model of a proton-exchange membrane fuel cell (PEMFC) are extracted and compared using various metaheuristic algorithms to analyze its behaviour in a fast and economical manner before setting up for an application, which will then be utilized on a marine vessel in this case. Sum-squared error is employed as the objective function to find the values of seven unknown modeling parameters. The parameter extraction is carried out by using the polarization curve data of a 1000 W commercial PEMFC. Three different multi-attribute decision-making methods are used to rank the metaheuristic algorithms in terms of performance.

3.1 Literature Review

3.1.1 Literature Review on Marine Vessels Utilizing Fuel Cell

There are several demonstration projects and a few commercial marine vessels utilizing fuel cells as a main propulsion unit or auxiliary power unit.

World's first fuel cell boat HYDRA used an Alkaline Fuel Cell (AFC) system with a 5.5 kW net power output. The passenger capacity of The Hydra is 22 passengers. A propulsion system is powered by an electric motor that gets electricity from Alkaline Fuel Cell. The debut was in June 2000 on the Rhine near Bonn, Germany. The vessel, which operated as a ferryboat in Ghent, Belgium during an electric boat conference in 2000, transported roughly 2,000 passengers from 1999 to 2000. The vessel is certified

by the Germanischer Lloyd for passenger transport, and its fuel cell system is capable of initiating operation even under sub-freezing temperature conditions, with an operating voltage between 64 - 88 V and an operating temperature of 70 °C (Etaing, n.d.).

Bristol City Council initiated a project named Green Capital in 2010. A local consortium is constituted which consists of directors of Bristol Packet Boat Trips, Number Seven Boat Trips, and Auriga Energy. A steel hull ferry is 11 meters long and a 3.6-meter breadth, two permanent magnets DC motors powered by a 12-kW fuel cell and named "Hydrogenesis" is constructed by Bristol Hydrogen Boats with CE marked. Hydrogenesis is the first hydrogen-powered ferry to operate in the United Kingdom which carries 12 passengers and 2 crew members. This is also the first commercially available fuel cell boat in the UK and the cost of hiring for private purposes costs 130 pounds per hour in 2016 (Bristol Hydrogen Boats, n.d.).

The purpose of the "Protium" project is to apply modem technologies to a traditional mode of transportation for use in a hybrid canal boat on the UK canal network. The boat is converted from British Waterways maintenance craft to a canal boat. The boat has a solid-state hydrogen store ($TiMn_2$- based metal hydride store), Proton Exchange Membrane (PEM) fuel cell (ReliOn Independence l000TM model), lead-acid battery pack and high efficiency, permanent magnet (NdFeB) electric motor. The speed limit for the majority of inland waterways in the UK is 6.4 kph. Thus, providing an excellent opportunity for testing a low-power PEM fuel cell in a marine environment. This boat is named "Ross Barlow" which is officially launched in September 2007 (Bevan, Züttel, Book, & Harris, 2011). The system has a large cylinder, each containing 30 kg of metal hydride power. The operating pressure of the system is lower than 10 bars. Approximately 4 kg of hydrogen is obtained from the solid-state hydrogen storage system. The forced air-cooled PEM fuel cell is rated at 1 kW and operates at 65 °C. The average fuel cell flow rate is measured at 15 L min^{-1}. There is a huge loss due to the purge of hydrogen to eliminate water management problems (Bevan et al., 2011). The system is most suitable for low-power demand applications. Therefore, speed limitation makes the system suitable for canals. A high-

power demand situation is provided by batteries. The converted boat and the designed hybrid system are more efficient than the traditional engine and also more silent and environmentally friendly.

The Zemships project was a groundbreaking initiative that marked the first instance of fuel cell technology being implemented onboard a passenger vessel. This project served as a tangible demonstration of the viability of fuel cell technology for use in inland passenger ships during daily operations. The project was spearheaded by Hamburg's Department for Urban Development and the Environment, and involved the collaborative efforts of several key partners, including but not limited to ATG Alster Touristik, Germanischer Lloyd, Hamburger University of Applied Sciences, Hochbahn, hySolutions, Linde Group, Proton Motor Fuel Cell GmbH, and UJV Nuclear Research Institute. Following the project's official conclusion in August of 2008, the FCS Alsterwasser has remained in normal line operation, overseen by ATG. The vessel is utilized for a variety of purposes, including Alster roundtrips, Hamburg channels, and charter trips (Dirk, 2013). Overall transported passengers are more than 43000 till the end of 2012 although no operation is possible in 2010 because of the fire accident. And also fuel cell system is operated for 2500 hours till the end of 2012 (Dirk, 2013).

The Nemo H_2 is the first boat powered by a fuel cell for 86 passengers and 2 crew in Amsterdam which is owned by Boat Company Lovers. The dimensions of the boat are 21.95-meter in length and 4.25-meter width. A propulsion system consists of 1 electrically powered, 75 kW stem thruster and 1 electrically powered, 11 kW bow thruster. It has two 30 kW PEMFCs and a 70-kWh battery, and the maximum speed of the boat is 8.6 knots per hour. Without refueling, the voyage time is 9 hours when the speed is approximately 7 knots. Hydrogen is stored in 6 cylinders at 350 bar for 24 kg of hydrogen. The canal boat meets all European regulations for barges. The boat is in operation on the canals in Amsterdam since December 2009 (Oldsailor, n.d.). The new boat cost more than double the cost to build than a canal boat running on a diesel engine. Needs to visit a hydrogen dispensing station for a refill once a day. Normal boats only need a fuel top-up once a week (The Green Light District, 2009).

Choi et al. (2016) developed and installed a hybrid proton exchange membrane fuel cell (PEMFC)/battery system for a 20-meter tourist boat with an output power of approximately 85 kW and a speed of 6.6-7.8 knots. Rivarolo, Rattazzi, Lamberti, & Magistri (2020) compared the energy efficiency, CO_2 emissions, and other fuels for the fuel cell system to be used in a ferry. The software was created at the University of Genoa to study the design and cost of a 200-passenger capacity ferry operating on the artificial lake of Itaipu. Rafiei, Boudjadar, & Khooban (2020) suggested a zero-emission hybrid fuel cell/battery/cold-ironing system and used real data from a ferry to examine hull design and energy resources. Balestra & Schjølberg (2021) created a simulation tool that evaluates a user-selected configuration in a battery and fuel cell power plant for marine applications that can produce the electricity required by the energy management system realistically. Dall'Armi, Micheli, & Taccani (2021) carried out simulations using different types of compressed hydrogen storage tanks (Type 1,3,4) to analyze the peak shaving point of the low temperature (LT)-PEMFC/battery system used for propulsion of a small-sized RoRo vehicle and passenger ferry.

3.1.2 Literature Review on Modeling of PEMFCs

The schematic of a hydrogen-fed PEMFC and redox reactions are given in Figure 3.1 and Equations 3.1-3.3, respectively. Hydrogen fed from the anode side is separated into positive and negative ions on the anode side of the FC. Positive ions move from the anode to the cathode, whereas negative ions move through the external circuit, thus electrical power is produced. Negative and positive ions reaching the cathode react with oxygen, which is found in the air fed to the cathode, to form water (Colpan, Nalbant, & Ercelik, 2018; Mench, 2008).

$$Anode: H_2 \rightarrow 2H^+ + 2e^- \quad (3.1)$$

$$Cathode: 0.5O_2 + 2H^+ + 2e^- \rightarrow H_2O \quad (3.2)$$

$$Overall: H_2 + 0.5O_2 \rightarrow H_2O \quad (3.3)$$

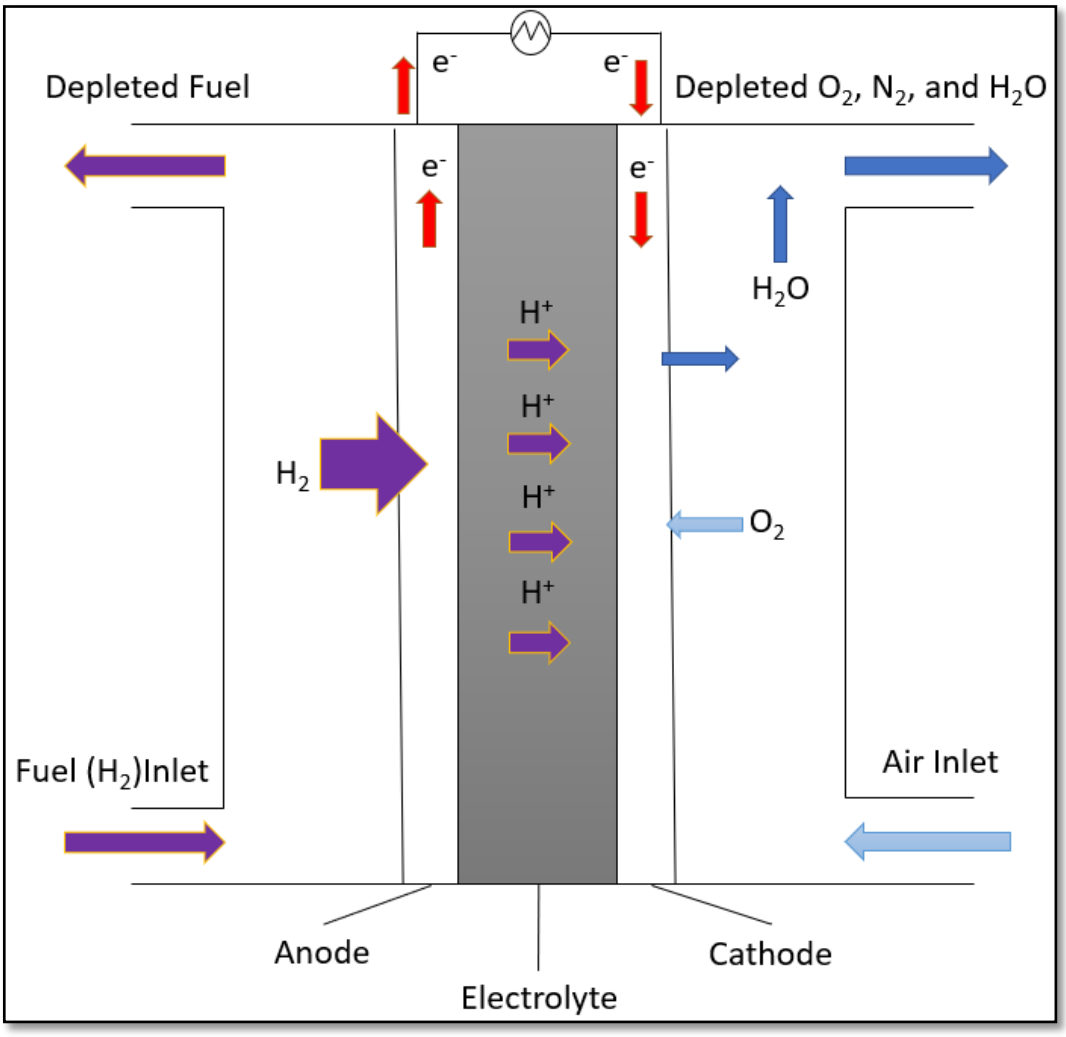

Figure 3.1. Schematic of the operation of a PEMFC

The performance assessment of fuel cells could be done through mathematical modeling or experimental methods. Installation of an experimental FC setup could have considerable disadvantages including the following: being time-consuming, dealing with challenging issues such as effective hydrogen supply and storage, and the high initial investment cost. However, developing a mathematical model is relatively cheap compared to an experimental setup, and it is also quite useful to develop an accurate mathematical model to study the feasibility of an FC-based system before its installation (Kirubakaran, Jain, & Nema, 2009). Various FC models exist in the literature and could be categorized as shown in Figure 3.2.

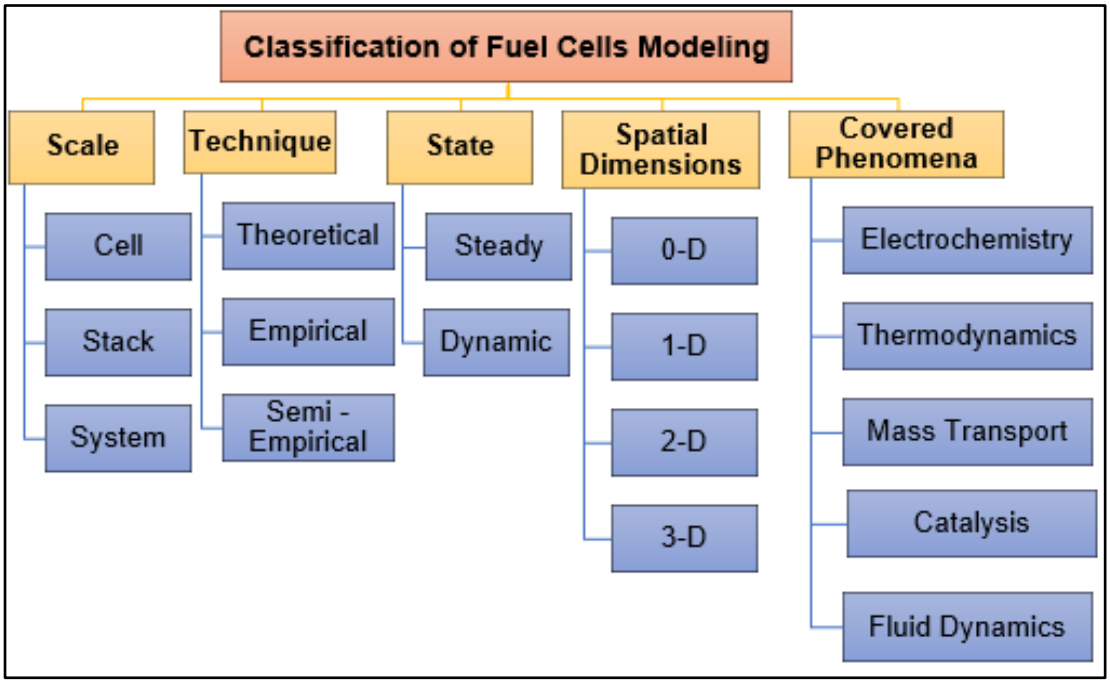

Figure 3.2 Classification of Fuel Cell Modeling (Adapted from (Ashraf, Abdellatif, Elkholy & El-Fergany, 2022a))

1D and 2D models are frequently used in literature to determine the performance analysis of the fuel cell. A non-isothermal, 1D, and 2-phase fuel cell model was created by (Jiang, Yang, Jiao & Du, 2018). Sensitivity analysis was used to choose the model's unknown parameters in a way that wouldn't compromise the model's dependability and validity. It was determined as a consequence that the parameters influence both model stability and cell performance and that the impacts of varying operating circumstances should be included in the validation study. A 1D and dynamic PEMFC model that is more suited for real-time applications was developed by (Lazar, Konradt & Rottengruber, 2019). To make the created model acceptable for usage in complex systems like real-time analysis, quick parameter studies, and comprehensive car models, authors lowered the computing load with simpler equations obtained. (Shan, Choe & Choi, 2007) created a 2D stack model and detailed the dynamic behavior of a stack with two neighboring cells and end plate assemblies. To examine the initialization behaviors and stack performance, simulations were conducted. The authors were able to determine the parameters impacting the source terms of the current density and the dynamic oxygen concentration distribution, as well as the dynamic temperature distribution of the fuel cell stack both in the plane direction and

along the channel. To analyze the heterogeneities, present on a cell's surface and to study the impact of operating conditions, (Robin et al., 2015) created a PEM fuel cell 2D and 1D model together. The fuel cell's activity is observed using the model developed by seeing how it interacts with the environment. Analyses of a GDL construct's effect on regional circumstances were also conducted. The PEM fuel cell's 3D and multiphase CFD model is frequently used to improve the cell's thermal and water management (Zhang & Jiao, 2018). To examine the impact of the PEMFC assembly stage on the mechanical condition of the active layer (MEA), (Carral & Mele, 2014) built a 3D model. By utilizing the developed 3D model, (Carral & Mele, 2014) conducted experimental investigations to examine the impact of several characteristics, including the number of cells and their placement within the stack, on the mechanical state of the active layer (MEA) during the PEMFC assembly stage. Consequently, the study revealed that optimal uniformity of MEA compression could be achieved by utilizing a higher number of cells and positioning them at the center of the stack. (Chen et al., 2021) have created a 3D polyphase PEMFC model with a wave flow channel to create the best flow field structure to improve the output performance of the fuel cell. Consequently, upon comparison of the wave flow channel with the straight channel, the superiority of the former in terms of reactant gas transport and removal of accumulated water in the microporous layer was established.

Among these models, semi-empirical 0-D models are generally advantageous to assess the performance of a specific FC under different operating conditions in a simple and fast manner. These 0-D models could be then integrated into system-level models easily and effectively.

3.1.3 Literature Review on Metaheuristic Algorithm for Parameter Extraction of PEMFCs

Optimization techniques are mostly classified as exact, heuristic, and metaheuristic methods (Talbi, 2009). Exact methods offer the advantage of guaranteeing a correct and exhaustive solution to the problem at hand. Nevertheless, the high computational load that these methods typically impose renders them impractical for real-life cases

in general. On the other hand, heuristics and metaheuristics do not guarantee the best solution but provide an acceptable and relatively fast solution. Therefore, heuristics and metaheuristics are the most common approaches to solving complex real-world optimization issues. Heuristic methods are specific to a particular problem. Thus, it yields satisfactory results in a reasonable runtime. However, on the other hand, the heuristic methods are problem-specific and cannot guarantee the optimal solution. Therefore, solutions are needed that can be applied to a specific range of problem groups, and metaheuristic methods have gained importance at this point. The “meta” as a prefix describes the MHAs as higher-level heuristics (Dokeroglu, Sevinc, Kucukyilmaz & Cosar, 2019) which are not problem-dependent solutions.

Figure 3.3 shows the number of papers published on several MHAs used for PEMFC parameter extraction. The selection criteria for these papers are as follows: articles in English published on or after 2018 and published in a journal listed in the Science Citation Index Expanded (SCI-Expanded) as of June 2022. Considering these results as well as algorithms with less run-time and parameter adjustment are chosen. Hence, DE, SSA, MFA, WOA, SCA, CS, GA, GWO, and JAYA optimization algorithms were run according to a predetermined objective function in the scope of this thesis.

Semi-empirical models give the coefficients used in the model by converging their output data to the FC’s experimentally acquired polarization curve, thus providing more reliable findings in determining the FC characteristic. There are various studies on this kind of model for PEMFCs. For example, Amphlett et al. (1995) created a semi-empirical mathematical model of a Ballard Mark IV solid PEMFC using Stefan Maxwell, Nernst, Tafel, Nernst-Planck, and Ohm's Law equations. The unknown parameters in the model were calculated using linear regression and experimental results. This study has pioneered many other studies in the same field.

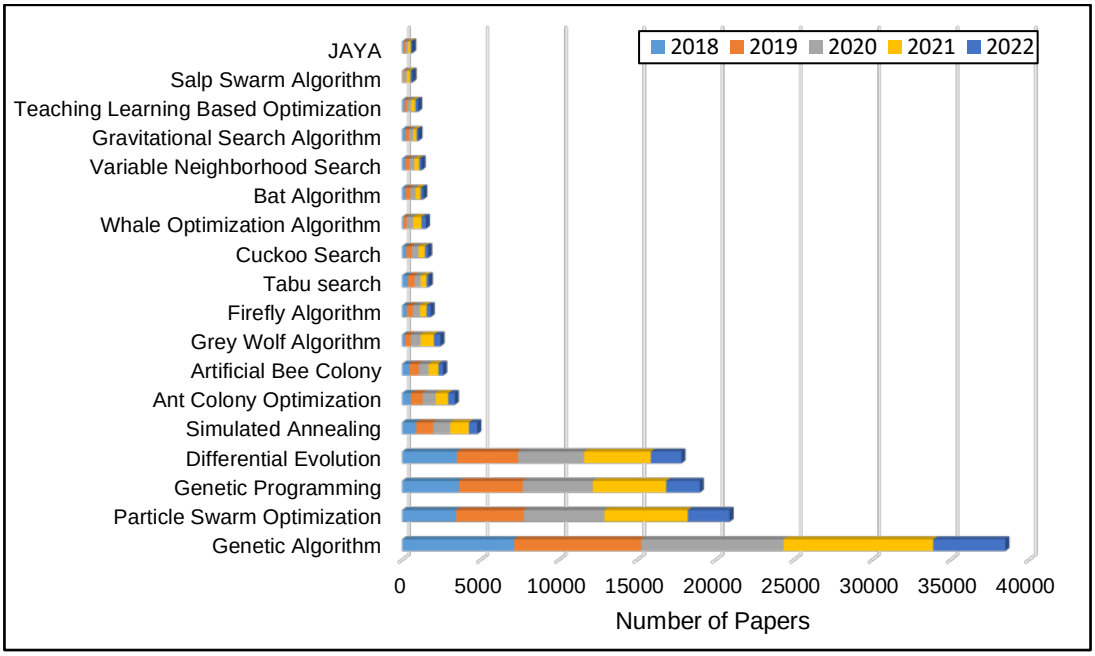

Figure 3.3 The number of related papers on the Web of Science for MHAs used in PEMFC parameter extraction

Mann et al. (2000) tested the performance of Ballard Mark IV and Mark V FCs at various membrane thicknesses, water contents, and different flow rates of oxygen using Amphlett et al. (1995)'s model with empirical formulas to find the unknown parameters of the model. In some studies, to optimize these parameters, metaheuristic algorithms (MHAs) were used to solve these non-linear equations.

Mo, Zhu, Wei & Cao (2006a) optimized the parameters required for the model by utilizing four data sets (two for identification and two for validation) with a niche Hybrid Genetic Algorithm (HGA). The authors utilized the difference between the measured and the calculated voltage values with the Sum of Squared Error (SSE) as the objective function. The work of Mo et al. (2006a) led various studies in the literature to implement new MHAs to validate the PEMFC model (e.g. (Ali, El-Hameed & Farahat, 2017; Turgut & Coban, 2016; Yang, Chellali, Lu, Li & Bo, 2016; Priya, Babu, Balasubramanian, Kumar & Rajasekar, 2015; Sun, Wang, Bi & Srinivasan, 2015)).

MHAs could be classified into four main categories: swarm-based, nature-based, physics-based, and evolutionary-based. All these categories have been studied in the literature to identify the best values for the FC model's unknown parameters, and researchers compared their findings with those of other studies in the literature.

Among these categories, swarm-based MHAs are the most diverse and extensively covered in the literature to extract the optimized PEMFC values. There are numerous studies to extract PEMFC parameters in the literature. Recent studies are discussed in detail. Xu, Wang & Wang (2019) proposed a simple two-stage eagle technique based on the JAYA algorithm and the Nelder-Mead simplex algorithm to effectively estimate the parameters required in the FC model, and the results obtained from this algorithm were compared with Gray Wolf Optimizer (GWO), Grasshopper Optimization Algorithm (GOA), Salp Swarm Algorithm (SSA), and Multi-Verse Optimizer (MVO). Chen & Wang (2019) adopted the adaptive strategy of step size to improve the search capability and proposed the Cuckoo Search with the Explosion Operator (CS-EO) Algorithm using the explosion operator to avoid stagnation in the local optimum. The authors compared the CS-EO with CS, Particle Swarm Optimization (PSO), Gravitational Search Algorithm (GSA), and Adaptive Cuckoo Search (A-CS). Cao, Li, Zhang, Jermsittiparsert & Razmjooy (2019) proposed a new Seagull Optimization Algorithm (SOA) that integrated the Lévy flight mechanism to give faster convergence rates and compared it with the different algorithms in the literature. Danoune, Djafour, Wang & Gougui (2021) created the Whale Optimization Algorithm (WOA) to improve the semi-empirical model and define the optimal parameter for different PEMFCs. The WOA was compared with various algorithms including the Genetic Algorithm (GA), PSO, and Artificial Bee Colony (ABC) Optimization. To experimentally validate the model, Heliocentris FC 50 was used together with the data of BCS 500 W and Ballard V. The accuracy of performance under different operating conditions was investigated. Ren & Eslami (2022) presented a new metaheuristic-based technique to extract the optimum unknown PEMFC parameters. To provide a more accurate and fast result, WOA was developed using the Fractional Order-Based (FO) design. The proposed algorithm utilizes SSE as the fitness function. FO-WOA was compared using six benchmark functions with the original WOA, World Cup Optimization (WCO)

algorithm, Elephant Herding Optimization (EHO), and Lion Optimization Algorithm (LOA). Validation of the proposed model was carried out using two well-known commercial FCs, which are Nexa PEMFC and 250 W PEM. Authors claimed that the best SSE values are obtained with a reasonable trade-off from convergence time by FO-WOA. Ashraf, Abdellatif, Elkholy & El-Fergany (2022b) utilized a newly developed swarm-based MHA called Hone Badger Optimizer (HBO). Three well-known PEMFCs (Mark V FC, SR-12, and 250 W) were selected to evaluate the performance of the HBO algorithm at diverse temperatures and supply pressures in steady-state circumstances. The Sum of Quadratic Errors (SQEs) was utilized as the fitness function to compare other well-known optimization algorithms. Tona-Swarm Optimizer (TSO) and Equilibrium Slime Mould Optimizer (ESMO), along with HBO, were also run by the authors and compared. The results of other algorithms used for comparison were obtained from literature. Various statistical comparisons and sensitivity analyses were done, and it was found that HBO is capable of handling the parameter extraction tasks effectively compared to others. Singh, Nijhawan, Singla, Gupta & Singh (2022) proposed a new hybrid algorithm to estimate the optimal PEMFC parameters. PSO and Dingo Optimizer (DOX) were combined to provide a robust algorithm. The proposed hybrid algorithm was tested with selected 10 benchmark test functions which are both uni-modal and multi-modal. Concerning convergence, stability, and efficiency, PSO, DOX, GWO, GWO-CS, and PSO-GWO hybrid algorithms were compared. The specifications of Ballard Mark V PEMFC were selected to extract the parameters. Friedman ranking test was also conducted, and hybrid PSO-DOX was found to perform better in terms of efficiency, accuracy, precision, computational time, and stability. Rezk, Wilberforce, Taha, Alahmadi & Olabi (2022) conducted a two-staged study that consists of modeling and optimization parts. An Adaptive Network-Based Fuzzy Inference System (ANFIS) was used to develop the PEMFC model with experimental datasets. The study aimed to find the optimum output power point which is tightly dependent on the fuel pressure, oxidant pressure, fuel flow rate, and oxidant flow rate. GWO was utilized to find the optimum power point by twenty-two datasets gathered from the experimental setup. Fifteen of these datasets were used for training and others for testing phases. Root Mean Square Error (RMSE) was used for evaluating the modeling accuracy. Integration of the

ANFIS model and GWO algorithm provided increased power output of up to %56. Bald Eagle Search (BES) is another robust newly developed MHA. Another study by Rezk, Olabi, Ferahtia, & Sayed (2022) applied this algorithm to estimate the unknown model parameters of two commercial PEMFCs (NedStack PS6 and BCS 500 W). The algorithm was compared with other algorithms using statistical validation methods, namely Analysis of Variance (ANOVA) and Tukey Honestly Significant Difference (HSD), in terms of accuracy, convergence rate, and robustness. SSE was used as the fitness function and the best, worst, mean, median, and standard deviation metrics were utilized to carry out statistical results. The authors revealed that the BES algorithm gives the best performance values among the compared algorithms.

Another algorithm category that stands out among various MHA-based optimization techniques is the evolutionary-based algorithms, which have been used for many years. There are several studies on these algorithms in the literature. Zhang & Wang (2013) used an adaptive RNA-GA algorithm inspired by the biological RNA mechanism and proposed an adaptive genetic strategy based on the coefficient of variation to preserve population diversity and avoid premature convergence. A multi-strategy Adaptive Differential Evolution (DE) developed for parameter optimization problems was presented by Gong & Cai (2014), briefly named rank-MADE. This algorithm was compared with the variants of the DE algorithm, Self-Adaptive DE (SaDE), JADE, Called Composite DE (CoDE), and DE with Differential Evolution with Global and Local Neighbourhoods (DEGL) algorithms. To improve the adaptive and dynamic performance of the DE algorithm, Sun et al. (2015) developed the Hybrid Adaptive DE (HADE) algorithm by utilizing the biological genetic strategy and compared the HADE algorithm with standard GA, PSO, DE, and adaptive DE. As a result, the authors showed that the HADE algorithm gives better results. Priya et al. (2015) created a new objective function with a zero derivative of power according to the current at the highest power point, which solved with a simple GA to determine the necessary parameters in the FC model. Kandidayeni, Macias, Khalatbarisoltani, Boulon & Kelouwani (2019) made parameter optimization for three different commercial FCs. The authors used the Shuffled Frog-Leaping Algorithm (SFLA), Firefly Optimization Algorithm (FOA), and Imperialist Competitive Algorithm (ICA)

for parameter optimization and compared their results with algorithms used in other studies in the literature.

Other types of MHA categories, physic-based and nature-based algorithms, are less commonly used compared to swarm-based and evolutionary-based algorithms. As an example of physic-based algorithms, Fathy, Elaziz & Alharbi (2020) presented a tried-and-tested new hybrid optimization approach, which includes a Vortex Search Algorithm (VSA) and DE. The authors used a new algorithm created for the optimization of 3 commercial FCs and compared the results with simple VSA and DE. Rezk et al. (2022) proposed a new methodology for Gradient-Based Optimizer (GBO) to find the optimal parameters for the semi-empirical FC model. The authors compared different algorithms from the literature for three different commercial FCs as 250 W FC stack, NedStack PS6, and SR-12 500 W. As an example of nature-based algorithms, Priya & Rajasekar (2019) applied a newly developed nature-based flower pollination algorithm that has the ability of high convergence speed, easy implementation, exceptional capacity to find the global optimum point, and less reliance on the initial solution. In the study, the authors made a comprehensive comparison in terms of SSE, individual absolute error, relative error values, and model parameter values and claimed Flower Pollination Algorithm (FPA) outperforms the GWO algorithm and all other methods in error analysis with the fewest number of iterations and curve fitting. Kandidayeni et al. (2019) used three different MHAs as mentioned above and one of them is the firefly optimization algorithm. Two different PEMFCs (NedStack PS6 and BCS 500 W) were used to compare the evaluated algorithms with the literature. Subsequently, 500-W Horizon PEMFC was utilized to verify the models. The study showed that FOA yields reasonable results with an insignificant difference compared to SFLA. Messaoud, Midouni & Hajji (2021) evaluated the Modified Moth-Flame Algorithm (M-MFA) with three frequently used PEMFCs - 250 W, NedStack PS6, and BCS 500W – in the literature. The authors applied the two SSE and RMSE as objective functions and integrated the uncertainty to analyze the performance of the algorithm. In the investigation, the effect of the number of unknown parameters on the results was also investigated. Comparison with other algorithms was conducted by gathering data from literature. It was claimed that

the estimated results by the proposed algorithm for the 250 W PEMFC with eleven unknowns exactly match the measured data.

The literature review indicates that researchers have substantially coded one or two novice algorithms as hybrid or non-hybrid in their studies. Then, the results have been compared with other studies found in literature. In addition, the parameter determination of certain commercial FCs (e.g., Ballard Mark V, BCS 500 W, NedStack PS6, SR-12, and Temasek) has been studied frequently. However, according to the authors' knowledge, there has been no parameter extraction study on the H-1000XP commercial FC, which has been commonly used in the Shell Eco-Marathon and Efficiency Challenge Hydromobil competitions.

3.2 Mathematical Modeling

3.2.1 0D Semi-empirical Electrochemistry Model of PEMFC Stack

The output voltage of the FC stack can be obtained in Equation 3.4:

$$V_{fc}=(V_{Nernst}-V_{act}-V_{ohmic}-V_{con}) \cdot N_{cell} \tag{3.4}$$

where V_{Nernst} is the reversible cell voltage known as Nernst voltage, V_{act} represents the activation polarization that is caused by the slowness of the reactions at the electrode surface, V_{ohmic} represents the ohmic polarization that is the resistance which implies all electrical and ionic conduction losses through the electrolyte, catalyst layers, cell interconnects, and contacts, V_{con} represents the concentration polarization that is associated with the concentration difference between the fuel/air channel and the chemical species on the electrode surface, and N_{cell} is the number of cells (Alpaslan et al., 2021). The Nernst voltage can be calculated with Equation 3.5 (Mo et al., 2006a; Amphlett et al., 1995).

$$V_{Nernst}=1.229-0.8\cdot 10^{-3}(T_{stack}-298.15)+4.3085\cdot 10^{-5}T_{stack}\cdot\left[ln\left(p_{H_2}\right)+0.5\cdot ln\left(p_{O_2}\right)\right] \quad (3.5)$$

where T_{stack} is the stack temperature (K), p_{H_2} is the partial pressure of the hydrogen (bar), and p_{O_2} is the partial pressure of the oxygen (bar). The partial pressure of the hydrogen can be obtained with Equation 3.6.

$$p_{H_2}=0.5\cdot RH_a\cdot P_{H_2O}^{sat}\left[\left(exp\left(\frac{1.635\left(\frac{I_{fc}}{A_{cell}}\right)}{T_{stack}^{1.334}}\right)\cdot\frac{RH_a\cdot P_{H_2O}^{sat}}{P_a}\right)^{-1}-1\right] \quad (3.6)$$

If the pure oxygen is fed to the cathode side of the FC, the partial pressure of oxygen at the cathode can be calculated using Equation 3.7.

$$p_{O_2}=P_c-\left(RH_c\cdot P_{H_2O}^{sat}\right)\cdot\left[\left(exp\left(\frac{4.192\left(\frac{I_{fc}}{A_{cell}}\right)}{T_{stack}^{1.334}}\right)\cdot\frac{\left(RH_c\cdot P_{H_2O}^{sat}\right)}{P_c}\right)^{-1}-1\right] \quad (3.7)$$

If the air is used instead of pure oxygen, the partial pressure of oxygen at the cathode can be calculated using Equation 3.8.

$$p_{O_2}=P_c-\left(RH_c\cdot P_{H_2O}^{sat}\right)-\frac{0.79}{0.21}\cdot p_{O_2}\cdot exp\left(\frac{0.291\left(\frac{I_{fc}}{A_{cell}}\right)}{T_{stack}^{0.832}}\right) \quad (3.8)$$

where RH_a and RH_c are relative humidity of vapors in the anode and cathode, respectively. I_{fc} is the FC operating current (A), A_{cell} is the active cell area (cm^2), P_a is the anode pressure (bar), and P_c is the cathode pressure (bar). $P_{H_2O}^{sat}$ is the saturation pressure of the water vapor (bar) and can be calculated as a function of the stack temperature using Equation 3.9 (Mo et al. 2006; Amphlett et al. 1995).

$$log_{10}(P_{H_2O}^{sat}) = 2.95 \cdot 10^{-2} \cdot (T_{stack} - 273.15) - 9.18 \cdot 10^{-5} (T_{stack} - 273.15)^2 + 1.44 \cdot 10^{-7} \cdot (T_{stack} - 273.15)^3 - 2.18 \quad (3.9)$$

The activation polarization can be calculated depending on the stack temperature and oxygen concentration with Equation 3.10,

$$V_{act} = -[\xi_1 + \xi_2 \cdot T_{stack} + \xi_3 \cdot T_{stack} \ln(C_{O_2}) + \xi_4 \cdot T_{stack} \cdot \ln(I_{FC})] \quad (3.10)$$

where ξ_k $(k = 1,2,3,4)$ are the semi-empirical coefficients based on theoretical equations with kinetic, thermodynamic, and electrochemical foundations (Mo et al. 2006), and C_{O_2} is the oxygen concentration (mol·cm^{-3}) that can be calculated using Equation 3.11 (Mann et al., 2000).

$$C_{O_2} = \left(\frac{p_{O_2}}{5.08}\right) \cdot 10^6 \exp\left(-\frac{498}{T_{stack}}\right) \quad (3.11)$$

The ohmic polarization depends on the membrane resistance (Ω), R_m, and contact resistance (Ω), R_C, as shown in Equation 3.12.

$$V_{ohmic} = I_{FC} \cdot (R_m + R_C) \quad (3.12)$$

The membrane resistance depends on the resistivity of the membrane (Ω.cm), ρ_m, membrane thickness (cm), l, and effective membrane area (cm^2), which is shown in Equation 3.13.

$$R_m = \frac{\rho_m \cdot l}{A_{cell}} \quad (3.13)$$

The membrane resistivity (ρ_m) can be calculated with Equation 3.14 for Nafion membranes.

$$\rho_m = \frac{181.6\left[1+0.03\cdot\left(\frac{I_{fc}}{A_{cell}}\right)+0.062\cdot\left(\frac{T_{stack}}{303}\right)^2\cdot(J)^{2.5}\right]}{\left[\lambda-0.643-3\left(\frac{I_{fc}}{A_{cell}}\right)\right]\cdot exp\left(4.18\cdot\left(\frac{T_{stack}-303}{T_{stack}}\right)\right)} \quad (3.14)$$

where λ is an adjustable parameter related to the membrane and its preparation process (Mo et al., 2006). The concentration polarization can be calculated using Equation 3.15.

$$V_{con} = -\beta\cdot ln\left(1-\frac{J}{J_{max}}\right) \quad (3.15)$$

where β is the parametric coefficient (V) that depends on the cell and its operation state (Mo et al. 2006), J is the actual current density (A·cm^{-2}), and J_{max} is the maximum current density (A·cm^{-2}).

3.2.2 Metaheuristic Optimization Algorithms for PEMFC Stack Parameter Extraction

3.2.2.1 Fitness Function Definition and Parameter Settings for MHAs

In this thesis, the model parameters were optimized using different MHAs to converge the results of the PEMFC model to the results obtained from the literature or manufacturer data to enhance the model. The output voltage was calculated at the points corresponding to each current value using the mathematical equations explained in Section 2.1. As a result, the suggested fitness function serves as a metric for the estimated parameters' quality. The SSE, given in Equation 3.16 was selected as the fitness function.

$$SSE = Min\left(\sum_{i=1}^{N}[V_{meas}(i) - V_{calc}(i)]^2\right) \quad (3.16)$$

where N is the amount of measured data points, i stands for the iteration counter, V_{meas} is the measured voltage of the FC, and V_{calc} denotes the calculated voltage of the FC. Several MADM methods with different principles were also described in Section 2.4. These methods were used to decide the best-performed MHAs for the H-1000XP case study. The MAE and the objective function efficiency were calculated with Equation 3.17 and Equation 3.18, respectively. The coefficient of determination (R^2), which is a well-known performance measurement metric, was used to evaluate the strength of the relation in regression using Equation 3.19.

$$MAE = \frac{\sum_{i=1}^{N} |V_{meas}(i) - V_{calc}(i)|}{N} \tag{3.17}$$

$$\eta = \frac{OF_{min}}{\overline{OF}} \times 100 \tag{3.18}$$

$$R^2 = \frac{\sum_{i=1}^{n} (V_{calc}(i) - \bar{V}(i))^2}{\sum_{i=1}^{n} \left(V_{meas}(i) - V_{calc}(i)\right)^2} \tag{3.19}$$

where OF_{min} is the lowest cost of the objective function, $\overline{OF}$ is the average value of 100 computed objective functions that can be calculated as $\overline{OF} = \sum_{i=1}^{100} OF_i/100$. $\bar{V}$ is the mean of the data. The parameter setting of the algorithms is given in Table 3.1. Maximum iterations were set to one thousand for each algorithm.

Table 3.1 Parameter setting of the algorithms

Algorithm	***Parameters***		
DE	*Number of Genes*	*Mutation Rate*	*Crossover Rate*
	30	0.85	0.2
CS	*Population size*	*α*	*β*
	30	0.01	1.5
SCA	*Population size*	*Linear Component*	
	30	2	
IWOA, WOA	*Population size*	*p*	
	30	0.5	
MFA	*Population size*	*b*	
	30	1	
GWO, IGWO, Jaya, SSA	*Population size*		
	30		

3.2.2.2 Genetic Algorithm (GA)

The genetic algorithm (GA) is one of the first and most well-regarded evolutionary algorithms in literature. GA is based on one of the most fundamental theories in the field of biology called the theory of evolution and was invented by Holland (1992) in the nineteen seventies. The main objective of all organisms is to be a survivor and Charles Darwin's theory claims that natural selection provides the survival of the fittest offspring in a competitive environment, and this is the basis of the GA. Natural selection refers to changes in an organism's genotype (crossover or mutation) that improve its chances of surviving in future generations. Those genetic variants that boost an organism's chances of survival are retained and passed down from generation to generation. Therefore, the genes of better-fitting organisms are passed down to future generations. Therefore, the future generation can also benefit from positive changes in the genotype (selection concept of GA by crossover, mutation, and elitism concepts). The interaction of organisms with one another in the form of cooperation or competition provides the foundation for the fulfillment of these changes. Because of its unique features, each creature has its concept of what constitutes a beneficial transformation, fit, or good, as the challenges encountered in daily life have their constraints and solution sets (fitness or objective function concept and constraints concept of GA). However, it is generally agreed that modifications that create a competitive edge on resources are beneficial (minimization or maximization concept GA). GA seeks the best solution by replicating all these principles within the framework of the restrictions and objective function established to solve our difficulties in practically every field.

3.2.2.3 Differential Evolution (DE)

Differential evolution (DE) presented by Storn & Price (1997), is a type of evolutionary algorithm that is used in searching for continuous optimization problems. In terms of robustness, ease of application, and quickness, it has remarkable advantages over other evolutionary methods and swarm-based techniques. The steps of the DE are mutation, crossover, and selection. While executing these stages, each

possible solution is evaluated by comparison with a target set. To reach the target, the mutation is utilized, and between the potential solution and gathered target a crossover is ensured. For instance, in Equation 3.20, S_a is a possible solution and, S_{aT} is the target vector for S_a from S_b, S_c, S_d (Karci, 2017; Storn & Price, 1997).

$$S_{aT} = S_b + f(S_c - S_d), \quad f \in [0,2] \tag{3.20}$$

Here, f is the scaling vector that supervises the amplification of alterations. The crossover is provided by the operator depicted in Equation 3.21, S_{aT}, and S_a are used in the operator.

$$S_{aU,i} = \begin{cases} S_{aT,i} & if\ rand \leq Cr \\ S_{a,i} & else \end{cases} \quad Cr \in [0,1] \tag{3.21}$$

where the rate of crossover is denoted as Cr. The selection process is executed using the operator in Equation 3.22.

$$S_{a,next} = \begin{cases} S_{aU} & if\ f(S_{aU}) \leq f(S_a) \\ S_a & else \end{cases} \tag{3.22}$$

3.2.2.4 Salp Swarm Algorithm (SSA)

The salp swarm algorithm (SSA) is one of the novice methods among swarm-based algorithms that mimic the behaviors of salps living in the ocean. SSA, demonstrated by (Mirjalili et al., 2017), has provided enhancements for some applications. SSA is a fast, comprehensive, and easy algorithm that can be applied to both single-objective and multi-objective optimization problems (Faris, Mirjalili, Aljarah, Mafarja & Heidari, 2020). The population of salps is split into two categories as followers and leaders. The leader is located at the beginning of the remaining salps, which are the followers. The salp position is stored in a matrix (x) with a dimension of the number of variables (n). The target of the swarm is the food source denoted as F. Equation 3.23 is executed to update the leader's location (Mirjalili et al., 2017).

$$x^1{}_j = \begin{cases} F_j + c_1 \cdot \left(c_2 \cdot \left(ub_j - lb_j\right) + lb_j\right) & c_3 \geq 0 \\ F_j - c_1 \cdot \left(c_2 \cdot \left(ub_j - lb_j\right) + lb_j\right) & c_3 < 0 \end{cases} \quad c_1 = 2e^{-\left(\frac{4I}{L}\right)^2} \tag{3.23}$$

Here $x^1{}_j$ is the location of the leader, F_j is the food source's location, lb_j and ub_j are the lower and upper bounds in the jth extent, respectively. The c numbers are defined randomly. The leader chooses the position regarding the food and c_1 is a crucial parameter for this operation. L is the maximum iteration number, and I is the present iteration. The followers' positions ($x^i{}_j$) are renovated rearranging Newton's law of motion presented in Equation 3.24 (Mirjalili et al., 2017).

$$x^i{}_j = \frac{1}{2}\left(x^i{}_j + x^{i-1}{}_j\right) \tag{3.24}$$

3.2.2.5 Moth-Flame Algorithm (MFA)

Moth-flame optimizer (MFA) mimics the pathfinding methods of moths named transverse orientation. Moths can travel among large areas using a straight path by retaining the fixed angle regarding the moon that provides effective navigation at night. In addition, artificial light sources such as flame allure the moths immensely. The algorithm is a recent method among the swarm optimization algorithms and was presented by Mirjalili (2015a). Initially, moths disperse indiscriminately, and a matrix denotes M stores their locations. The columns of N indicate the number of variables (d) the rows depict the number of moths (n). The fitness values of M are assessed and saved in an array (OM) for all moths ,(Nadimi-Shahraki, Fatahi, Zamani, Mirjalili & Abualigah 2021). Equation 3.25 illustrates the matrix M and the array OM.

$$\mathrm{M} = \begin{bmatrix} m_{1,1} & m_{1,2} & \dots & m_{1,d} \\ m_{2,1} & m_{2,2} & \dots & m_{2,d} \\ \vdots & \vdots & \vdots & \vdots \\ m_{n,1} & m_{n,2} & \dots & m_{n,d} \end{bmatrix} \quad OM = \begin{bmatrix} OM_1 \\ OM_2 \\ \vdots \\ OM_n \end{bmatrix} \tag{3.25}$$

A similar procedure is executed for flames tracked by moths. The positions of flames are saved in a similar matrix F and their fitness values are stored in an array

OF. At the beginning of the algorithm, the OF array is commenced by depending ascending order of the OM array. In the following iterations, the algorithm will update the F according to the best agent. Equation 3.26 indicates a logarithmic spiral determined for the algorithm. The positions of each moth (M_i) and flames (F_j) are updated using the spiral formula (S (M_i, F_j)).

$$S(M_i,F_j)=D_i \cdot e^{bt} \cdot cos(2\pi t)+F_j \quad (3.26)$$

where the distance between ith moth and jth flame is denoted as D_i, t defines the required closeness between moth and flame (t=1 is the farthest and t=-1 is the closest), and b is a random constant that varies between -1 and 1, which determines the shape of the spiral. D_i is found using Equation 3.27 (Nadimi-Shahraki et al. 2021; Mirjalili 2015).

$$D_i = \left|F_j - M_i\right| \quad (3.27)$$

3.2.2.6 Whale Optimization Algorithm (WOA)

Whale optimization algorithm (WOA) is also a novice swarm-inspired MHA presented by Mirjalili & Lewis (2016). WOA is inspired by hunting strategies named bubble-net feeding behavior of humpback whales. The whales usually hunt small fishes close to the surface of the water by forming bubbles to approach their prey. This provides to keep the small fishes together and to come near their prey without being noticed. The main parts of the algorithm are encircling prey, bubble-net attacking, and searching for prey (Celik & Karadeniz, 2020; Mirjalili & Lewis, 2016). Initially, the whales identify their prey and surround them. The position of the best agent is assumed to be the best candidate and other agents update their position according to the best. This strategy is modeled using Equations 3.28-3.29) (Lee & Zhuo, 2021; Mirjalili & Lewis, 2016):

$$\vec{D} = \left|\vec{C} \cdot \vec{X}^{*} - \vec{X}(t)\right| \quad (3.28)$$

$$\vec{X}(t+1) = \left|\vec{X}^{*}(t) - \vec{A} \cdot \vec{D}\right| \tag{3.29}$$

where t is the iteration number, $\vec{X}$ is the position vector, $\vec{X}^{*}$ represents the position vector of the ideal solution achieved so far, calculation of coefficient vectors denoted as $\vec{A}$ and $\vec{C}$ is depicted in Equations 3.30-3.31:

$$\vec{A} = 2 \cdot \vec{a} \cdot \vec{r} - \vec{a} \tag{3.30}$$

$$\vec{C} = 2 \cdot \vec{r} \tag{3.31}$$

where $\vec{r}$ is a vector formed randomly between 0 and 1, $\vec{a}$ is lowered linearly from 2 to 0. After the location of the prey is designated, using shrinking encircling or spiral updating position methods the bubble-net strategy can be simulated. The first method can be modeled utilizing the decrease of $\vec{a}$ value. This decrease provides the variation limits of $\vec{A}$ vector. The latter behavior is presented in Equations 3.32-3.33:

$$\vec{X}(t+1) = \vec{D}' \cdot e^{bl} \cdot \cos(2\pi l) + \vec{X}^{*}(t) \tag{3.32}$$

$$\vec{D}' = \left|\vec{X}^{*}(t) - \vec{X}(t)\right| \tag{3.33}$$

where $\vec{D}'$ is the margin of the whale to the prey, b is the shape constant of the logarithmic spiral, and l is a random number that varies between -1 and 1. In the WOA, the whales come to their prey with a linear (shrinking encircling) or spiral movement. The possibility of each movement is 50% and the movement is determined in Equation 3.34:

$$\vec{X}(t+1) = \begin{cases} \vec{X}^{*}(t) - \vec{A} \cdot \vec{D} & \text{if } p < 0.5 \\ \vec{D}' \cdot e^{bl} \cdot \cos(2\pi l) + \vec{X}^{*}(t) & \text{if } p \geq 0.5 \end{cases} \tag{3.34}$$

where p is a random scalar between 0 and 1. The whales explore their prey randomly regarding the location of each other. $\vec{A}$ can be used to model this behavior, if $\vec{A}$ is

greater than 1 or less than -1, the agent is compelled to move away from the reference agent. This strategy is modeled with Equations 3.35-3.36:

$$\vec{D} = \left|\vec{C} \cdot \vec{X}_{rand} - \vec{X}\right| \tag{3.35}$$

$$\vec{X}(t+1) = \left|\vec{X}_{rand} - \vec{A} \cdot \vec{D}\right| \tag{3.36}$$

3.2.2.7 Sine Cosine Algorithm (SCA)

Sine cosine algorithm (SCA) is based on behaviors of mathematical sine and cosine functions. It is a population-based algorithm and was introduced by Mirjalili (2016). SCA initializes different initial solution sets randomly and makes them glide through to the best solution by utilizing sine and cosine functions. It is a responsive and simple algorithm that can be easily implemented to tackle several optimization issues including feature selection, parameter estimation, and scheduling (Abualigah & Diabat, 2021). The algorithm starts with the optimization phase of random solution sets iteratively. Then the solution sets are updated for exploration and exploitation stages using Equations 3.37-3.38. In the former stage, random solutions are formed to find the possible best regions of the search space. The latter phase decreases the randomness and variations, which are less compared to the first stage (Abualigah & Diabat, 2021; Mirjalili, 2016).

$$X_i^{t+1} = X_i^t + r_1 \cdot sin(r_2) \cdot |r_3 P_i^t - X_i^t| \tag{3.37}$$

$$X_i^{t+1} = X_i^t + r_1 \cdot cos(r_2) \cdot |r_3 P_i^t - X_i^t| \tag{3.38}$$

where X_i^t represents the location of the current solution and P_i^t is the target position in the iteration t, dimension i, and r_1, r_2, r_3 typifies random numbers. The usage condition of these equations is specified with the random number r_4. If the r_4 is smaller than 0.5, Equation 3.37, else Equation 3.38 is used to update the position.

3.2.2.8 Cuckoo Search Algorithm (CS)

Based on the combination of cuckoo breading strategies and Levy Flight mechanism of the birds, the Cuckoo Search (CS) Algorithm is a swarm-inspired global optimization algorithm that mimics the searching nest and reproduction strategies. The algorithm is introduced by Yang & Deb (2009) and to define the algorithm, three idealized rules were determined (Bindu & Reddy, 2013):

- One egg is spawned by each cuckoo, and the egg is dropped into a random nest.
- The highest quality nests will be inherited by the following generations.
- Available nests are considered constant and the probability of discovery by a cuckoo P_a is between 0 and 1.

The algorithm is initialized by generating possible solutions, and it continues with determining the optimal decision. Candidate solutions were formed using Equation 3.39 based on the given three rules (Zhang, Yu, Luo & Zhang, 2020).

$$X_i^{t+1} = X_i^t + a \oplus L(\beta) \tag{3.39}$$

where X is the position vector, t is the iteration number, and I is the number of bird nests. The step-size factor a controls the random search limits and it is greater than 0. The point-to-point multiplication is referred to as $\oplus$, and $L(\beta)$ is the optimization route determined randomly. The required distance that the cuckoo searches are defined by the Levy flight step size ($a \oplus L(\beta)$). The relation of Levy flight route and t is named as Levy probably distribution indicated in Equations 3.40-3.41 (Zhang et al. 2020).

$$X_i^{t+1} = X_i^t + a \oplus L(\beta) \tag{3.40}$$

$$L(\beta) \sim u = t^{\beta},\ (1 < \beta \leq 3) \tag{3.41}$$

3.2.2.9 JAYA

Rao (2019) created the algorithm "JAYA", which means "victory", in 2016 in Sanskrit. It is a modern population-based MHA that combines the advantages of evolutionary and Swarm Intelligence algorithms. While evolutionary algorithms provide an advantage in finding the best result around a local search space, Swarm Intelligence algorithms are better at locating the global optima for the entire search space. JAYA algorithm combines these two specifications and has several benefits over other population-based algorithms, including being simple to use, adaptable, with the least tuning requirement, and flexible. The JAYA algorithm can handle constrained or unconstrained problems within the scope of single or multi-objective (Zitar, Al-Betar, Awadallah, Doush & Assaleh, 2022). The algorithm depends on the difference between the candidate solution with the best and the worst candidates multiply with random numbers between zero and one for every iteration. The formula of the JAYA algorithm is given in Equation 3.42.

$$X'_{j,k,i}=X_{j,k,i}+r_{1,j,i}\cdot\left(X_{j,best,i}-\left|X_{j,k,i}\right|\right)-r_{2,j,i}\cdot\left(X_{j,worst,i}-\left|X_{j,k,i}\right|\right) \quad (3.42)$$

where $X_{j,k,i}$ is the current solution, $X'_{j,k,i}$ is the newly updated solution, and $r_{1,j,i}$ and $r_{2,j,i}$ are two random numbers generated uniformly for each iteration to balance the exploitation and exploration processes. $X_{j,best,i}$ and $X_{j,worst,i}$ are the best and the worst solution for the variable j at i_{th} iteration. The distances between the current-best and current-worst candidates indicate higher exploitation for closer ranges and higher exploration for higher ranges. If $X'_{j,k,i}$ provides a superior solution, $X_{j,k,i}$ is dropped in favor of $X'_{j,k,i}$. Every accepted solution serves as the input for the following iteration.

3.2.2.10 Grey Wolf Optimizer (GWO)

The grey wolf optimizer (GWO) was presented in 2014 by (Mirjalili, Mirjalili & Lewis 2014). The algorithm is inspired by the leadership structure and social hunting system of grey wolves. The GWO utilizes the alpha, beta, delta, and omega wolves to

find the optimal solution to the issue. The three steps of the hunting technique include tracking, encircling, and attacking prey. The hunting (optimization) is guided by α, β, and δ wolves in the GWO algorithm, and in each step of the hunt, have always those three best solutions and update it whenever a better solution is discovered. The mathematical model of the algorithm for encircling prey and attacking modeled between Equation 3.43 to Equation 3.44 as follows:

$$\vec{D}= \left|\vec{C} \cdot \vec{X}_p(t)-\vec{X}_p(t)\right| \tag{3.43}$$

$$\vec{X}(t+1)=\vec{X}_p(t)-\vec{A} \cdot \vec{D} \tag{3.44}$$

where $\vec{A}$ and $\vec{C}$ are coefficient vectors, $\vec{D}$ is the distance vector, t indicates the current iteration, $\vec{X}_p$ is the position vector of the prey, and $\vec{X}$ is the position vector of a grey wolf. $\vec{A}$ and $\vec{C}$ are computed in Equations 3.45-3.46:

$$\vec{A}=2\vec{a} \cdot \vec{r}_1-\vec{a} \tag{3.45}$$

$$\vec{C}=2 \cdot \vec{r}_2 \tag{3.46}$$

where $\vec{r}_1$ and $\vec{r}_2$ are random vectors between zero to one and components of $\vec{a}$ are linearly decreasing from two to zero to reduce the randomness and the magnitude of the movement proportional to the iteration number. At the beginning of the mathematical model, the best three solutions are assumed as α, β, and δ grey wolves. Other wolves update their location favorably to these wolves, as calculated in Equations 3.47-3.49 are derived in this regard (Mirjalili et al., 2014):

$$\vec{D}_\alpha= \left|\vec{C}_1 \cdot \vec{X}_\alpha-\vec{X}\right|, \vec{D}_\beta= \left|\vec{C}_2 \cdot \vec{X}_\beta-\vec{X}\right|, \vec{D}_\delta= \left|\vec{C}_3 \cdot \vec{X}_\delta-\vec{X}\right| \tag{3.47}$$

$$\vec{X}_1=\vec{X}_\alpha-\vec{A}_1 \cdot (\vec{D}_\alpha), \vec{X}_2=\vec{X}_\beta-\vec{A}_1 \cdot (\vec{D}_\beta), \vec{X}_3=\vec{X}_\delta-\vec{A}_3 \cdot (\vec{D}_\delta) \tag{3.48}$$

$$\vec{X}(t+1)=\frac{\vec{X}_1+\vec{X}_2+\vec{X}_3}{3} \tag{3.49}$$

where the subscripts as α, β, and δ indicate the wolves. Equation 45 analysis reveals that $\vec{A}$ lies between -2$\vec{a}$ and 2$\vec{a}$. Attacking the prey is provided by decreasing the $\vec{a}$ value from two to zero. Thus, the exploitation part of the algorithm is achieved successfully. To carry out the exploration (search) part of the algorithm random $|\vec{A}|$ values are selected higher than one to allow the divergence of wolves to search for prey.

3.2.3 Multi-attribute Decision-Making Methods (MADM)

MADMs are used to order the algorithms and the most optimal single-objective metaheuristic optimization techniques are determined for the FC parameter extraction problem. Technique for Order of Preference by Similarity to Ideal Solution (TOPSIS), Multi-Objective Optimization on the Basis of Ratio Analysis (MOORA), and Preference Ranking Organization Method for Enrichment of Evaluations (PROMETHEE) are the decided methods for the ranking process due to their wide usage and reliability. In addition, the ranking alterations of three methods that use different principles are aimed to be demonstrated and discussed. The SSE and runtime are considered non-beneficial, and objective function efficiency is taken as the beneficial criteria. The equal-weighting method, which is one of the objective weighing techniques, is utilized to appoint the weights of criteria. Since it is an initial benchmarking study conducted to determine the optimal algorithms for further applications of the stated PEMFC parameter optimization process, this weighting method is decided.

3.2.3.1 Technique for Order of Preference by Similarity to Ideal Solution

TOPSIS is a frequently utilized MADM that can be applied to problems consisting of many criteria and alternatives and is easy to use. TOPSIS was developed by Hwang

and Yoon in 1980 (Yuksel & Koseoglu, 2022; Tzeng & Huang, 2011). The first step of the TOPSIS method is to normalize the decision matrix (n_{ij}) with vector normalization in Equation 3.50.

$$n_{ij}=\frac{x_{ij}}{\sqrt{\sum_{i=1}^{m} x_{ij}^2}},\ i=1,\ldots,m\ ;=1,\ldots,n \tag{3.50}$$

The weighted normalized decision matrix (r_{ij}) is then calculated and the positive ideal (PIS) and negative ideal solutions (NIS) are determined using Equations 3.51-3.53.

$$r_{ij}=w_j \cdot n_{ij},\ i=1,\ldots,m\ ;j=1,\ldots,n \tag{3.51}$$

$$PIS=\{r_1^+,\ldots,r_j^+,\ldots,r_n^+\}\ where\ v_j^+=\begin{cases} max(r_{ij}/i=1,\ldots,m) & if\quad j\in B \\ max(r_{ij}/i=1,\ldots,m) & if\quad j\in C \end{cases} \tag{3.52}$$

$$NIS=\{r_1^-,\ldots,r_j^-,\ldots,r_n^-\}\ where\ v_j^-=\begin{cases} max(r_{ij}|i=1,\ldots,m) & if\quad j\in B \\ max(r_{ij}|i=1,\ldots,m) & if\quad j\in C \end{cases} \tag{3.53}$$

Finally, the distance of each alternative (S_i^+ and S_i^-) is determined with Equations 3.54-3.55 and the closeness coefficients (CC_i) of each alternative are calculated with Equtaion 3.56. The highest CC_i value gives the best result (Çelikbilek & Tüysüz, 2020; de Farais Aires & Ferreira 2019).

$$S_i^+=\sqrt{\sum_{i=1}^{m}\left(r_{ij}-r_j^+\right)^2},i=1,\ldots,m \tag{3.54}$$

$$S_i^-=\sqrt{\sum_{j=1}^{m}\left(r_{ij}-r_j^-\right)^2},i=1,\ldots,m \tag{3.55}$$

$$CC_i=\frac{S_i^-}{S_i^+ + S_i^-} \tag{3.56}$$

3.2.3.2 Multi-Objective Optimization on the Basis of Ratio Analysis

MOORA is a weighted normalization method that is frequently used and proposed by Brauers & Zavadskas (2006). This method considers all possible alternatives and criteria. It offers straightforward implementation, quick computation, less mathematical burden, and excellent reliability. The ratio, reference point, full multiplicative, and important factors are four different types of MOORA (Yuksel & Koseoglu, 2022; Kundakci, 2016).

Ratio and reference point formats were used in this study. Each criterion is assumed to have an equal weight by the MOORA-Ratio (Yuksel & Koseoglu, 2022; Kundakci, 2016; Brauers & Zavadskas, 2006). Creating a decision matrix is the first stage in the MOORA-Ratio process. After that, the decision matrix is normalized in Equation 3.57.

$$x_{ij}^{*} = \frac{x_{ij}}{\sqrt{\sum_{j=1}^{n} x_{ij}^{2}}} \tag{3.57}$$

Weighted normalized decision matrix (v_{ij}) with the multiplication of weights (w_j) is used to find the normalized matrix with Equation 3.58.

$$v_{ij} = x_{ij}^{*} \cdot w_j \tag{3.58}$$

The performance of decision choices is calculated with Equation 3.59 and preference values (y_i^{*}) are obtained. Finally, the y_i^{*} values are sorted in descending order.

$$y_i^{*} = \sum_{j=1}^{g} v_{ij} - \sum_{j=g+1}^{n} v_{ij} \tag{3.59}$$

3.2.3.3 Preference Ranking Organization Method for Enrichment of Evaluations

The PROMETHEE I (partial ranking) and PROMETHEE II (full ranking) were invented by J.P. Brans and first presented in 1982 by Nadeau and Landry at a conference held in Québec, Canada (Brans & De Smet, 2016). To ensure detailed analysis, PROMETHEE allows obtaining both partial and certain priorities. Firstly, to create the dataset, the decision points, evaluation factors, and weights should be determined by the decision-maker. After that, the decision-maker should choose a selection function to indicate the evaluation factors and illustrate the internal interactions. The preference function must be the standard evaluation criterion employed in the study if the decision-maker lacks an evaluation criterion (Yuksel & Koseoglu, 2022; Brans & De Smet, 2016; Şenkayas & Hekimoğlu, 2013). It is necessary to ensure pairwise comparisons between each evaluation factor and each decision point. Equation 3.60 may be used to display the common preference function when A and B exhibit two distinct decision points.

$$P_{(A,B)} = \begin{cases} 0 & f(A) \leq f(B) \\ p[f(A)-f(B)] & f(A) > f(B) \end{cases} \tag{3.60}$$

Equation 3.60 can be used to calculate the preference indices using typical preference functions in Equation 3.61.

$$\pi(A,B) = \sum_{i=1}^{k} (w_i \cdot P_i \cdot (A,B)) \tag{3.61}$$

In the next, positive (φ^+) and negative (φ^-) superlative degrees are obtained using Equation 3.62 and Equation 3.63.

$$\varphi^+ = \frac{1}{n-1} \sum \pi(A,x) \tag{3.62}$$

$$\varphi^{-} = \frac{1}{n-1}\sum \pi(x,A) \tag{3.63}$$

where x shows the decision points except for A. PROMETHEE I is used to determine a partial ranking. The method makes sure that positive and negative superlative degrees are compared pairwise to get the best choice point. Finally, PROMETHEE II can be used to precisely rank the choice points. Priority degrees can be calculated with Equation 3.64 and sorted in descending order. Consistent with this, if $(A) > \varphi(B)$, alternative A is superior (Yuksel & Koseoglu, 2022; Brans & De Smet, 2016; Şenkayas & Hekimoğlu, 2013; Behzadian, Kazemzadeh, Albadvi & Aghdasi, 2010).

$$\varphi(A) = \varphi^{+}(A) + \varphi^{-}(A) \tag{3.64}$$

3.3 Results and Discussion

In this section, results are presented and discussed through the sub-sections. In sub-section 3.3.1, validation of the semi-empirical mathematical model and the results of the various algorithms used were examined comparatively. Sub-section 3.3.2 provides the performance evaluation and comparison of various metaheuristic optimization algorithms on the described fitness function.

3.3.1 PEMFC Model Validation Results

The basic parameters of the 250 W FC (Mo et al., 2006) are used for the validation of the E-CGA, and those of the H-1000XP is used for the comparison of the different algorithms. The main parameters of these fuel cells are shown in Table 3.2.

Table 3.2 The main parameters of the PEMFCs

Parameters	***250 W***	***H-1000XP***
Number of cells, N_{cell}	24	50
Active cell area, A_{cell} (cm^2)	27	77
Maximum current density, J_{max} , $(A{\cdot}cm^{-2})$	0.86	0.56
Membrane thickness, l (μm)	127	125
Rated power (W)	250	1000
Inlet anode pressure, P_a (atm)	1 – 3	0.56
Inlet cathode pressure, P_c (atm)	1 – 5	1
Stack temperature, T (K)	343.15 – 353.15	328
Relative humidity in the anode, RH_a*(-)*	1	1
Relative humidity in the cathode, RH_c*(-)*	1	1

The study of Mo et al. (2006) was used as the reference for the validation of the semi-empirical mathematical model. In their study, a niche genetic algorithm was used to calculate the unknown modeling parameters. In this thesis, E-CGA was used to compare the results of this algorithm-based model with the study of Mo et al. (2006). Four data sets (two for validation and two for identification) were used. In the reference study (Mo et al., 2006), Range 2 was used for parameter estimation, as shown in Table 3.3. Range 1 was used in this study to better understand algorithm convergence since it has a greater range than range 2 (Xu et al., 2019). In the reference study (Mo et al., 2006), the SSE value for four data sets was calculated as 16.6081. In this thesis, the SSE value was calculated as 13.467.

Table 3.3 Ranges taken for the parameters' estimation (Xu et al. 2019)

		ξ_1	ξ_2	ξ_3	ξ_4	β	R_c (V)	λ
Range 1	*Min*	-1.19969	1e-3	3.6e-5	-2.6e-4	0.0136	1e-4	10
	Max	-0.8532	5e-3	9.8e-5	-9.54e-5	0.5	8e-4	24
Range 2	*Min*	-0.952	1e-3	7.4e-5	-1.98e-4	0.016	1e-4	14
	Max	-0.944	5e-3	7.8e-5	-1.88e-5	0.5	8e-4	23

The comparison of the parameters is given in Table 3.4 and the comparison of the polarization curves between the reference study and this study is given in Figure 3.4. It can be seen from this figure that the results of the reference study and this study are well matched.

Table 3.4 Results of parameters for 250 W FC in Range 2

Algorithm	ξ_1	ξ_2	ξ_3	ξ_4	β	$R_c\ (V)$	λ	***SSE***
HGA	-0.944	3.01e-3	7.4e-5	-1.8e-4	0.02914	1e-4	23	16.6081
E-CGA	-0.949	3.07e-3	7.696e-5	-1.88e-4	0.0315	1.04e-4	22.99	13.4670

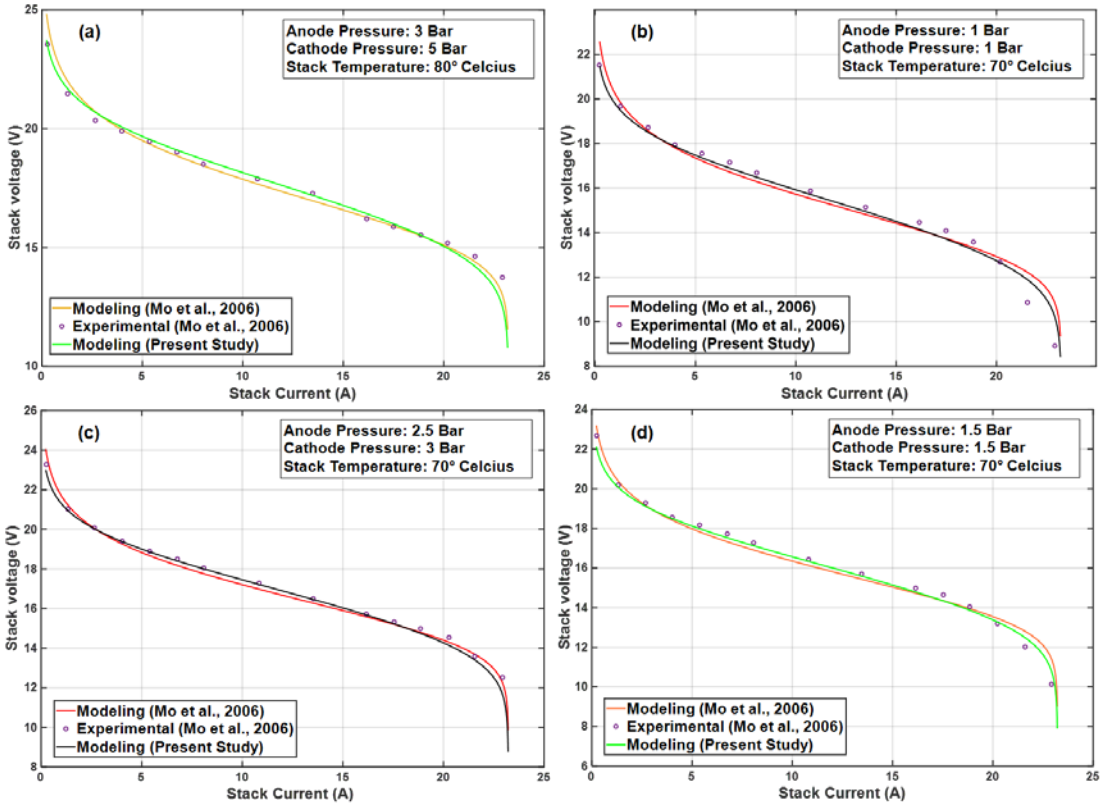

Figure 3.4 The comparison of the polarization curves of the 250 W PEMFC using the E-CGA as in this study and HGA as in the study of Mo et al. (2006): (a) and (b) for identification and (c) and (d) for validation

The polarization curve of the H-1000XP was obtained using the unknown model parameters given in Table 3.4 found by E-CGA. The polarization curve obtained using the E-CGA is compared with the manufacturer's datasheet, as shown in Figure 3.5 (Horizon Educational [HE], 2021). In conclusion, comparing the polarization curve obtained with the E-CGA with that from the manufacturer's datasheet, it is clear that these are very close, and the SSE value is low, as shown in Table 3.4 The high accuracy of the model proves the accuracy of the equation set used. In the rest of the study, this equation set was used to calculate the unknown model parameters by applying various MHAs to find the best suitable MHA.

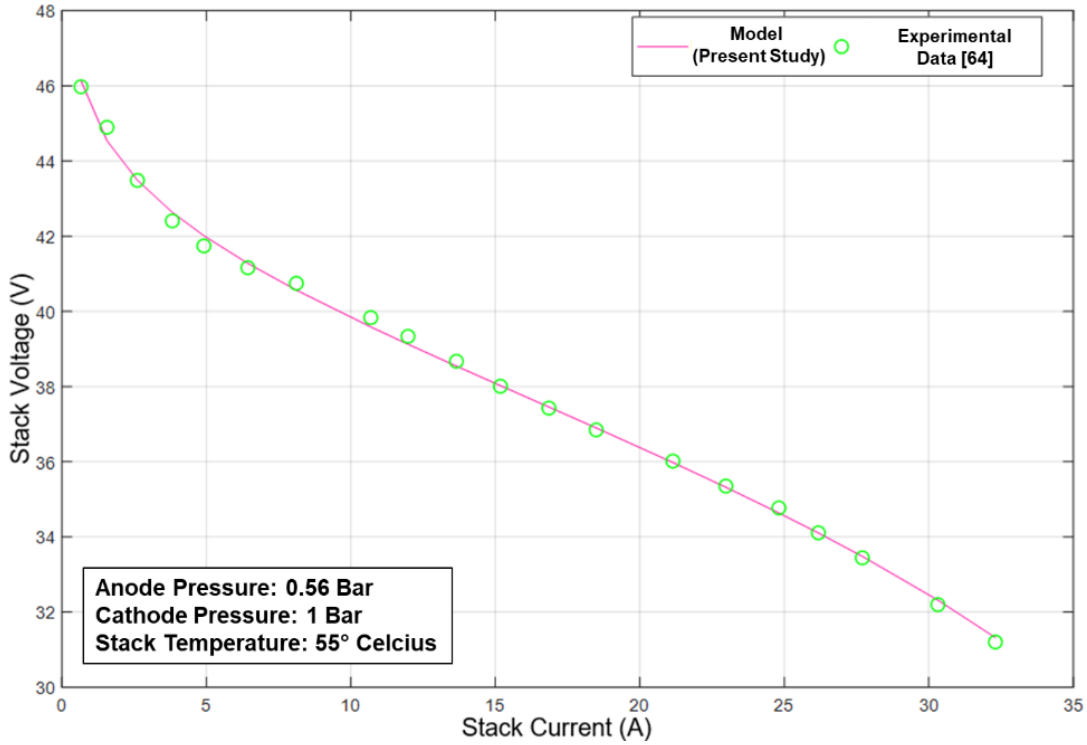

Figure 3.5 Polarization curve of H-1000XP (Experimental data were taken from (HE, 2021))

3.3.2 Metaheuristic Algorithms and MADM Methods Results

The selected 10 algorithms were run using Python 3.10, all on the same computer. The specifications of the computer are Intel(R) Core(TM) i5-9400 CPU @ 2.90GHz, 8GB Ram, and the operating system is Windows 10 (64 bits). The algorithms were assessed regarding different error measurement methods for ensuring a precise comparison of the performance and were ranked by TOPSIS, MOORA, and PROMETHEE according to SSE, run time, and objective function efficiency. This efficiency was considered beneficial, and the run-time and SSE were taken as non-beneficial criteria. Runtimes were selected as the overall duration of 100 runs for each algorithm. The weights of the criteria were calculated using one of the objective-weighing methods called equal weighting. The method relies on assigning equal weights to each criterion so that sum equals one. The rankings and performance of algorithms were compared and discussed. Table 3.5 specifies the performance metrics of each algorithm.

Table 3.5 Results of the statistical comparison

Algorithm	Runtime (S)	Best SSE	Worst SSE	Mean SSE	η	R^2	MAE
WOA	1316.7	0.4449	0.7681	0.5030	88.4558	0.9987	0.1097
IWOA	2946.3	0.4449	0.5140	0.4595	96.8143	0.9987	0.1097
GWO	1485.4	0.4456	0.5779	0.4749	93.8367	0.9987	0.1096
IGWO	2787.7	0.4450	0.4781	0.4513	98.6034	0.9987	0.1097
JAYA	1298.5	0.5599	118.1836	10.8045	5.1817	0.9983	0.1276
MFA	1054	0.4389	0.6368	0.4523	97.0298	0.9987	0.1141
SCA	1238.9	0.4916	1.6004	0.7358	66.8123	0.9985	0.1133
SSA	1298.8	0.4486	0.6448	0.5080	88.3112	0.9987	0.1098
DE	1067.7	0.4457	0.5035	0.4698	94.8669	0.9987	0.1101
CS	2354.1	0.7864	11.4660	3.5792	21.9723	0.9976	0.1538

Table 3.6 indicates the rank of each algorithm according to the specified MADMs (TOPSIS, MOORA, and PROMETHEE) methods considering decided weighting factors.

Table 3.6 The rank of each algorithm determined by selected MADM methods

ALGORİTHM	TOPSIS RANK	MOORA RANK	PROMETHEE RANK
WOA	5	4	3
IWOA	10	10	8
GWO	6	5	5
IGWO	9	7	7
JAYA	7	9	9
MFA	1	1	1
SCA	4	6	6
SSA	3	3	4
DE	2	2	2
CS	8	8	10

The results of MADM methods ranking with equal weights showed that MFA is ranked as the first, and DE is the second optimal algorithm for this problem regarding all three methods. MFA has the lowest runtime and SSE and the second-highest objective function efficiency among all. TOPSIS ranked GWO and IWOA as the last two algorithms due to their remarkably higher run times. The last two choices of MOORA were IWOA and JAYA. On the other hand, PROMETHEE pointed out JAYA and CS for the last two spots. Among the algorithms, GWO has the highest

objective function efficiency. Considering the MAE and R^2 values of the algorithms, GWO and IGWO offered the lowest error rates. In other words, MFA provided the lowest error on a total error basis, while GWO on a mean error basis ensured the lowest error for this problem. CS has the poorest SSE among the others and its run time is the third, and its objective function efficiency is the second worst. Because of these, it was ranked last by PROMETHEE and eighth by the other MADM methods. Although JAYA ensured a relatively fast solution, its objective function efficiency and consistency were inadequate for this problem. Table 3.7 depicts the parameters found by the best solution for each algorithm.

Table 3.7 The estimated parameters by the algorithms

Algorithm	ξ_1	ξ_2	ξ_3	ξ_4	λ	R_c (V)	β
MFA	-1.2516	0.0042	0.0001	0.0001	11.0198	-0.0014	0.0967
DE	-0.9689	0.0029	0.00004	-0.0001	24	0.0001	0.0979
SSA	-0.9638	0.0034	0.0001	-0.0001	21.4509	0.0001	0.0955
SCA	-0.8532	0.0025	0.0000	-0.0001	24	0.0004	0.0951
WOA	-0.8532	0.0031	0.0001	-0.0001	23.9949	0.0001	0.0982
IGWO	-1.0637	0.0031	0.0000	-0.0001	23.9330	0.0001	0.0983
JAYA	-1.1997	0.0034	0.0000	-0.0001	17.4219	0.0003	0.0888
CS	-1.1997	0.0038	0.0001	-0.0001	17.1406	0.0001	0.0870
GWO	-0.8734	0.0025	0.00004	-0.0001	23.9792	0.0001	0.0981
IWOA	-1.0731	0.0031	0.00004	0.0001	24	0.0001	0.0983

For comparison purposes, the top two positions by all three MADM methods (MFA, DE) and four algorithms ranked in the last two places by at least one of the methods (IWOA, GWO, JAYA, CS) are illustrated and discussed. Figure 3.6 illustrates the convergence of the polarization curves to the experimental data when employing the parameters obtained through the designated algorithms.

TOPSIS method with equally weighted criteria ranked the GWO and IWOA as the worst-performed algorithms since the run time of these algorithms was remarkably higher. However, for applications that do not require fast solutions, these algorithms can be preferable options. Especially, GWO was the most consistent algorithm in 100 runs, and its performance was the best according to MAE and R^2 metrics. GWO provided the same performance regarding MAE and R^2 metrics with a more acceptable

run time, however, its objective function efficiency was slightly lower than JAYA, while CS ensured the poorest error rates and objective function efficiency among the algorithms. Although JAYA provided an acceptable run time, the consistency and objective function efficiency of the algorithm was not admissible for this problem. The run time of the CS was the third worst, and it did not perform well regarding the objective function efficiency and error rates. PROMETHEE method ranked these algorithms as the poorest for this problem set.

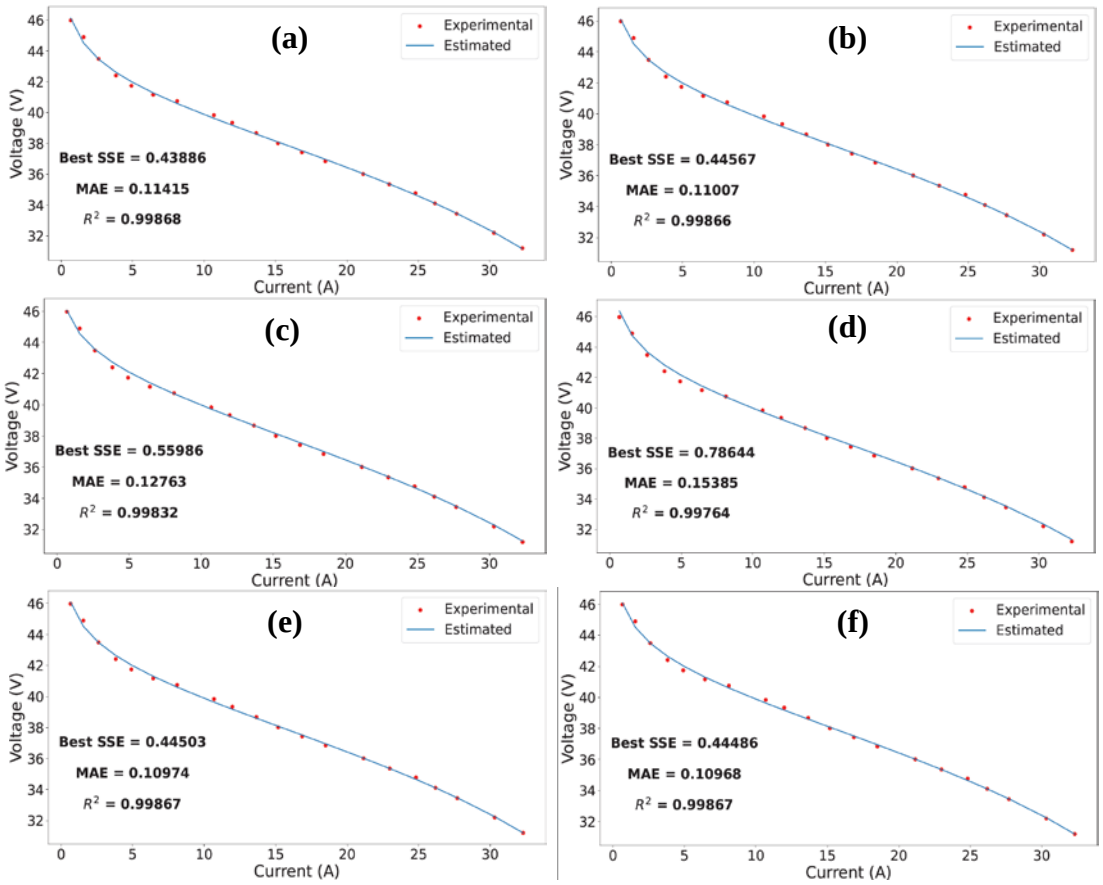

Figure 3.6 Polarization curves when estimated parameters of (a) MFA, (b) DE, (c) JAYA, (d) CS, (e) IWOA, (f) GWO were used (Experimental data were taken from (HE, 2021))

The consistency of the algorithms was determined numerically using the objective function efficiency metric. Figure 3.7. illustrates the convergence curves of each algorithm's best solutions. Figure 3.8. shows the distribution of the lowest error rates found by the algorithms in each run. Enlarged versions are also given in the figure to highlight where the values are close to zero.

Fig.7 shows that JAYA is the algorithm that reached the best SSE value with the lowest iteration number. However, the best SSE value of JAYA is higher than other algorithms. IWOA and MFA followed the JAYA by converging the global optimum solution time. Especially, IWOA found the ideal solution before the 100th iteration which indicates that its runtime can be lowered significantly with the adjustment of the number of iterations. In Fig. 3.8., the illustration of the objective function efficiency metric was ensured. GWO, MFA, and IWOA are the most consistent algorithms as can be seen in the figure.

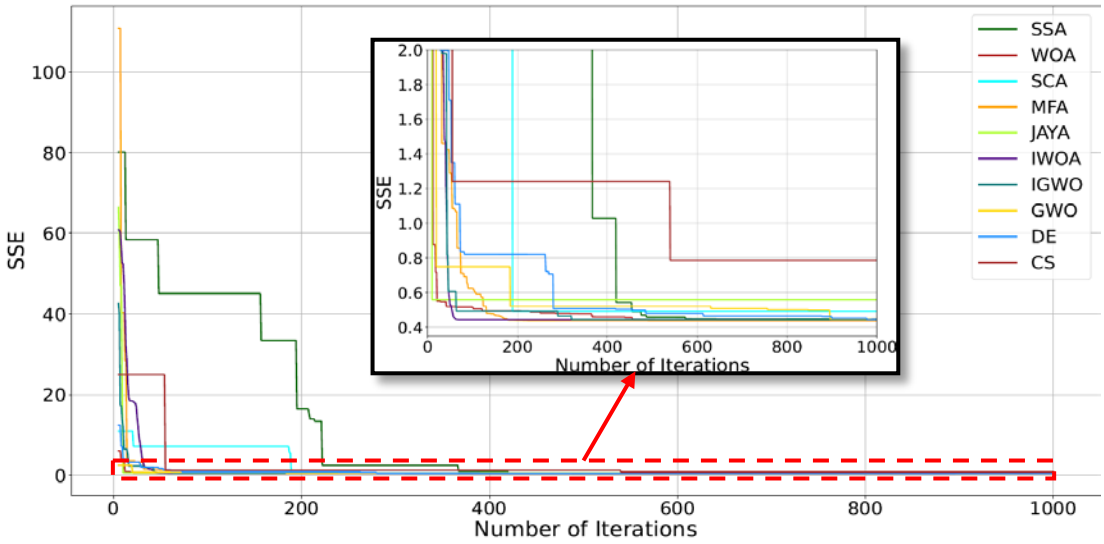

Figure 3.7 Convergence curves of each algorithm's best solutions

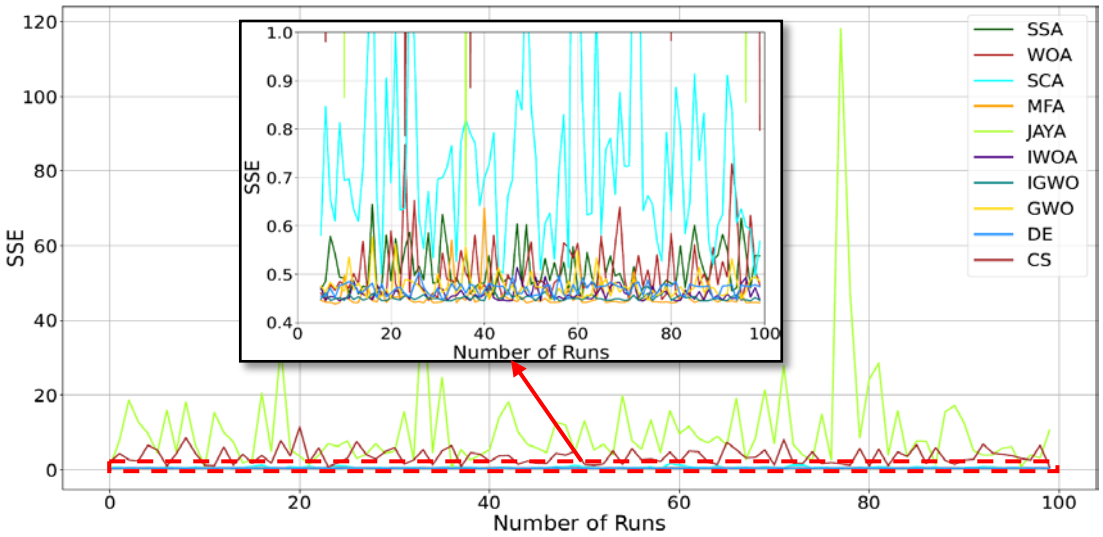

Figure 3.8 Distribution of the lowest error obtained by the algorithms in each run

The convergence performances of the algorithms were evaluated with the objective function efficiency metric. 1000 iterations and 100 runs were selected to benchmark the algorithms. However, it should be noted that algorithms with high efficiencies obtained the best results significantly earlier than 1000 iterations. Particularly, MFA and GWO ensured consistent and fast convergence which can be seen in Figure 3.9. and Figure 3.10. The number of iterations can be optimized, and lower run times can be achieved for these algorithms. This adjustment can make GWO preferable for this problem and boost the performance of MFA to even higher regarding the run time.

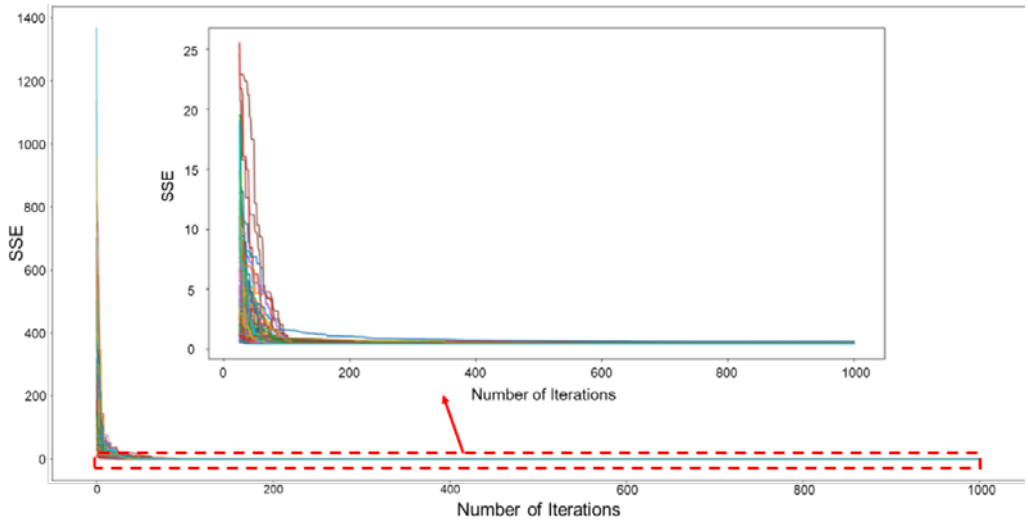

Figure 3.9 Convergence curve of MFA

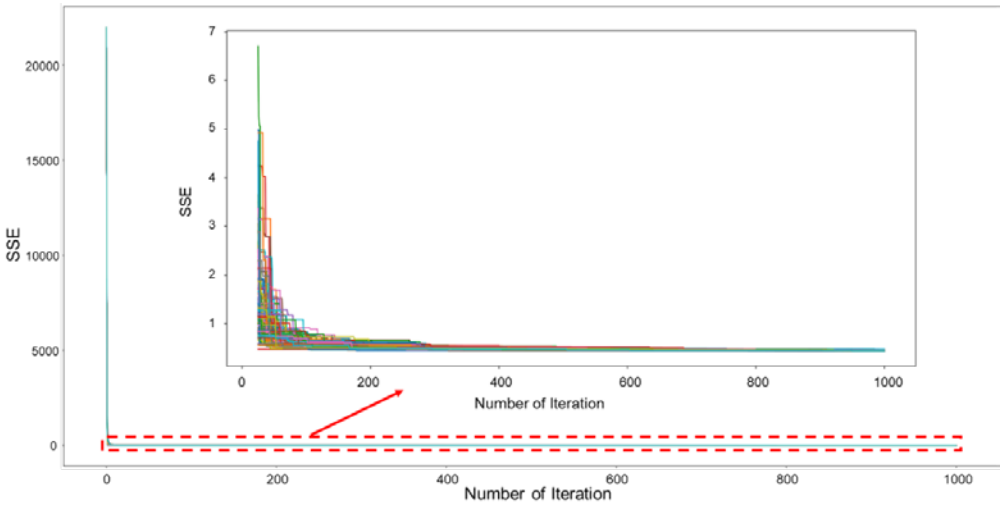

Figure 3.10 Convergence curve of GWO

Figure 3.9 indicates that MFA reached the optimum solution before the 200th iteration in the majority of runs. In Figure 3.10, the convergence is sharper for GWO which means, the optimum solution was approached at the beginning of the iterations. Before the 400th iteration, the algorithm commonly found the optimum result for the specific run. The algorithms having low efficiencies could not achieve low error rates even in the 1000th iteration in most of the runs. Figure 3.11 and Figure 3.12 demonstrate the convergence curves of CS and JAYA, respectively.

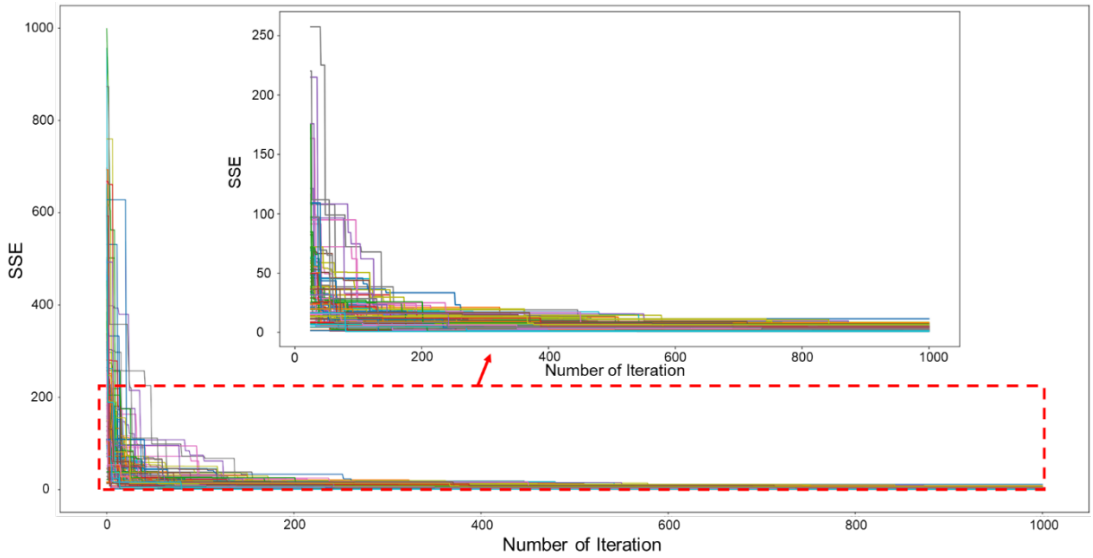

Figure 3.11 – Convergence curve of CS

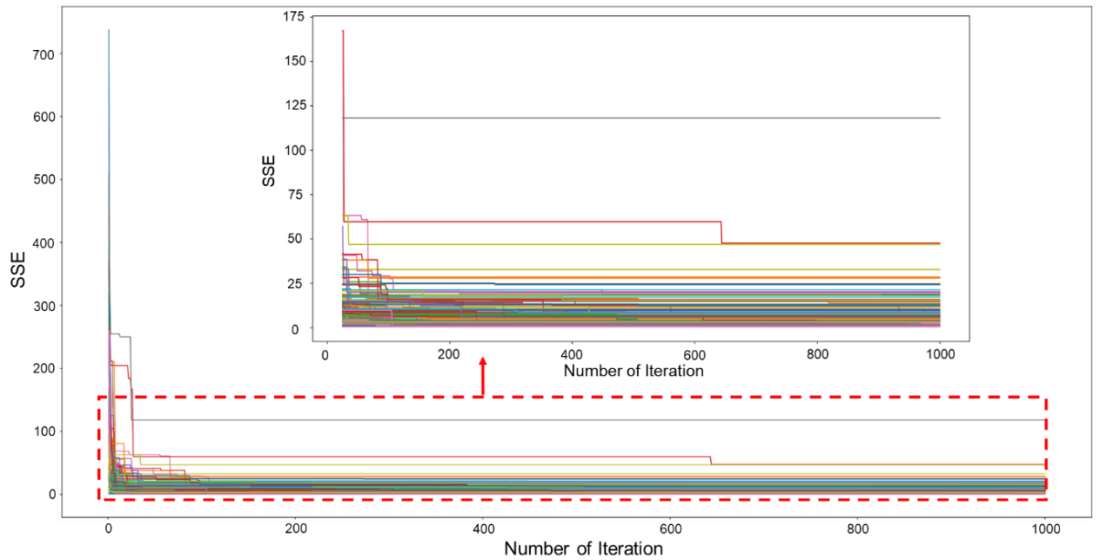

Figure 3.12 – Convergence curve of JAYA

CS detected the optimum solution slightly more efficiently than JAYA. However, at the end of the 100 runs, its error rate remained the highest. The algorithm becomes insufficient for the fields that require a low error rate. The convergence of JAYA seemed stacked in the local optima depicted in Figure 3.12. Even though the lowest SSE was found as 0.56, the mean SSE was absurdly high can be seen in Table 3.5. For applications where stability is a top priority, instability makes the algorithm unusable.

CHAPTER 4
ENVIRONMENTAL AND ECONOMIC ANALYSES OF FUEL CELL AND BATTERY-BASED HYBRID SYSTEMS UTILIZED AS AUXILIARY POWER UNITS ON A CHEMICAL TANKER VESSEL

This chapter investigates the environmental and economic impacts of implementing fuel cell and battery-based hybrid configurations. Phosphoric acid and molten carbonate fuel cell systems in the place of diesel generators of a large tanker to supply the vessel's total electricity demand. Environmental and economic analyses of the utilization of the specified fuel cell systems with $LiNiCoALO_2$ and $LiNiMnCoO_2$ chemical types of battery cells on a large marine vessel are provided in this thesis. In addition, the assessment of the most suitable battery cell and charge-discharge hours for fuel cell systems is carried out with a grid-search algorithm. Six different fuel cell and battery configurations are investigated to obtain the optimum system layout.

4.1 Literature Survey on Marine Transport Applications

The studies on fuel cell-based marine systems have increased nowadays. There are some EU projects and theoretical studies found in the literature that are discussed in detail through this sub-section both commercial vessels and demonstration projects.

The "Fuel Cell Technology for SHIPs" (FCSHIP) project, which ran from 2002 to 2004, had the main goals of evaluating safety concerns, assessing not only the economic but also the environmental aspects of FC usage, and assessing the potential of FC use for both main propulsion and auxiliary power units. During the project, various types of fuels and FCs (PEMFC, MCFC, and SOFC) were studied. As a consequence of the project, PEMs are chosen for small-medium power systems, while MCFC and SOFC systems are appropriate for high-power applications requiring high volumetric power density hydrocarbon-based fuels. The only method to minimize GHG emissions among these fuels is to utilize natural gas or green hydrogen (Coppola et al., 2020). Another project that utilizes LNG as fuel is the FELICITAS subproject II, which was completed between 2005 and 2008. 250 kW SOFC developed by Rolls-

Royce for stationary systems evaluated on sea conditions. Furthermore, the utilization of alternative hydrocarbon-based fuels that could be used instead of hydrogen and the waste heat recovery potential of SOFC were also investigated and proven tests held on board a mega yacht (Klingner, 2009). MultiSchiBZ project is the successor of the SchiBZ projects funded by the German Federal Ministry of Transport and Digital Infrastructure on the large cargo vessel MS Forester that has two phases development phase between 2018-2020, and a demonstration phase between 2020-2022. The main goal of the project is to develop a SOFC system that has more than 50% efficiency and is operated with low-sulfur diesel fuel or LNG as an energy source. Other goals of the project are to design a more realistic heat exchanger that includes the effects of temperature variance and heat transfer to optimize the reforming process of LNG (e4Ships, n.d.-a). Worthy to note that the “RiverCell2” (e4ships, n.d.-b) and “Pa-X-ell 2” (e4ships, n.d.-c) projects carried out between 2017-2021 facilitate HT-PEMFC with methanol as a primary energy source and LNG as optional.

The MC-WAP project (Centro Per Gli Studi Di Tecnica Navale [CETENA] 2011), which received funding from the EU, was conducted between 2005 and 2010 to design and develop onboard MCFCs with an output ranging from 100 kW to 500 kW as auxiliary power units (APUs) for RoPax, RoRo, and cruise vessels. The project encompassed several main objectives, including the development of an integrated MCFC system capable of meeting auxiliary loads of up to 500 kWe fueled by diesel oil, enhancing the safety, performance, and reliability of the balance of plant components, and reformer technology in the maritime environment. In selected typologies of vessels, the conventional diesel generators were partially or entirely replaced with the MCFCs. The project's principal outcomes included the identification of new rules for reforming procedures and marine applications of FCs, as well as the determination of the operating conditions of MCFC-APUs under vibrations, motions, and marine environment. As a case study, Micoli, Coppola & Turco (2021) selected a SOFC powered by LNG as an auxiliary power unit for a cruise ship. The authors investigated the assumption that a 20 MW SOFC system was installed on the ship and conducted a comparison using three generations of dual-fuel engines. The study revealed that significant reductions in SO_x, CO, NO_x, and PM pollutants could be

achieved while decreasing CO_2 emissions by 11%. Additionally, the authors calculated the placement of the SOFC system in terms of weight and volume according to the most recent international norms and proposed a system. Based on the calculations, it was determined that the SOFC system is both heavier and takes up more room. However, it was discovered that this circumstance had no significant impact on the ship's stability and buoyancy. The EU-funded project “NAUTILUS” began on July 1, 2020, intending to develop LNG-fueled SOFC-battery hybrid gensets that would gradually replace internal combustion engine-based generators for long-haul passenger ships. The generated energy is used to meet the ship's entire heating and power requirements (German Aerospace Center [DLR], n.d.). In the FellowSHIP project carried out between 2003 and 2011, a 320 kW MCFC, fed with LNG, was installed as an auxiliary power unit on an offshore-supply vessel named “Viking Lady” (Tronstad, Høgmoen, Haugom & Langfeldt, 2017). The main findings from the FellowSHIP project are slow response time of fuel cells could be compensated with batteries to provide improved safety, fuel savings, and a significant amount of emissions reduction. Other benefits are related to reductions in machinery maintenance costs, and noise and vibration reduction. The project also helped remove impediments to the commercialization of fuel cell and battery hybrid technology and alleviate safety concerns (Alnes, 2018).

Inal & Deniz (2020) assessed the fuel cell types for ships in their study based on multi-criteria decision analysis including PEMFC, MCFC, PAFC, and SOFC. The cost analysis of the fuel cell types showed that the PEMFC has the lowest installation cost, followed by PAFC and MCFC, respectively. However, the operational cost of PEMFC was found to be the highest due to the costs of pure hydrogen and storage equipment. The average cost ranking between PAFC and LNG-fueled MCFC was reported slightly in favor of PAFC due to its lower initial cost. Another study conducted by the same authors (Inal & Deniz, 2021) also revealed the usage of a 2.8 MW MCFC operating with LNG instead of a conventional diesel engine for a chemical tanker, utilizing 27 trip data of a chemical tanker for 10 months in 2018. Fuel transitions in ECAs are also considered in the computations to get more precise results. As a consequence, it is claimed that the emission values are calculated correctly and obtained a 99% decrease

in SO_x, PM, and NO_x emissions, and a 33% reduction in CO_2 emissions. Seyam, Dincer & Agelin-Chaab (2022) proposed a propulsion system design for ships utilizing a hybridized 4 MW SOFC system with organic Rankine cycle and gas Brayton cycle systems. The results showed that the utilization of sustainable fuels of LNG and hydrogen in the system would reduce carbon emissions by 80% and improve the energy efficiency of the propulsion system by 14%. Roh, Kim, Jeon & Yoon (2019) set up a test bench consisting of LNG-fueled MCFC, lead-acid battery, and D/G to consider fuel consumption and emission reduction compared to the standalone operation of a commercial diesel generator for selected five different types of vessels with various operation modes. A simple rule-based EMS is proposed according to the load and SoC of lead-acid batteries. As a result, the average CO_2 reduction potential is reported between 70% to 74%.

Tronstad et al. (2017) reviewed the use of fuel cells in marine applications. It has been seen that all mentioned fuel cell projects and applications have used PEM, SOFC, or MCFC, and none of them used PAFC (Tronstad et al., 2017). However, the only study that mentioned the usage of PAFC in a maritime application was carried out by (Winkler, 2009). The project was funded by United States Maritime Administration (MARAD) to meet auxiliary loads of a power barge with PAFCs. No other information about the project could be found in the literature. Bassam (2017) conducted a more in-depth analysis of the literature on fuel cell maritime applications, looking at 62 research published since 2000. PAFC was not utilized in these theoretical research and initiatives, according to the study. For researchers who want to examine the maritime applications of the fuel cell in more detail, some of the notable studies could be summarized (Sürer & Arat 2022; Dall'Armi et al., 2021; Xing, Stuart, Spence & Chen, 2021; Coppola et al., 2020; Markowski & Pielecha, 2019; Leites, 2016; Van Biert et al., 2016). However, when studies in the other fields are examined, current studies are encountered in which the use of PAFC as a stationary power unit is investigated as a thermo-economic (Wilailak et al., 2021), potential replacement with utilizing NG as fuel (Nam, Nam & Lee, 2021), and combined heat, power, and hydrogen generation systems (Park et al., 2021). Besides, a commercial PAFC-type fuel cell named

PureCell Model 400, produced by Doosan company, and sold commercially, can use hydrogen or LNG as fuel, used in commercial applications.

The studies in the literature show that the continued use of conventional internal combustion diesel engines as the main engine or auxiliary power unit is the biggest obstacle to reducing the emissions by seaborne trade to the targeted levels in 2050. There is only one study found in the literature related to environmental and economic analyses of fuel cell-battery hybrid system design that can fully meet the electricity demand of ocean-going tanker ships by considering different operation modes (Korkmaz et. al, 2023). Despite the commercial availability of PAFC products, their suitability for marine applications remains largely unexplored. The marine application of MCFC systems, on the other hand, has been limited to their use as main propulsion units on small vessels, and they have not yet been utilized to fulfill the entirety of the auxiliary power demand of large vessels. The literature survey shows that there have been no studies by the author that evaluate the most suitable battery brand and charge-discharge hours for PAFC and MCFC systems with a grid-search algorithm. One part of this thesis aimed to analyze and discuss the potential environmental and economic impacts of implementing various fuel cell/battery hybrid configurations instead of marine D/Gs to compensate for the auxiliary power demand of the vessel.

4.2 System Description

The ship electricity generation plant of an oceangoing tanker vessel was modeled using Python language. The plant consists of three equivalent marine diesel generators and can produce electricity up to 3.15 MW. The data gathered from ship trial tests of marine diesel generators were used to construct the mathematical model of the plant. Six different operation modes of the system and their electrical loads were obtained from electrical load tests also carried out during ship trail tests. Specifications of one generator in the simulated system and electrical loads of the operation modes are demonstrated in Table 4.1. The utilization hours of these modes were obtained from port calls and position history data collected from (Marine Traffic, 2021). Figure 4.1 illustrates the utilization hours of the operation modes between 06 December 2019/06

December 2021. The route of the ship involved oceangoing navigations mainly on the Europe-North America route. 67% of the utilization hours were spent during navigational operations, and the remaining were coastal operations. Yuksel & Koseoglu (2022) provided the mathematical background, validation, and operating principle for the conventional ship power distribution system model. The emissions of diesel fuels were calculated using emission factors published by Kuzu, Bilgili & Kiliç (2021).

Table 4.1 Specifications of the marine diesel generators and electrical load

Prime Mover		**Alternator**	
Engine/Generator MCR	960/900 kW	**Output Capacity**	1,312.5 kVA
Rpm	900	**Voltage**	450 V
Cylinder Bore/ Piston Stroke (mm)	210/320	**Frequency**	60 Hz
Swept Volume per Cylinder (dm^3)	11.1	**Poles**	8
Piston Mean Speed (m/s)	9.6	**Voltage Variation**	2.50%
Compression Ratio	17:1	**Voltage Adjust**	5%
Mean Effective Pressure (bar)	24.1	**Power Factor**	0.8 Lagging

Electrical Load		
Operational Mode	**Load (kW)**	**Current (A)**
On navigation	850.6	1,364.152
On navigation with tank heating	1,195.7	1,917.607
At berth	1,122	1,799.410
During cargo handling	1,781.5	2,857.085
During anchorage	571.3	916.224
During anchorage with tank heating	863	1,384.038

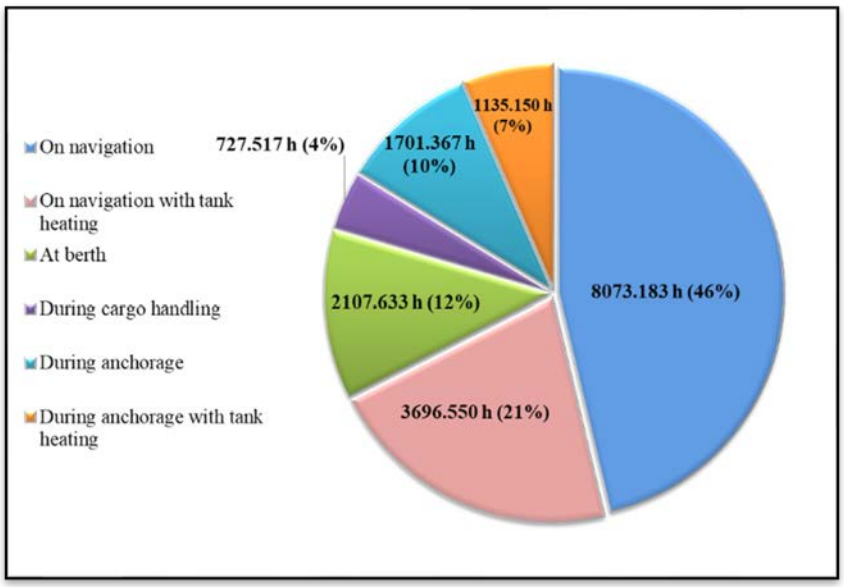

Figure 4.1 Utilization hours of the plant according to operation modes

The proposed system configurations involve the usage of commercial fuel cells supported by battery packs instead of marine diesel generators in the plant. The first fuel cell type used in the study is the PAFC which uses phosphoric acid electrolytes. The mean electrical efficiency of PAFCs varies between 40-50%, but the implementation of heat recovery systems could rise the efficiency up to 80% (Tronstad et al., 2017), and the operating temperature is 150-200 °C. Equation 4.1, Equation 4.2, and Equation 4.3 demonstrate the electrochemical reactions of PAFC (Lindorfer, Rosenfeld & Böhm, 2020). Catalog data of Doosan PureCell Model 400 (Doosan Fuel Cell America INC [DFCA], 2018), which is a PAFC, is used in the mathematical model. Table 4.2 indicates the technical specifications of the commercial PAFC.

$$Anode:\ H_2 \rightarrow 2H^+ + 2e^- \tag{4.1}$$

$$Cathode:\ \frac{1}{2}O_2 + 2H^+ + 2e^- \rightarrow H_2O \tag{4.2}$$

$$Total:\ O_2 + 2H_2 \rightarrow 2H_2O \tag{4.3}$$

Table 4.2 Technical specifications of the commercial PAFC (DFCA, 2018)

Fuel Cell Type	PAFC
Electric Power Output	440 kW
Electrical Efficiency	45%
Peak Overall Efficiency	90%
LNG Consumption	98.4 (m^3/h)
NO_x	0.009 (kg/MWh)
CO_2	454 (kg/MWh) without heat recovery
VOC	0.005 (kg/MWh)
CO	0.005 (kg/MWh)

The second type of fuel cell used in the proposed system layouts is the MCFC. The molten carbonate salts are used as electrolytes and these are heated up to 700 °C (Marefati & Mehrpooya, 2019). The high operating temperatures provide fuel-type flexibility to MCFCs. The electrical efficiency of an MCFC changes between 50-60%, but the total efficiency could be up to 85% with heat recovery systems. This type of fuel cell is considered suitable for higher energy applications. Equation 4.4, Equation

4.5, and Equation 4.6 depict the electrochemical reactions of MCFC (Tronstad et al., 2017). SureSource 1500 model of Fuelcell Energy company is selected as the MCFC type (Fuelcell Energy [FE], n.d.). Table 4.3 demonstrates the main specifications of the MCFC.

$$\begin{aligned} Anode:\ H_2 + CO_3^{-2} &\rightarrow O_2 + H_2O + 2e^- \\ CO + CO_3^{-2} &\rightarrow 2CO_2 + 2e^- \end{aligned} \tag{4.4}$$

$$Cathode:\ \frac{1}{2}O_2 + CO_2 + 2e^- \rightarrow CO_3^{-2} \tag{4.5}$$

$$Total:\ 2H_2 + O_2 \rightarrow 2H_2O \tag{4.6}$$

Table 4.3 Technical specifications of the commercial MCFC (Inal & Deniz, 2021; FE, n.d.)

Fuel Cell Type	**MCFC**
Electric Power Output	1400 kW
Electrical Efficiency	47% +- 2%
LNG Consumption	615.12 (m^3/h)
NO_x	0.0045 (kg/MWh)
CO_2	444.5 (kg/MWh) without heat recovery
PM	$9.07 \cdot 10^6$ (kg/MWh)
SO_x	0.000045 (kg/MWh)

Figure 4.2 illustrates the proposed electricity distribution system layout of the vessel. The conventional system consists of three equivalent marine diesel generators with 1.05 MW power output and one emergency generator. The CO_2 value given in Table 4.3 involves the required CO_2 loop for the startup process of the MCFC. In the study, marine diesel generators are replaced with fuel cells and battery packs to meet the electrical load of the ship. The emergency generator (E/G) is kept for safety concerns. As seen in Figure 4.2, the air is supplied with a blower to the cathode side of the fuel cell. The produced water in the system is pumped to the water tank and it is also used in the system for mixing with LNG. With the help of the mixer and heat exchanger, a water gas shift reaction is occurred to produce hydrogen for utilization in the fuel cell plant (Inal & Deniz, 2021).

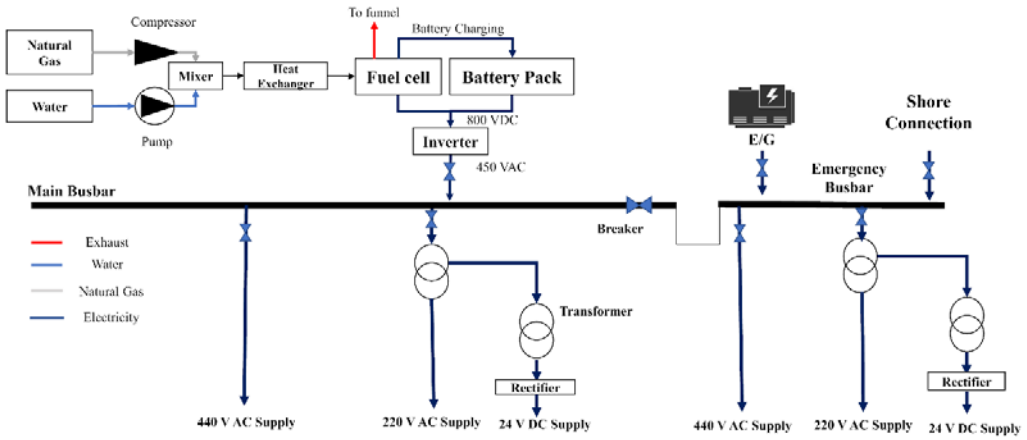

Figure 4.2. FC/battery hybrid electricity distribution system scheme (Adapted from (Cahyagi & Koenhardono, 2018; İnal & Deniz, 2021; Oways, 2019))

The system configurations are depicted in Table 4.4. The installed auxiliary power generation capacity of the vessel has remained at 3.15 MW which is the cumulative capacity of the existing three generator sets onboard.

The first and second configurations were designed to meet the electrical load with fuel cells, and battery packs are placed to compensate for operational loads when the vessel requires fast response time during quick load changes. In the other four configurations, batteries and fuel cells meet the load together. C3 and C4 cases utilize batteries during navigation to compare the environmental and economic results with C5 and C6 cases. While the batteries meet the majority of the electrical load in the discharge state, the fuel cells meet both the system load and the charge load in the charging state. The case of battery usage during navigation is examined to observe the impacts of battery life on the economic performance of the systems.

Table 4.4 Proposed system configurations

Configuration Code	Fuel Cell Power	Fuel Cell Type	Battery Capacity	Battery usage during navigation
C1	2 x 1.4 MW	MCFC	0.35 MWh	No
C2	6 x 0.44 MW	PAFC	0.51 MWh	No
C3	2 x 1.4 MW	MCFC	0.95 MWh	Yes
C4	5 x 0.44 MW	PAFC	0.95 MWh	Yes
C5	2 x 1.4 MW	MCFC	0.95 MWh	No
C6	5 x 0.44 MW	PAFC	0.95 MWh	No

The suitable battery for the different system configurations and the optimum charging-discharging times were obtained from a grid-search iterative selection algorithm that calculates the LNG consumption with possible charging-discharging hours. Battery usage during navigation operations was evaluated to increase battery life. The ship's electricity grid requires 450 V AC and the inverter demands 800 V DC input to give this output (Yuksel & Koseoglu, 2022). This is achieved by connecting 320 serial cells. Table 4.5 illustrates the specifications of the selected battery cells on the system.

Table 4.5 Selected battery cells for system configurations ((Panasonic, 2021; PowerXtra, 2021; Molicel, 2018; LGChem, 2014))

Battery Code	Capacity (mAh)	Nominal Voltage (V)	Price ($)	Weight (kg)
B1	3,350	3.6	11.82	0.048
B2	3,500	3.7	10	0.048
B3	3,500	3.7	8,82	0.049
B4	3,200	3.7	5.45	0.049

In this regard, initially, the conventional ship power distribution plant of 50,000 deadweight tons (DWT) oceangoing oil/chemical tanker vessel involving three equivalent D/Gs was modeled according to six different operation modes. The realistic fuel consumption calculation of D/Gs was ensured according to varying load sharing regarding the power demand in each operation with a numerical model. Then, commercially available PAFC, MCFC, and battery sets were selected. Six different fuel cell/battery configurations were investigated to obtain the optimum system layout. A state-based EMS was designed to control the charge/discharge processes of the batteries. Hybrid configurations were proposed in the first two configurations (C1 and C2) as the batteries are only utilized to meet the rapid load changes required from the vessel. C3 and C4 configurations were modeled to continuously utilize the batteries on all operations of the vessel. C5 and C6 used batteries only in coastal operations having frequent load changes to increase the battery life, thus the navigation operations were not included. The performance of the proposed fuel cell/hybrid system configurations was evaluated using environmental and economic analyses, and the results of utilizing

fuel cell/hybrid system configurations as auxiliary power units in the vessel were compared with the utilization of the existing D/G plant onboard.

4.3 Modeling of Fuel Cell and Battery Configuration

There have conducted two case studies in the scope of the thesis. The first case study involves a large oil/chemical tanker working with PAFC and battery hybrid configuration. The environmental and economic analyses of this case study are carried out using catalog data of a commercial PAFC unit; thus, no fuel cell modeling equations are utilized.

4.3.1 Mathematical Modeling of the Hybrid Power Plants

The mathematical model of the plant with fuel cell and battery configurations is created using Python programing language. A state-based energy management strategy (EMS) is proposed to control the battery charging and discharging processes. Figure 4.3 illustrates the mathematical model's algorithm scheme whereas Figure 4.4 depicts the EMS's working logic.

EMS function takes the battery state and previous state of charge (SoC) as inputs, and it starts with calculating the available maximum battery capacity from the function obtained from battery aging curves. The curves are gathered from the technical data sheet of the selected battery cells (Panasonic, 2021; PowerXtra, 2021; Molicel, 2018; LGChem, 2014). Then, the function computes the state of health (SoH) and checks through the battery state. According to the SoC and battery state, the decision of keeping or updating the state is taken. Finally, available battery capacity and updated SoC are calculated.

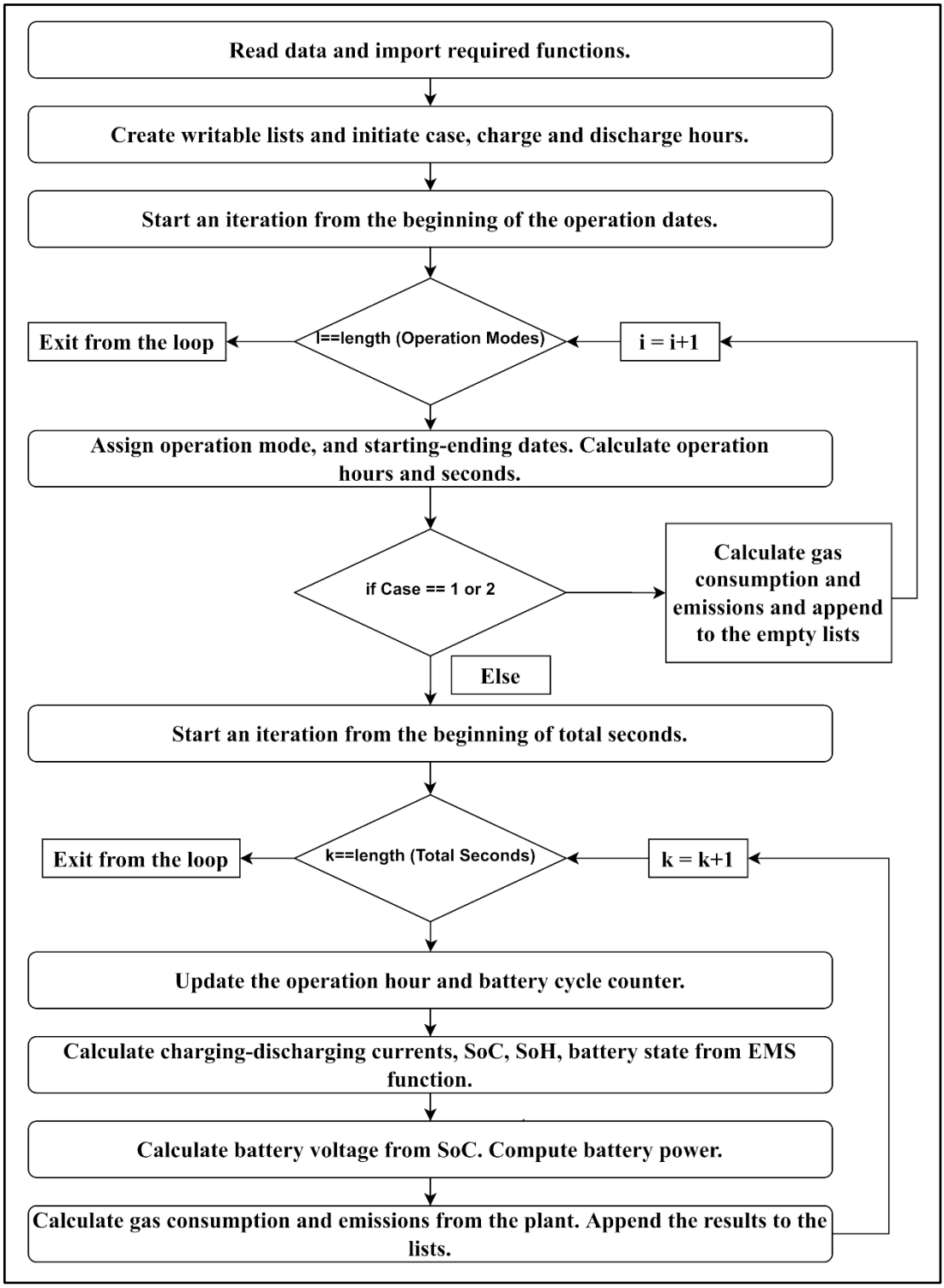

Figure 4.3 Ship power distribution system model algorithm scheme

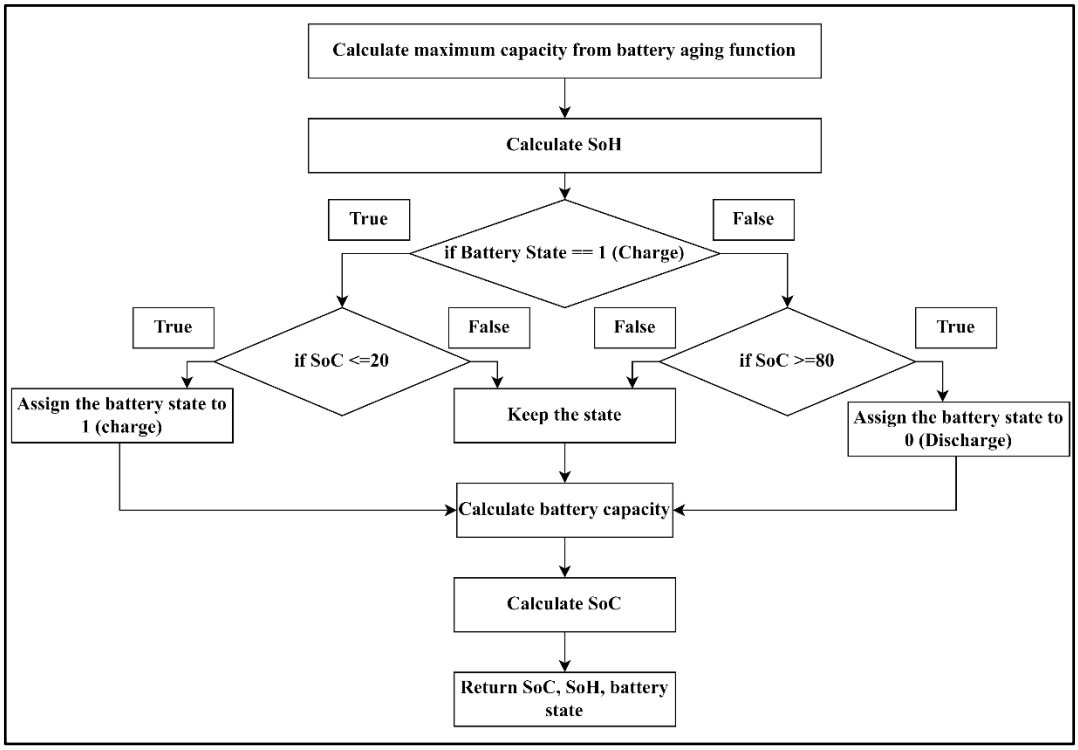

Figure 4.4 State-based EMS algorithm scheme

The algorithm of numerical simulation of fuel cell-battery powered ship electricity distribution plant is initiated with reading data and importing necessary libraries and functions. The model computes the operation hour and reads the operation mode from the data. Then, the fuel cell-battery configuration and battery charge-discharge hours are determined. Empty lists to save calculations of iterations are also created in this step. In the next step, an iteration over operation dates is initiated and for cases 1 and 2 LNG consumption and emissions are computed. If the case is 3 or 4, battery usage is to be considered, so a nested iteration is started over total operation seconds. To control the loop, cycle and operation hour counters are constructed and updated through the loop. Inside the loop, using pre-written functions by authors, battery charge-discharge currents were calculated. SoC, SoH, and battery state are determined and updated using the EMS function explained above. Battery voltage is computed using SoC-voltage curves provided by the technical datasheets of the battery cells. Finally, the gas consumption and emissions from the plant are calculated and saved to the initiated empty lists. The LNG consumption resulting in emissions of PAFC and MCFC based on the power output (in kW) has been obtained from the technical

datasheets of the fuel cells. Assuming that the fuel cells operate at constant efficiency values shown in Tables 4.2 and 4.3 where their characteristics are given, fuel consumption values are calculated depending on the required power generation determined according to the specified configuration and operating modes. The grid-search iterative selection algorithm tried the combinations of battery charging-discharging hours within the limits permitted by the manufacturer to obtain the optimum system performance for each configuration. While the minimum LNG consumption for each system design is the target of the algorithm, the ideal charging/discharging times have shaped the optimum EMS logic and schematic.

SoC is computed using the Coulomb counting method (Saxena, Hendricks & Pecht, 2016; Sepasi, Ghorbani & Liaw, 2015). Equation 4.7 shows the mathematical expression of the SoC calculation over time.

$$\mathrm{SoC(t)=SoC(0)-}\left(\int_0^t \eta \cdot \mathrm{I(t)}/\mathrm{C_{av}}\right) \tag{4.7}$$

where $SoC(t)$ is the SoC at time t, $SoC(0)$ is the SoC at the beginning of the operation, C_{av} is the available capacity of the battery, $I(t)$ discharging or charging current at the time t, η is the coulombic efficiency which is taken as 1 in this study. The charging procedure is constant current with constant voltage, and the discharging protocol is constant current with a constant C rate. To avoid increased inner resistance and improve battery life, the SoC range of the batteries in the model is kept between 20% and 80% (Saxena et al., 2016). Voltage is calculated from the function obtained from SoC-voltage curves (Panasonic, 2021). Equation 4.8 indicates the charge voltage (V_c) and Equation 4.9 depicts the discharge voltage (V_a) calculations from the SoC for the selected battery cell.

$$\begin{gathered} V_{c,2,3,4}=-\left(0.93 \cdot SoC^2\right)+\left(2.02 \cdot SoC\right)+3.13 \\ V_{c,1}=\left(-29.91 \cdot SoC^5\right)+\left(65.73 \cdot SoC^4\right)-\left(51.8 \cdot SoC^3\right)+\left(17.84 \cdot SoC^2\right) \\ -(3.55 \cdot SoC)+4.19 \end{gathered} \tag{4.8}$$

$$V_{d,2,3,4} = \left(2.45 \cdot SoC^3\right) - \left(4.95 \cdot SoC^2\right) + (04.15 \cdot SoC) + 2.48$$
$$V_{d,1} = \left(4.042 \cdot SoC^5\right) - \left(9.2056 \cdot SoC^4\right) + \left(7.87 \cdot SoC^3\right) - \left(3.144 \cdot SoC^2\right) + (0.6 \cdot SoC) + 2.63 \quad (4.9)$$

The state of health (SoH) is calculated using Equation 4.10 (Omar et al., 2014).

$$SoH(t) = C_{act}(t) / C_{init} \quad (4.10)$$

where C_{act} is actual and C_{init} is the initial battery capacity. Equation 4.11 depicts the calculation of C_{act} obtained from the battery aging curves of specified battery cells (Panasonic, 2021; PowerXtra, 2021; Molicel, 2018; LGChem, 2014).

$$\begin{aligned} C_{act} &= -0.3607 \cdot c_b + 3412.86 && \text{for battery 1} \\ C_{act} &= -0.2374 \cdot c_b + 3479.6 && \text{for batteries 2 and 3} \\ C_{act} &= -0.2171 \cdot c_b + 3181.4 && \text{for battery 4} \end{aligned} \quad (4.11)$$

where c_b is the number of battery cycles. Equation 4.12 depicts the battery-inverter power conversion calculation.

$$\begin{cases} P_{con} = \eta_{con} \cdot P_{bat}, & discharging \\ P_{bat} = \eta_{con} \cdot P_{con,} & charging \end{cases} \quad (4.12)$$

The efficiency factor (η_{con}) of the AC/DC converters in the system are assumed as 0.99 (Ovrum & Bergh, 2015). Battery power is denoted as P_{bat} and P_{con} represents the converted power.

4.3.2 Environmental Analysis of Hybrid System

The mathematical model computes the emission amounts sourced by diesel fuels by using emission factors taken over from Kuzu et al. (2021). Equation 4.13 is the emission calculation and Table 4.6 indicates the emission factors for the MDO and HFO.

$$E_i = \sum_k \theta_k \cdot EF_i \tag{4.13}$$

where E is the total emission, θ is the fuel consumption of the vessel, EF is the emission factor, k is the operation mode and i represents the pollutant type.

Table 4.6 EF of diesel fuels (g emission/ g fuel) (Kuzu et al., 2021)

Pollutant	**CO_2**	**N_2O**	**NO_x**	**VOC**	**CO**	**PM**	**SO_x**
EF MDO	3.206	0.00015	0.0961	0.00308	0.00277	0.00097	0.01
EF HFO	3.114	0.00015	0.0903	0.00308	0.00277	0.00278	0.025

LNG consumption and emissions of the fuel cell-battery configurations are calculated using Equation 4.14.

$$m_i = \sum_k P_k \cdot t_k \cdot \partial_i \tag{4.14}$$

where m is the pollutant or LNG mass in kg, P is the required total power of the operation, t is the operation time in hours, and ∂ is the emission or gas consumption coefficient given in Tables 4.2 and 4.3.

4.3.3 Economic Analysis of Hybrid System

Economic analyses of the specified configurations have been carried out to detect the feasibility of systems. Investment costs are calculated considering the inflation between the year of gathered price information and 2022 by using the Chemical Engineering Plant Cost Index (CEPCI). The prices are obtained as $1,125,000/unit for the PAFC project in 2006 and $4,992,000/unit for the MCFC project in 2010. The current prices are estimated as shown in Equation 4.15 and Equation 4.16:

$$Cost_{2022,PAFC} = Cost_{2006,PAFC} \cdot (CEPCI_{2022}/CEPCI_{2006}) \tag{4.15}$$

$$Cost_{2022,MCFC} = Cost_{2010,MCFC} \cdot (CEPCI_{2022}/CEPCI_{2010}) \tag{4.16}$$

where $CEPCI_{2006}$ = 499.6, $CEPCI_{2010}$ = 550.8 (Turton, Shaeiwitz, Bhattacharyya & Whiting, 2018), $CEPCI_{2022}$ = 806.3 (Jenkins, 2022).

Following the cost determination, the capital recovery factor (CRF) is shown in Equation 4.17, which converts the entire current value to a flow of even yearly payments at the annual interest rate (i = 5%) over the system life (LT) of 10 years for fuel cells (Kanuri, 2012), and the life span of batteries computed using the ordinary least squares regression (Tian, Zeng, Gu, Zhang & Yuan, 2021; Yang & Yeh, 2018).

$$CRF = i \cdot (1+i)^{LT} / [(1+i)^{LT}-1] \tag{4.17}$$

The levelized energy cost (LEC) is the ratio of the entire cost, including maintenance and operating costs (C_{om}), to the annual energy produced by the plant, as established in Equation 4.18 by (Tian et al., 2021):

$$LEC=(CRF \cdot Cost_{2022} + Cost_{om})/(\dot{W}_{net} \cdot t) \tag{4.18}$$

where C_{om} is taken as 1.5% of the total cost ($Cost_{2022}$), W_{net} is the net power output from the plant, and t is the working hours. The working hours are computed using the reference tanker ship's real-time operational data acquired from port calls and position histories. c_{ele} is the cost of electricity, which is computed from fuel prices and total energy production of plants as given in Equation 4.19 (Yang & Yeh, 2018):

$$c_{ele} = \sum_{k} \theta_k \cdot Cost_{fuel,j}/(\dot{W}_{net} \cdot t)_k \tag{4.19}$$

where k is the operation mode, $Cost_{fuel}$ is the fuel price, and j is the fuel type used in the specified operation modes. The conventional plant utilizes very low sulfur fuel oil (VLSFO) during navigation and marine gas oil (MGO) near coastal areas. The average prices for the specified date range and current prices that have risen due to global political agenda were taken for both diesel fuels (for twenty ports average) and

LNG (for Rotterdam port) from (Ship and Bunker, 2022). Current prices were obtained on May 30th, 2022, and given in Table 4.7.

Table 4.7 Bunker prices for diesel fuels and LNG (Ship and Bunker 2022)

Fuel	Price Reference	Bunker Price ($/t)
VLSFO	Two-years average	461.5
	Current	988
MGO	Two-years average	530
	Current	1,275
LNG	Two-years average	810.5
	Current	1,509

4.4 Results and Discussion

4.4.1 Mathematical Modeling Results of the Fuel Cell/Battery Hybrid System on Chemical Tanker Vessel

The grid-search iterative selection algorithm iterated over specified batteries and charging-discharging hour combinations that targeted to find the configurations having minimum fuel consumptions. Charge and discharge times were tried between 3 and 8 hours. Table 4.8 indicates the optimum batteries and charging-discharging combinations retrieved from grid-search iterative selection algorithm results. Results provided that the lowest LNG consumption is achieved when B2 batteries are used during navigation, and B4 batteries give the best results when these are not used during navigation phases. The fastest charging and the slowest discharging combination gave the best results for all battery-utilized combinations. The long-term support of the batteries to the system has had a positive effect on reducing the LNG consumption of the FCs.

Table 4.8 Optimum batteries and charge-discharge hours

Configuration Code	Battery Code	Charge Hour	Discharge Hour	Battery Usage During Navigation
C3	B2	3	8	Yes
C4	B2	3	8	Yes
C5	B4	3	8	No
C6	B4	3	8	No

The environmental and economic analyses were carried out using the calculated fuel consumption of D/Gs and fuel cell/battery hybrid systems for six different configurations. The fuel consumption of each operation mode and their environmental effects were taken into consideration in the analyses. It is important because the calculations are based on the utilization of VLSFO during navigational phases and MGO during non-navigational phases. Figure 4.5 indicates the total fuel consumption of the combinations and fuel consumption distribution according to operation modes for 2 years of operation of the reference vessel.

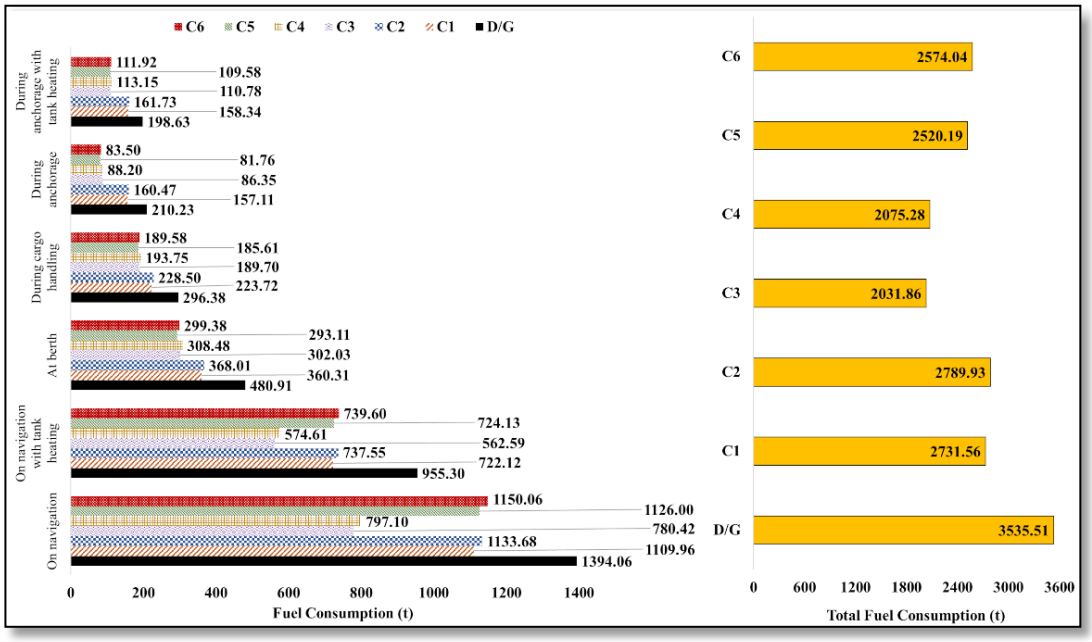

Figure 4.5 Fuel consumptions on different operation modes and total fuel consumption of the proposed combined systems and D/G plant

The conventional D/G plant consumes 2,349.36 t of VLSFO during navigation operations and 1,186.15 t of MGO for port and anchorage operations. Without using the batteries, fuel cell configurations of C1 and C2 consume 2,731.56 t and 2,789.93 t of LNG, respectively. 211.37 t of LNG saving was attained for the MCFC/battery hybrid configuration (C5) when the batteries support port and anchorage operations in comparison with the C1 configuration. The PAFC/battery system with battery usage during coastal operations (C6) provided an LNG saving of 215.89 t when compared with the PAFC/battery hybrid system of C2.

The most remarkable fuel consumption reductions were achieved in C3 and C4 cases where the batteries support all operations. Especially, LNG consumption of C3 and C4 configurations during navigation was reduced to 1,343.01 t and 1,371.71, respectively. It indicates that an LNG saving of %26.7 during navigation operations and a total of 25.6% fuel savings could be achieved by utilizing batteries with fuel cells at all operations. For the port and anchorage operations, C5 and C6 ensured slightly lower LNG consumption due to the increased SoH of batteries compared to C3 and C4. The total LNG consumptions are higher for PAFC systems because of the higher specific LNG fuel consumption compared to MCFC systems. Since the power output of the PAFC system is less, the system design was made to run more than one PAFC in parallel. In the MCFC system, on the other hand, the number of operating MCFCs mostly remained constant due to the higher power output. The impact of battery usage in reducing LNG consumption was greater in PAFC systems because battery usage reduces the number of PAFCs utilized for the operation. In general, the battery-pack utilization during the navigation decreases the LNG consumption remarkably for each FC type.

4.4.2 Environmental Analysis of the Hybrid System

This section highlights the environmental impacts of the selected combinations and their potential to reduce air pollutant emissions. Table 4.9 depicts the potential emission reduction percentages of each combination compared to a conventional D/G plant. The emission coefficients provided by the commercial PAFC and MCFC catalogs were used to calculate the air pollutant amount. N/A values represent that the emission coefficient is neglected in the fuel cell catalog.

Potential N_2O emissions were completely prevented and the production of NO_x, PM, SO_x, VOC, and CO emissions can be largely avoided by utilizing proposed system configurations. Especially for increasing the air quality near coastal areas, fuel cell plants can be promising alternatives. Although LNG usage still caused CO_2 production, a remarkable amount of CO_2 emissions can be prevented by fuel cell plants. The battery support to fuel cells reduced LNG consumption, which also impacts

CO_2 reduction positively. Figure 4.6 shows the total CO_2 production and distribution of CO_2 emissions according to operation modes for each fuel cell/battery hybrid configuration and D/G plant.

Table 4.9 The emission reduction potential of the proposed system configurations compared to conventional diesel generators

Pollutant Type	C1 (%)	C2 (%)	C3 (%)	C4 (%)	C5 (%)	C6 (%)
CO_2	32.44%	31.00%	49.75%	48.67%	37.67%	36.34%
N_2O	100%	100%	100%	100%	100%	100%
NO_x	99.98%	99.95%	99.98%	99.97%	99.98%	99.96%
VOC	N/A	98.60%	N/A	98.96%	N/A	98.71%
CO	N/A	99.14%	N/A	99.36%	N/A	99.20%
PM	99.998%	N/A	99.999%	N/A	99.998%	N/A
SO_x	99.9989%	N/A	99.9992%	N/A	99.999%	N/A

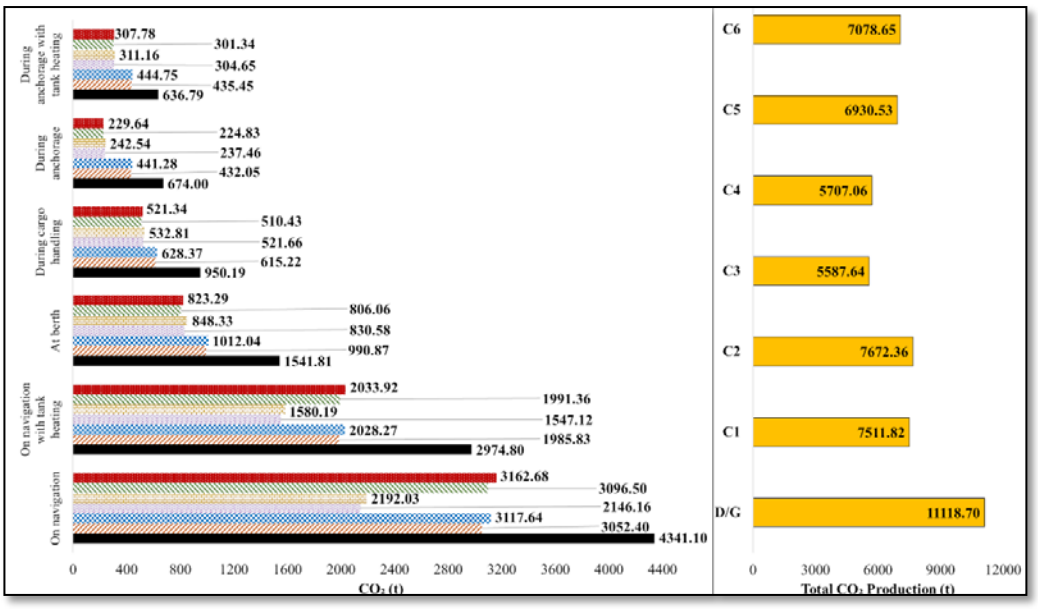

Figure 4.6. CO_2 production on different operation modes and total fuel consumption from the fuel cell/battery hybrid systems and D/G plant according to operation modes

The fuel-cell battery hybrid system configurations produced fewer CO_2 emissions compared to the conventional D/G plant. Particularly, the C3 and C4 reduced the total CO_2 emission in two years by 5,531.06 t and 5,411.64 t respectively. Lowering the LNG consumption with battery support provided CO_2 emission reductions of 1,006.35 t and 977.65 t during navigation for the respective system designs. Battery support on fuel cells also made a difference to lower CO_2 for the other operations. The

environmental effect of C3 and C4 are considerably lower than other combinations regarding CO_2 reductions. Especially, to achieve the decarbonization goals set by IMO and European Union, the utilization of FC plants as the auxiliary power units on large commercial marine vessels is a feasible option according to the analysis. If the infrastructure of fuel-related resources is prepared, installing commercially available FC units in newly constructed ships, and retrofitting older ships can be a solution for reducing CO_2 emissions. Figure 4.7 illustrates the remaining emissions from the D/G plant and fuel cell/battery hybrid systems according to each operation mode. In the subplots of Figure 4.7, the left vertical axes represent the D/G emissions, and the right vertical axes show the fuel cell/battery hybrid system-based emission productions.

Figure 4.7 highlights that the fuel cell/battery hybrid configurations can prevent approximately 326 t of NO_x and 70 t of SO_x emissions in two years. These values are crucial considering that the emission reduction calculation involves only the auxiliary engines of one vessel. Among fuel cell-battery systems, the configurations that utilize the battery support provided a greater reduction potential for these emissions. In terms of the prevention of emissions from marine vessels, fuel cell plants showed satisfactory performance. The investment related to capturing SO_x and NO_x on board can be shifted towards the FC technology to achieve sustainable transportation.

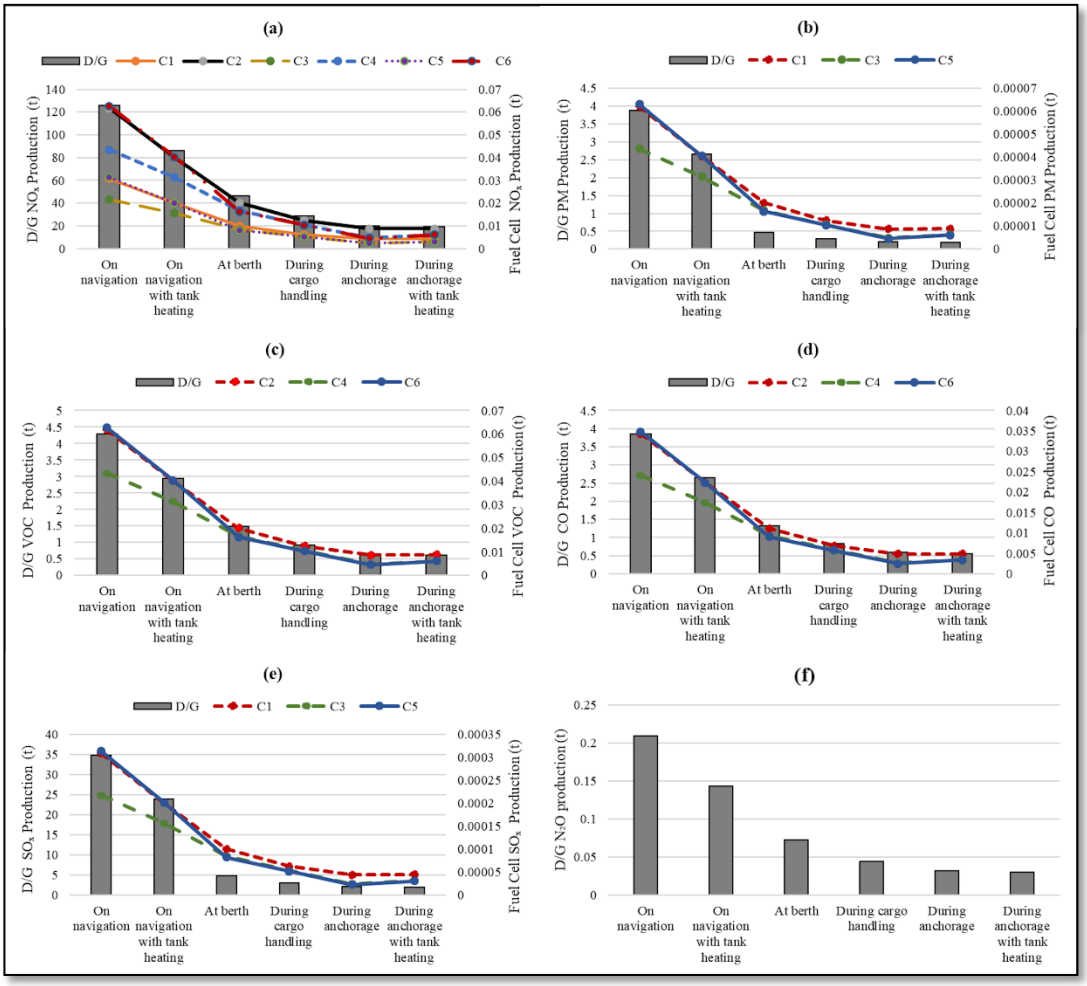

Figure 4.7. The production of (a) NO_x, (b) PM, (c) VOC, (d) CO, (e) SO_x, (f) N_2O emissions from plants for different operation modes

4.4.3 Economic Analysis of Hybrid System

The environmental analysis results showed that all fuel cell/battery hybrid configurations could reduce fuel consumption and CO_2 emissions by 31 - 49.75% when compared with D/G utilization. The utilization of batteries during navigation, given as C3 and C4 configurations, increased the energy efficiency of the vessel. The utilization of batteries for longer service periods will increase the completed charge/discharge cycles, cause a reduction in the battery life and increase the systems' investment costs throughout their lifetime. In this section, the economic performance of the six-fuel cell/battery hybrid configurations was investigated considering LEC and c_{ele}.

The estimation of the battery lifespans was ensured from SoH variation curves. SoH curves of the cases that examine battery usage during the navigation are shown in Figure 4.8. Ordinary least square regression was fitted to these curves to predict the life of the battery.

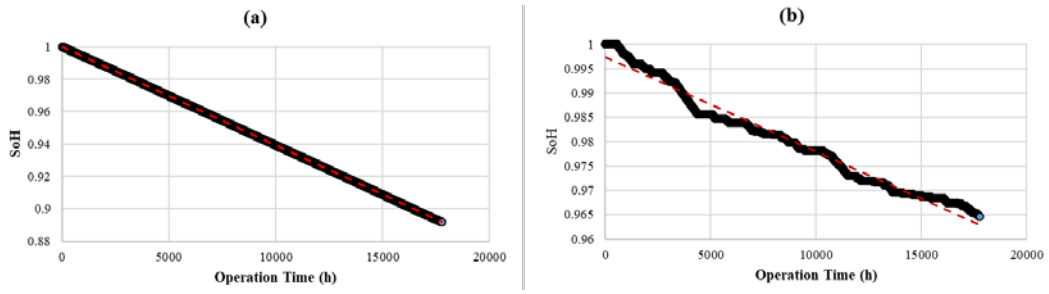

Figure 4.8 SoH curves of batteries were (a) utilized (b) not utilized during the navigation

When the batteries were utilized during navigation, battery life was calculated as 3.75 years. The battery life can be expanded up to 11.62 years without using the batteries when the ship is on the course. Even though battery utilization during navigation provides remarkable emission reduction, the battery lifespan is affected negatively by this type of usage frequency. Table 4.10 highlights the battery lifespans, weight, volume, and costs of the fuel cell-battery configurations. PAFC systems have slightly lower weights and volumes compared to MCFC units. C4 has the lowest weight and volume compared to other combinations due to the lower number of fuel cells. The investment cost of the PAFC units was also lower than MCFC units. C5 and C6 require one set of battery packs during the system's lifetime. On the other hand, battery sets should be replaced three times for C3 and C4, which vastly increases the costs of the combinations.

LEC is defined as the investment costs including operation and maintenance costs per unit of energy production of the hybrid configurations. The normalized values indicate comparable data to assess the economic performance of the proposed configurations regarding the investment costs. LEC values for each configuration were calculated by using Eq. 18 and the results were depicted in Figure 4.9. It can be seen that the LECs of PAFC configurations (C2-C4-C6) were found lower than MCFC configurations (C1-C3-C5). The lowest LEC was obtained from the C6 configuration.

This result is expected because the battery sets of C3 and C4 configurations need to be changed two times in the given system lifetime of 10 years due to high utilization time in total voyages, which causes rapid degradation of batteries and an increased number of charge/discharge cycles. It is also lower than the C2 configuration because of one more fuel cell utilized in C2, and non-utilized batteries added to the C2 configuration for safety concerns.

Table 4.10 Weights, volumes, costs, and battery lifespans of the system configurations

Configurations	**C1**	**C2**	**C3**	**C4**	**C5**	**C6**
$Cost_{2022}$ **[$]**	14,847,237	11,232,101	17,869,685	12,332,537	15,262,309	9,725,161
$Cost_{om}$ **[$]**	222,708	168,481	268,045	184,988	228,934	145,877
Battery Code	B4	B4	B2	B2	B4	B4
Number of parallel cells	133	194	339	339	371	371
System Volume (m^3)	564.98	533.86	569.68	448.94	570.33	449.59
Weight (t)	200.31	175.02	203.43	148.52	204.04	149.13
Battery Life [years]	-	-	3.75	3.75	11.62	11.62

However, the LEC values should be evaluated by considering the environmental and remaining economic analysis results because LEC values do not involve the fuel consumption of specified systems and can be considered as a base for comparing the investment costs.

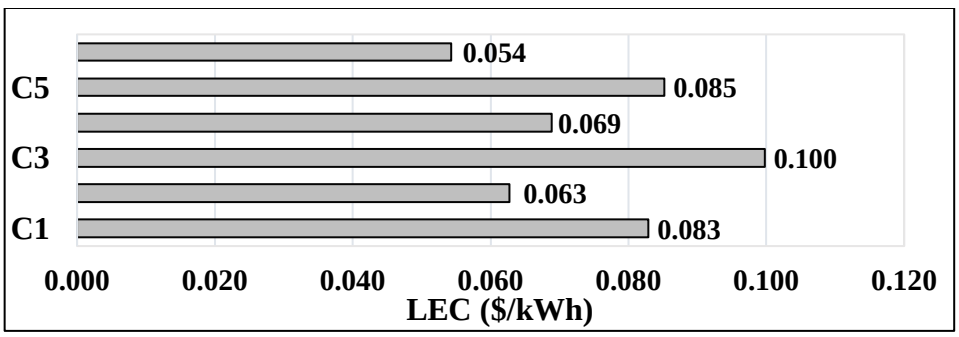

Figure 4.9. LEC values obtained for each configuration mode

c_{ele} of all configuration modes were obtained by using the fuel prices of LNG in Eq. 20 and given in Figure 4.10 VLSFO utilization during navigation and MGO utilization near coastal areas were taken into consideration for the calculation of c_{ele} values of D/G usage onboard to compare the existing electricity production cost of the vessel with the results of proposed configuration modes. The economic analyses for c_{ele} values were carried out using two parameters as current fuel prices and average fuel prices of 2 years when the operational data of the vessel were taken. The analysis results showed that c_{ele} of C3 configuration is the lowest. High price hikes in the MGO market decreased the economic feasibility of electricity generation with D/Gs. Although LNG fuel prices are higher than MGO and VLSFO prices for both scenarios, it can be seen that c_{ele} of C3-C4 configurations are very competitive when compared to onboard electricity production with D/Gs, considering the decrease in the fuel consumption of the vessel with the proposed fuel cell/battery hybrid configurations. c_{ele} of the proposed systems increased by almost 2 times compared to average fuel prices of 2 years.

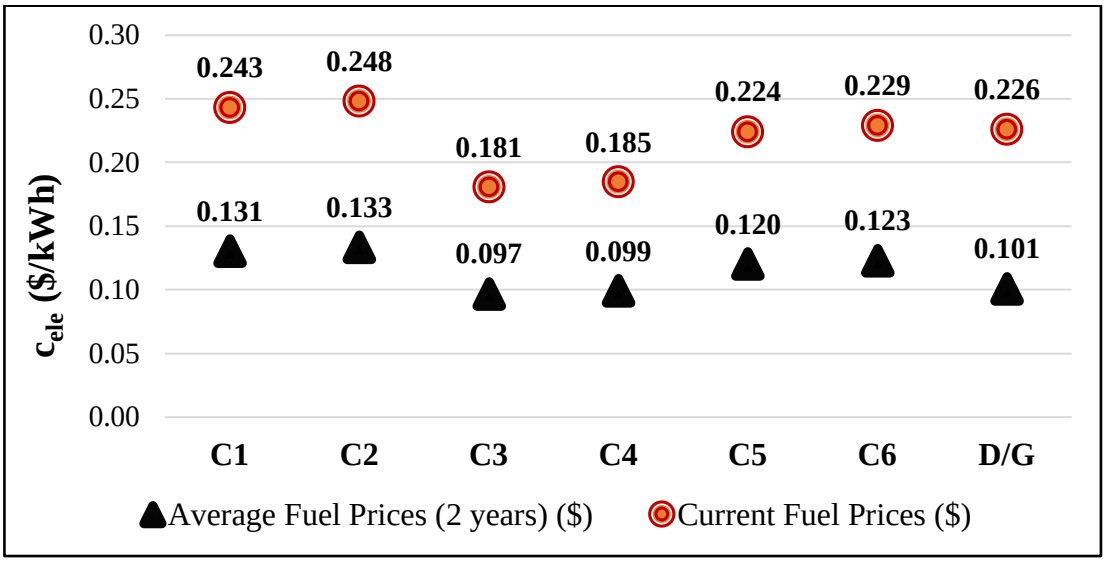

Figure 4.10 Electricity production costs of utilizing fuel cell/battery hybrid configurations and D/Gs onboard

CHAPTER 5
CONCLUSIONS

In this thesis, the parameter optimization problem for H-1000XP PEMFC was handled using nine relatively novel algorithms. Initially, to validate this solution methodology, the results found by E-CGA were compared with experimental test values of a 250 W PEMFC gathered from (Mo et al. 2006). The manufacturer data for the H-1000XP PEMFC was used for the comparison of the different algorithms. The algorithms were evaluated regarding error rate with various metrics, run time, and objective function efficiency. Three MADM methods were utilized to rank the algorithms according to the mentioned criteria. The main conclusions derived from the thesis are listed below:

- MFA algorithm was ranked as the best by all MADM methods and ensured the optimum solution set with low SSE, runtime, and high objective function efficiency. One of the evolution-based algorithms, DE, also offered reliable performance and was placed second. These two methods were found suitable for the given issue, and their performances could be further improved with targeted hyper-parameter tuning.

- In terms of objective function efficiency, R^2 and MAE, IGWO, and GWO provided the best results. However, the runtime was remarkably higher for this algorithm yielded be ranked 9th by TOPSIS. Due to the same reason, MOORA and PROMETHEE selected GWO for the 7th rank which is not a satisfactory ranking either. However, in the consistency requiring applications, it could be considered a valid option. Its runtime could be optimized, and SSE could be lowered with a hyper-parameter tuning either.

- Convergence speeds of the MFA and IGWO were also found as the best which means the 1000 iterations could be lowered to decrease the running times of these algorithms.

- Among the convergence speeds of the best solution sets, IWOA was the fastest algorithm for finding the ideal solution before the 100th iteration. Its running time could be decreased remarkably by ensuring parameter tuning.

- JAYA and CS algorithms were found to be not suitable for this problem. JAYA solved the problem with a competitive runtime, but its objective function efficiency and convergence speed was the worst among others. The runtime of the CS was lower than GWO and IWOA however, compared to other algorithms it remained slow. The objective function efficiency of the CS was slightly better than JAYA, but its error metrics were the worst which made it unsuitable for the application. MADM methods ranked these two algorithms in low spots either.

In conclusion, this study provides valuable insights into the parameter optimization of H-1000XP PEMFC and suggests several areas for future research. The parameter optimization of PEMFC has been a frequently studied topic and numerous algorithms were tried on various FCs. This thesis presented an optimization algorithm benchmarking to detect the parameters of H-1000XP PEMFC. The results of this thesis could be useful for scientists that aim to build a mathematical model or investigate the algorithms to solve a similar problem for the specified FC. Some recommended areas for future studies include expanding the benchmarking with the addition of different algorithms, a more specialized hyperparameter tuning of mentioned algorithms with various prominent features, and a verification process of the determined parameters using the experimental data which will be obtained by laboratory trials of H-1000XP PEMFC.

In this thesis, the conventional ship power distribution plant of a 50,000 DWT oceangoing tanker vessel involving three equivalent D/Gs was simulated using a Python environment. The realistic fuel consumptions of D/Gs are calculated by regarding the power demand of the vessel at varying loads in each operation with a numerical model. The ship trial test data of onboard D/Gs were used to model the plant according to six different operation modes. The utilization hours of these modes were obtained from port calls and position history data between 06 December 2019/06

December 2021. The route of the ship involved oceangoing navigations mainly on the Europe-North America route.

This thesis aimed to analyze and discuss the potential environmental and economic impacts of implementing fuel cell/battery hybrid configurations instead of marine D/Gs to compensate for the electricity demand of the vessel. The novelty of the theis is as follows:

- There have found no studies in the literature related to environmental and economic analyses of fuel cell-battery hybrid system designs that can fully meet the electricity demand of ocean-going tanker ships.

- Although there are commercially available PAFC products, they have not yet been evaluated for marine applications.

- Marine applications of MCFC systems are found to be limited with MCFC utilization on main propulsion units of small vessels. They have not been used to supply all of the auxiliary power demand of large vessels.

- The literature survey shows that there have been no studies that evaluate the most suitable battery brand and charge-discharge hours for PAFC and MCFC systems with a grid-search algorithm.

In this regard, commercially available PAFC, MCFC, and battery sets were selected. Six different configurations of fuel cell-battery combinations were investigated to obtain the optimum system layout. A state-based EMS was designed to control the charge/discharge processes of the batteries. Hybrid configurations were proposed in the first two configurations (C1 and C2) as the batteries are only utilized to meet the rapid load changes required from the vessel. C3 and C4 configurations were modeled to continuously utilize the batteries on all operations of the vessel. C5 and C6 used batteries only in coastal operations having frequent load changes to

increase the battery life, thus the navigation operations were not included. The main conclusions derived from the thesis were given as follows:

- Results show that the lowest LNG consumption is achieved when B2 batteries are used during navigation, and B4 batteries give the best results when they are not used during navigation phases.

- The fastest charging and the slowest discharging combination gave the best results for all battery-utilized combinations.

- LNG consumption of C3 and C4 configurations during navigation was reduced to 1,343.01 t and 1,371.71, respectively. It indicates that an LNG saving of %26.7 during navigation operations and a total of 25.6% fuel savings could be achieved by utilizing batteries with fuel cells at all operations.

- Potential N_2O emissions were completely prevented and the production of NO_x, PM, SO_x, VOC, and CO emissions can be largely avoided by utilizing proposed system configurations.

- Although LNG usage still caused CO_2 production, a remarkable amount of CO_2 emissions can be prevented by fuel cell plants. The battery support to fuel cells reduced LNG consumption, which also impacts CO_2 reduction positively. The utilization of fuel cell/battery hybrid configurations could reduce fuel consumption and CO_2 emissions by 31 - 49.75% when compared with D/Gs.

- When the batteries were utilized during navigation, battery life was calculated as 3.75 years. The battery life can be expanded up to 11.62 years without using the batteries when the ship is on the course.

- The LECs of PAFC configurations (C2-C4-C6) were found to be lower than MCFC configurations (C1-C3-C5). The lowest LEC was obtained from the C6 configuration as 0.054 $/kWh. This result is expected because the battery sets of C3

and C4 configurations need to be changed two times in the given system lifetime of 10 years due to high utilization time in total voyages, which causes rapid degradation of batteries and an increased number of charge/discharge cycles.

- The lowest c_{ele} was found to be a C3 configuration with the values of 0.181 and 0.097 $/kWh for the current fuel prices and average fuel prices of 2 years when the operational data of the vessel were taken, respectively.

- C3-C4 configurations are very competitive when compared to onboard electricity production with D/Gs, considering the decrease in the fuel consumption of the vessel with the proposed fuel cell/battery hybrid configurations. c_{ele} of the proposed systems increased by almost 2 times compared to average fuel prices of 2 years.

The limitations of the thesis are as follows:

- The LNG consumption of fuel cells was calculated from technical datasheets at the given efficiency values.

- In the utilization times of the operation modes, maneuvering durations were added to the port operations' utilization due to the close electric demand, and lack of exact maneuvering times.

- The small changes in the operational load during operations were neglected and assumed constant loads.

In future studies, the analyses can be extended with different fuel cell technologies, e.g., PEMFC and SOFC. A detailed mathematical model of the specified fuel cell types can be implemented to deepen the analyses. The operational load and utilization time data of the marine diesel generators can be improved by collecting from a commercial ship in more detail with more frequent timestamps to improve the accuracy of the

electric load model. Different types of EMS algorithms can be utilized in the model to evaluate the system performance by comparing the outputs of the algorithms.

REFERENCES

Abualigah, L., & Diabat, A. (2021). Advances in sine cosine algorithm: a comprehensive survey. *Artificial Intelligence Review, 54*(4), 2567-2608.

Ali, M., El-Hameed, M. A., & Farahat, M. A. (2017). Effective parameters' identification for polymer electrolyte membrane fuel cell models using grey wolf optimizer. *Renewable energy, 111*, 455-462.

Alnes, Ø. Å. (2018). (02.06.2022) *FellowSHIP project concludes 15 years of maritime battery and fuel cell research*. https://www.dnv.com/expert-story/maritime-impact/FellowSHIP-project-concludes-15-years-of-maritime-battery-and-fuel-cell-research.html.

Alpaslan, E., Çetinkaya, S. A., Yüksel Alpaydın, C., Korkmaz, S. A., Karaoğlan, M. U., Colpan, C. O., ... & Gören, A. (2021). A review on fuel cell electric vehicle powertrain modeling and simulation. *Energy Sources, Part A: Recovery, Utilization, and Environmental Effects*, 1-37.

Amphlett, J. C., Baumert, R. M., Mann, R. F., Peppley, B. A., Roberge, P. R., & Harris, T. J. (1995). Performance modeling of the Ballard Mark IV solid polymer electrolyte fuel cell: I. Mechanistic model development. *Journal of the Electrochemical Society, 142*(1), 1.

Andújar, J. M., & Segura, F. (2009). Fuel cells: History and updating. A walk along two centuries. *Renewable and Sustainable Energy Reviews, 13*(9), 2309-2322.

Aouaini, F., Bouazizi, N., Almoneef, M. M., Al-Ghamdi, H., & Lamine, A. B. (2021). Absorption and desorption of hydrogen in Ti 1.02 Cr 1.1 Mn 0.3 Fe 0.6 RE 0.03: experiments, characterization and analytical interpretation using statistical physics treatment. *RSC advances, 11*(26), 15905-15920.

Artkın, F. (2018). The Renewable Energy Sources and Technologies of Potential in Turkey. *The Eurasia Proceedings of Science Technology Engineering and Mathematics*, (4), 285-295.

Ashraf, H., Abdellatif, S. O., Elkholy, M. M., & El-Fergany, A. A. (2022a). Computational techniques based on artificial intelligence for extracting optimal parameters of PEMFCs: Survey and insights. *Archives of Computational Methods in Engineering*, *29*(6), 3943-3972.

Ashraf, H., Abdellatif, S. O., Elkholy, M. M., & El-Fergany, A. A. (2022b). Honey badger optimizer for extracting the ungiven parameters of PEMFC model: Steady-state assessment. *Energy Conversion and Management*, *258*, 115521.

Balestra, L., & Schjølberg, I. (2021). Modelling and simulation of a zero-emission hybrid power plant for a domestic ferry. *International Journal of Hydrogen Energy*, *46*(18), 10924-10938.

Bassam, A. (2017). *Use of voyage simulation to investigate hybrid fuel cell systems for marine propulsion* [Doctoral dissertation]. University of Southampton.

Behzadian, M., Kazemzadeh, R. B., Albadvi, A., & Aghdasi, M. (2010). PROMETHEE: A comprehensive literature review on methodologies and applications. *European Journal of Operational Research*, *200*(1), 198-215.

Berry, G. D., Martinez-Frias, J., Espinosa-Loza, F., Aceves, S. M., & Cutler, J. C. (2004). Hydrogen Storage and Transportation, Encyclopedia of Energy.

Bevan, A. I., Züttel, A., Book, D., & Harris, I. R. (2011). Performance of a metal hydride store on the “Ross Barlow” hydrogen powered canal boat. *Faraday Discussions*, *151*, 353-367.

Bindu, A. H., & Reddy, M. D. (2013). Economic load dispatch using cuckoo search algorithm. *Int. Journal Of Engineering Research and Apllications*, *3*(4), 498-502.

Boretti, A. (2022). Which thermochemical water-splitting cycle is more suitable for high-temperature concentrated solar energy?. *International Journal of Hydrogen Energy*, *47*(47), 20462-20474.

Brans, J. P., & De Smet, Y. (2016). Multiple criteria decision analysis: state of the art surveys. In S. Greco, M. Ehrgott, & J.R. Figueira (Eds.), *PROMETHEE methods* (pp.187-219). New York, NY: Springer New York.

Brauers, W. K., & Zavadskas, E. K. (2006). The MOORA method and its application to privatization in a transition economy. *Control and Cybernetics*, *35*(2), 445-469.

Bristol Hydrogen Boats. (2023, March 28). *About Hydrogenesis*. Bristolhydrogenboats. http://www.bristolhydrogenboats.co.uk/about.html

Cahyagi, D., & Koenhardono, E. S. (2018). Study of shipboard power distribution system: review on an aplication of ac zonal distribution. *IPTEK The Journal of Engineering*, *4*(1), 1-6.

Cao, Y., Li, Y., Zhang, G., Jermsittiparsert, K., & Razmjooy, N. (2019). Experimental modeling of PEM fuel cells using a new improved seagull optimization algorithm. *Energy Reports*, *5*, 1616-1625.

Carral, C., & Mele, P. (2014). A numerical analysis of PEMFC stack assembly through a 3D finite element model. *International Journal of Hydrogen Energy*, *39*(9), 4516-4530.

Celik Y., Karadeniz A. (2020). Whale Optimization Algorithm for Numerical Constrained Optimization. *Academic Platform Journal of Engineering and Science*, *8(3)*, 547 - 554.

Çelikbilek, Y., & Tüysüz, F. (2020). An in-depth review of theory of the TOPSIS method: An experimental analysis. *Journal of Management Analytics*, *7*(2), 281-300.

Centro Per Gli Studi Di Tecnica Navale (2022, June 24). Cordiseuropa. *Molten-carbonate fuel Cells for Waterborne Application. https://cordis.europa.eu/project/id/19973*

Chen, Y., & Wang, N. (2019). Cuckoo search algorithm with explosion operator for modeling proton exchange membrane fuel cells. *International Journal of Hydrogen Energy*, *44*(5), 3075-3087.

Chen, X., Yu, Z., Yang, C., Chen, Y., Jin, C., Ding, Y., ... & Wan, Z. (2021). Performance investigation on a novel 3D wave flow channel design for PEMFC. *International Journal of Hydrogen Energy*, *46*(19), 11127-11139.

Choi, C. H., Yu, S., Han, I. S., Kho, B. K., Kang, D. G., Lee, H. Y., ... & Kim, M. (2016). Development and demonstration of PEM fuel-cell-battery hybrid system for propulsion of tourist boat. *International Journal of Hydrogen Energy*, *41*(5), 3591-3599.

Colpan, C.O., Nalbant, Y. & Ercelik, M., (2018). Fundamentals of Fuel Cell Technologies. In: *Comprehensive Energy Systems*. Elsevier. (pp. 1107–1130).

Coppola, T., Micoli, L., & Turco, M. (2020, June). State of the art of high temperature fuel cells in maritime applications. In *2020 International Symposium on Power Electronics, Electrical Drives, Automation and Motion (SPEEDAM)* (pp. 430-435). IEEE.

Dall'Armi, C., Micheli, D., & Taccani, R. (2021). Comparison of different plant layouts and fuel storage solutions for fuel cells utilization on a small ferry. *InternatIonal Journal of Hydrogen Energy*, *46*(26), 13878-13897.

Danoune, M. B., Djafour, A., Wang, Y., & Gougui, A. (2021). The Whale Optimization Algorithm for efficient PEM fuel cells modeling. *International Journal of Hydrogen Energy*, *46*(75), 37599-37611.

de Farias Aires, R. F., & Ferreira, L. (2019). A new approach to avoid rank reversal cases in the TOPSIS method. *Computers & Industrial Engineering*, *132*, 84-97.

Demirbaş, A. (2001). Biomass resource facilities and biomass conversion processing for fuels and chemicals. *Energy Conversion and Management*, *42*(11), 1357-1378.

Department of Energy. (2022a, June 2). *Comparison of Fuel Cell Technologies*. https://www.energy.gov/eere/fuelcells/comparison-fuel-cell-technologies

Department of Energy. (2022b, June 2). *Physical Hydrogen Storage*. https://www.energy.gov/eere/fuelcells/physical-hydrogen-storage.

Department of Energy. (2022c, June 2). *Metal Hydride Storage Materials*. https://www.energy.gov/eere/fuelcells/metal-hydride-storage-materials.

Dirk, S. (2013). Venice,“. In *Fuel Cell Solutions for Maritime and Harbour Applications Proton Motor Fuel Cell GmbH”. Fuel Cells and Hydrogen for Maritime and Harbour Applicarions FCH Workshop* (Vol. 13).

Det Nortsle Veritas. (2022, 2 June). *EEXI – Energy Efficiency Existing Ship Index*. https://www.dnv.com/maritime/insights/topics/eexi/index.html?gclid=CjwKCAjwv-GUBhAzEiwASUMm4nww5onoBP7iRtliXLhyuRqfcYtTBM7bnA66oJf49bR2SmogZA8QRoCSFQQAvD_BwE

Dokeroglu, T., Sevinc, E., Kucukyilmaz, T., & Cosar, A. (2019). A survey on new generation metaheuristic algorithms. *Computers & Industrial Engineering*, *137*, 106040.

Doosan Fuel Cell America INC. (2022, June 6). *PureCell Model 400*. https://www.doosanfuelcellpower.com/download/pdf/catalog/pafc-400kw_en.pdf

e4Ships. (2023a, March 29). *MultiSchiBZ*. https://www.e4ships.de/english/maritime-shipping/multischibz/

e4Ships. (2023b, March 29). *RiverCell2*. https://www.e4ships.de/english/inland-shipping/rivercell2/

e4Ships. (2023c, March 29). *Pa-X-ell 2*. https://www.e4ships.de/english/maritime-shipping/pa-x-ell-2/

El-Eskandarany, M. S. (2020). *Mechanical Alloying: Energy Storage, Protective Coatings, and Medical Applications.* Andrew Publishing: Norwich.

Etaing. (2023, March 28). *The Passenger Boat The Hydra*. http://www.hydrogencarsnow.com/documents/hydra.pdf.

Faris, H., Mirjalili, S., Aljarah, I., Mafarja, M., & Heidari, A. A. (2020). Salp swarm algorithm: theory, literature review, and application in extreme learning machines. *Nature-inspired Optimizers: Theories, Literature Reviews and Applications*, 185-199.

Fathy, A., Abd Elaziz, M., & Alharbi, A. G. (2020). A novel approach based on hybrid vortex search algorithm and differential evolution for identifying the optimal parameters of PEM fuel cell. *Renewable Energy*, *146*, 1833-1845.

Fremaux, S., Beheshti, S. M., Ghassemi, H., & Shahsavan-Markadeh, R. (2015). An experimental study on hydrogen-rich gas production via steam gasification of biomass in a research-scale fluidized bed. *Energy Conversion and Management*, *91*, 427-432.

Fuelcell Energy. (2022, June 6). *SureSource 1500*. https://www.fuelcellenergy.com/wp-content/uploads/2017/02/Product-Spec-SureSource-1500.pdf

German Aerospace Center [DLR]. (2023, March 25). *Nautical Integrated Hybrid Energy System for Long-haul Cruise Ships*. https://cordis.europa.eu/project/id/861647

Gerretsen, I. (2022, June 2). *EU carbon tax puts a price on shipping emissions*. Chinadialogue. https://chinadialogue.net/en/transport/eu-carbon-tax-puts-a-price-on-shipping-emissions/#:~:text=

Ghosal, M. K. (2022). *Entrepreneurship in Renewable Energy Technologies*. CRC Press.

Gong, W., & Cai, Z. (2014). Parameter optimization of PEMFC model with improved multi-strategy adaptive differential evolution. *Engineering Applications of Artificial Intelligence*, *27*, 28-40.

Grove, W. R. (1839). Voltaic Series and the Combination of Gases by Platinum. *London and Edinburgh Philosophical Magazine and Journal of Science, 14*, 127–130.

Grove, W. R. (1843). On the gas voltaic battery. *Philosophical Transactions of the Royal Society of London, 133,* 91–112.

Holland, J. H. (1992). *Adaptation in natural and artificial systems: an introductory analysis with applications to biology, control, and artificial intelligence*. MIT press.

Horizon Educational. (2023, March 29). *H-1000XP User Manual*. https://www.horizoneducational.com/h-1000-xp-fuel-cell-stack/p1407

Hota, P., Das, A., & Maiti, D. K. (2022). A short review on generation of green fuel hydrogen through water splitting. *International Journal of Hydrogen Energy*, 48(2), 523-541.

Inal, O. B., & Deniz, C. (2020). Assessment of fuel cell types for ships: Based on multi-criteria decision analysis. *Journal of Cleaner Production*. 265, 121734.

Inal, Ö. B., & Deniz, C. (2021). Emission analysis of LNG fuelled molten carbonate fuel cell system for a chemical tanker ship: a case study. *Marine Science and Technology Bulletin*. 10(2):118–133.

Ingeborg. (2023, 27 March). *Fuel Cell Boat Through The Canals*. The Green Light District. http://thegreenlightdistrict.nl/2009/11/30/fuel-cell-boat-through-the-canals/.

International Maritime Organization. (2022, June 2). *EEDI and SEEMP*. https://www.marpol-annex-vi.com/eedi-seemp/

International Maritime Organization. (2000). *First IMO GHG Study 2000*. London, UK. https://www.imo.org/en/OurWork/Environment/Pages/IMO-GHG-studies.aspx

International Maritime Organization. (2009). *Second IMO GHG Study 2009*. London, UK. https://www.imo.org/en/OurWork/Environment/Pages/Greenhouse-Gas-Study-2009.aspx

International Maritime Organization. (2014). *Third IMO GHG Study*. London, UK. https://www.imo.org/en/ourwork/environment/pages/greenhouse-gas-studies-2014.aspx

International Maritime Organization. (2018). *Initial IMO Strategy on Reduction of GHG Emissions from Ships. https://www.imo.org/en/MediaCentre/HotTopics/Pages/Cutting-GHGemissions.aspx*

International Maritime Organization. (2020). *Fourth IMO GHG Study 2020*. London, UK. https://www.imo.org/en/OurWork/Environment/Pages/Fourth-IMO-Greenhouse-Gas-Study-2020.aspx.

Jenkins, S. (2022, June 24). *CEPCI Updates: April (Prelim.) and March (Final)*. Chemengonline. https://www.chemengonline.com/2022-cepci-updates-april-prelim-and-march-final/

Jiang, Y., Yang, Z., Jiao, K. & Du, Q. (2018). Sensitivity analysis of uncertain parameters based on an improved proton exchange membrane fuel cell analytical model. *Energy Conversion and Management. 164*, 639–654.

Kaltschmitt, M., Streicher, W. & Wiese, A. (2007). *Renewable energy: technology, economics and environment*. Springer Science & Business Media.

Kandidayeni, M., Macias, A., Khalatbarisoltani, A., Boulon, L., & Kelouwani, S. (2019). Benchmark of proton exchange membrane fuel cell parameters extraction with metaheuristic optimization algorithms. *Energy*, *183*, 912-925.

Kanuri, S. V. (2012). UTC Power and the PureCell Model 400 fuel cell power plant finding wide application. *Fuel Cells Bulletin*, *2012*(2), 12-15.

Karci, A. (2017). Differential Evolution Algorithm and Its Variants. *Anatolian Journal of Computer Sciences. 2(1)*, 10–14.

Kaya, A. Y., & Erginer, K.E. (2021). An analysis of decision-making process of shipowners for implementing energy efficiency measures on existing ships: The case of Turkish maritime industry. *Ocean Engineering, 241*, 110001.

Kirubakaran, A., Jain, S., & Nema, R. K. (2009). A review on fuel cell technologies and power electronic interface. *Renewable and Sustainable Energy Reviews, 13*(9), 2430-2440.

Klingner, M. (2009). *Fuel cell power trains and clustering in heavy-duty transports. Cordis.* https://cordis.europa.eu/docs/results/516/516270/127976021-6_en.pdf.

Korkmaz, S. A., Erginer, K. E., Yuksel, O., Konur, O., & Colpan, C. O. (2023). Environmental and economic analyses of fuel cell and battery-based hybrid systems utilized as auxiliary power units on a chemical tanker vessel. *International Journal of Hydrogen Energy*.

Kundakci, N. (2016). Combined Multi-Criteria Decision Making Approach Based On Macbeth And Multi-MOORA Methods. *Alphanumeric Journal*, *4*(1), 17-26.

Kuzu, S. L., Bilgili, L., & Kiliç, A. (2021). Estimation and dispersion analysis of shipping emissions in Bandirma Port, Turkey. *Environment, Development and Sustainability*. *23*(7), 10288–10308.

Langmi, H. W., Engelbrecht, N., Modisha, P. M., & Bessarabov, D. (2022). Hydrogen storage. In T. Smolinka, & J. Garche (Eds). *Electrochemical Power Sources: Fundamentals, Systems, and Applications* (pp. 455-486). Elsevier.

Lazar, A. L., Konradt, S. C., & Rottengruber, H. (2019). Open-source dynamic Matlab/Simulink 1D proton exchange membrane fuel cell model. *Energies*, *12*(18), 3478.

Lee, C. Y., & Zhuo, G. L. (2021). A hybrid whale optimization algorithm for global optimization. *Mathematics*, *9*(13), 1477.

Leites, K. (2016). Fuel Cells for Marine Applications. In D. Stolten, R. C. Samsun, N. Garland. *Fuel Cells: Data, Facts, and Figures.* John Wiley & Sons, Ltd.

LGChem. (2014). *Product specification, rechargeable lithium ion battery model: INR18650 MJ1 3500mAh.* https://birikimpilleri.net/Resim/900817503007_1.pdf

Lindorfer, J., Rosenfeld, D. C., & Böhm, H. (2020). Fuel cells: Energy conversion technology. In T. Letcher (Ed), *Future Energy: Improved, Sustainable and Clean Options for Our Planet* (pp. 495-517). Elsevier.

Liu, G., Xu, Y., Yang, T., & Jiang, L. (2020). Recent advances in electrocatalysts for seawater splitting. *Nano Materials Science*. *5*(1), 101-116.

Loyd Register. (2022, June 2). *EEXI and CII Regulation Awareness.* https://www.lr.org/en/training/understanding-rules-and-regulations/eexi-and-cii-regulation-awareness/

Mann, R. F., Amphlett, J. C., Hooper, M. A., Jensen, H. M., Peppley, B. A., & Roberge, P. R. (2000). Development and application of a generalised steady-state electrochemical model for a PEM fuel cell. *Journal of Power Sources, 86*(1-2), 173-180.

Marefati, M., & Mehrpooya, M. (2019). Introducing and investigation of a combined molten carbonate fuel cell, thermoelectric generator, linear fresnel solar reflector and power turbine combined heating and power process. *Journal of Cleaner Production, 240,* 118247.

Marine Traffic. (2021, December 31). *MarineTraffic*. https://www.marinetraffic.com/en/ais/home/centerx:-12.0/centery:15.0/zoom:4

Markowski, J., & Pielecha, I. (2019). The potential of fuel cells as a drive source of maritime transport. In *IOP Conference Series: Earth and Environmental Science* (Vol. 214, No. 1, p. 012019). IOP Publishing.

Mench, M. M. (2008). *Fuel cell engines*. John Wiley & Sons.

Messaoud, R. B., Midouni, A., & Hajji, S. (2021). PEM fuel cell model parameters extraction based on moth-flame optimization. *Chemical Engineering Science*, *229*, 116100.

Micoli, L., Coppola, T., & Turco, M. (2021). A case study of a solid oxide fuel cell plant on board a cruise ship. *Journal of Marine Science and Application*, *20*(3), 524-533.

Ministry of Transport and Infrastructure. (2021). *Ulaşan ve Erişen Türkiye*. https://www.uab.gov.tr/uploads/pages/bakanlik-yayinlari/ulasan-ve-erisen-turkiye-2021.pdf

Mirjalili, S. (2015). Moth-flame optimization algorithm: A novel nature-inspired heuristic paradigm. *Knowledge-based Systems*, *89*, 228-249.

Mirjalili, S. (2016). SCA: a sine cosine algorithm for solving optimization problems. *Knowledge-based Systems*, *96*, 120-133.

Mirjalili, s.., & Lewis, A. (2016). The Whale Optimization Algorithm. *Advances in Engineering Software*, *95*, 51-67.

Mirjalili, S., Mirjalili, S. M., & Lewis, A. (2014). Grey wolf optimizer. *Advances in Engineering Software*, *69*, 46-61.

Mirjalili, S., Gandomi, A. H., Mirjalili, S. Z., Saremi, S., Faris, H., & Mirjalili, S. M. (2017). Salp Swarm Algorithm: A bio-inspired optimizer for engineering design problems. *Advances in Engineering Software*, *114*, 163-191.

Mo, Z. J., Zhu, X. J., Wei, L. Y., & Cao, G. Y. (2006). Parameter optimization for a PEMFC model with a hybrid genetic algorithm. *International Journal of Energy Research*, *30*(8), 585-597.

Molicel. (2023, March 20). *Approval Sheet Lithium-Ion Rechargeable Battery. https://www.molicel.com/product/inr-18650-m35a/*

Nadimi-Shahraki, M. H., Fatahi, A., Zamani, H., Mirjalili, S., & Abualigah, L. (2021). An improved moth-flame optimization algorithm with adaptation mechanism to solve numerical and mechanical engineering problems. *Entropy*, *23*(12), 1637.

Nam, H., Nam, H., & Lee, D. (2021). Potential of hydrogen replacement in natural-gas-powered fuel cells in Busan, South Korea based on the 2050 clean energy Master Plan of Busan Metropolitan City. *Energy*, *221*, 119783.

Nikolaidis, P., & Poullikkas, A. (2017). A comparative overview of hydrogen production processes. *Renewable and Sustainable Energy Reviews*, *67*, 597-611.

Nixon, N. (2023, March 28). *Timeline: The history of wind power*. Theguardian. https://www.theguardian.com/environment/2008/oct/17/wind-power-renewable-energy

National Renewable Energy Laboratory. (2022, April 17). *Interactive Best Research-Cell Efficiency Chart*. https://www.nrel.gov/pv/interactive-cell-efficiency.html.

Oldsailor. (2022, February 2). *Nemo H2: Worlds First Fuel Cell Powered Canal Boat Launched in Amsterdam*. Marinebuzz. http://www.marinebuzz.com/2009/12/15/nemo-h2-worlds-first-fuel-cell-powered-canal-boat-launched-in-amsterdam/

Omar, N., Monem, M. A., Firouz, Y., Salminen, J., Smekens, J., Hegazy, O., & Van Mierlo, J. (2014). Lithium iron phosphate based battery–Assessment of the aging parameters and development of cycle life model. *Applied Energy*, *113*, 1575-1585.

Ovrum, E., & Bergh, T. F. (2015). Modelling lithium-ion battery hybrid ship crane operation. *Applied Energy*, *152*, 162-172.

Oways. (2022, June 8). *Electrical Distribution*. Available from: https://owaysonline.com/electrical-distribution/

Panasonic. (2022, June 7). *Specification for NCR18650GA*. https://birikimpilleri.net/Resim/900095503030_1.pdf

Park, C., Jung, Y., Lim, K., Kim, B., Kang, Y., & Ju, H. (2021). Analysis of a phosphoric acid fuel cell-based multi-energy hub system for heat, power, and hydrogen generation. *Applied Thermal Engineering*, *189*, 116715.

PowerXtra. (2022, June 24). *Power-Xtra PX18650-32E - 3.7 V 3200 Mah Li-ion Battery- 3C*. Available from: https://birikimpilleri.net/Resim/900600503339_1.pdf

Priya, K., & Rajasekar, N. (2019). Application of flower pollination algorithm for enhanced proton exchange membrane fuel cell modelling. *International Journal of Hydrogen Energy*, *44*(33), 18438-18449.

Priya, K., Babu, T. S., Balasubramanian, K., Kumar, K. S., & Rajasekar, N. (2015). A novel approach for fuel cell parameter estimation using simple genetic algorithm. *Sustainable Energy Technologies and Assessments*, *12*, 46-52.

Rafiei, M., Boudjadar, J., & Khooban, M. H. (2020). Energy management of a zero-emission ferry boat with a fuel-cell-based hybrid energy system: Feasibility assessment. *IEEE Transactions on Industrial Electronics*, *68*(2), 1739-1748.

Ramirez-Vidal, P., Sdanghi, G., Celzard, A., & Fierro, V. (2022). High hydrogen release by cryo-adsorption and compression on porous materials. *International Journal of Hydrogen Energy*.

Rao, R. V. (2019). *Jaya: An Advanced Optimization Algorithm and its Engineering Applications*. Cham: Springer International Publishing.

Raza, R., Akram, N., Javed, M. S., Rafique, A., Ullah, K., Ali, A., ... & Ahmed, R. (2016). Fuel cell technology for sustainable development in Pakistan–An over-view. *Renewable and Sustainable Energy Reviews*, *53*, 450-461.

Ren, X., & Eslami, M. (2022). Optimum parameters extraction of proton exchange membrane fuel cells using Fractional-Order Whale Optimization Algorithm. *Energy Science & Engineering*, *10*(9), 3237-3249.

Rezk, H., Wilberforce, T., Sayed, E. T., Alahmadi, A. N., & Olabi, A. G. (2022). Finding best operational conditions of PEM fuel cell using adaptive neuro-fuzzy inference system and metaheuristics. *Energy Reports*, *8*, 6181-6190.

Rezk, H., Ferahtia, S., Djeroui, A., Chouder, A., Houari, A., Machmoum, M., & Abdelkareem, M. A. (2022). Optimal parameter estimation strategy of PEM fuel cell using gradient-based optimizer. *Energy*, *239*, 122096.

Rezk, H., Olabi, A. G., Ferahtia, S., & Sayed, E. T. (2022). Accurate parameter estimation methodology applied to model proton exchange membrane fuel cell. *Energy*, *255*, 124454.

Ritchie, H, Roser, M & Rosado, M. (2023, March 28). *Energy mix*. Ourworldindata. https://ourworldindata.org/energy-mix

Rivarolo, M., Rattazzi, D., Lamberti, T., & Magistri, L. (2020). Clean energy production by PEM fuel cells on tourist ships: A time-dependent analysis. *International Journal of Hydrogen Energy*, *45*(47), 25747-25757.

Robin, C., Gerard, M., d'Arbigny, J., Schott, P., Jabbour, L., & Bultel, Y. (2015). Development and experimental validation of a PEM fuel cell 2D-model to study heterogeneities effects along large-area cell surface. *International Journal of Hydrogen Energy*, *40*(32), 10211-10230.

Roh, G., Kim, H., Jeon, H., & Yoon, K. (2019). Fuel consumption and CO2 emission reductions of ships powered by a fuel-cell-based hybrid power source. *Journal of Marine Science and Engineering*, *7*(7), 230.

Saxena, S., Hendricks, C., & Pecht, M. (2016). Cycle life testing and modeling of graphite/LiCoO2 cells under different state of charge ranges. *Journal of Power Sources*, *327*, 394-400.

Şenkayas, H., & Hekimoğlu, H. (2013). Çok kriterli tedarikçi seçimi problemine PROMETHEE yöntemi uygulaması. *Verimlilik Dergisi*, (2), 63-80.

Sepasi, S., Ghorbani, R., & Liaw, B. Y. (2015). Inline state of health estimation of lithium-ion batteries using state of charge calculation. *Journal of Power Sources*, *299*, 246-254.

Seyam, S., Dincer, I., & Agelin-Chaab, M. (2023). Investigation and comparative evaluation of a hybridized marine engine powered by eco-friendly fuels including hydrogen. *International Journal of Hydrogen Energy*, *48*(12), 4812-4829.

Shan, Y., Choe, S. Y., & Choi, S. H. (2007). Unsteady 2D PEM fuel cell modeling for a stack emphasizing thermal effects. *Journal of Power Sources*, *165*(1), 196-209.

Ship and Bunker. (2022, May 30). *Global Average Bunker Prices*. https://shipandbunker.com/prices/av/global

Singh, B., Nijhawan, P., Singla, M. K., Gupta, J., & Singh, P. (2022). Hybrid algorithm for parameter estimation of fuel cell. *International Journal of Energy Research*, *46*(8), 10644-10655.

Sohani, A., Naderi, S., Torabi, F., Sayyaadi, H., Akhlaghi, Y. G., Zhao, X., ... & Said, Z. (2020). Application based multi-objective performance optimization of a proton exchange membrane fuel cell. *Journal of Cleaner Production*, *252*, 119567.

Stetson, N., McWhorter, S., Ahn, C., & SRNL, C. (2015). Introduction to hydrogen storage. In R. Gupta, A. Basile, & T. N. Veziroğlu (Eds.), *Compendium of Hydrogen Energy*. *2* (pp. 4-25). Woodhead Pusblishing Series in Energy.

Storn, R., & Price, K. (1997). Differential evolution-a simple and efficient heuristic for global optimization over continuous spaces. *Journal of Global Optimization*, *11*(4), 341.

Sun, Z., Wang, N., Bi, Y., & Srinivasan, D. (2015). Parameter identification of PEMFC model based on hybrid adaptive differential evolution algorithm. *Energy*, *90*, 1334-1341.

Sürer, M. G., & Arat, H. T. (2022). Advancements and current technologies on hydrogen fuel cell applications for marine vehicles. *International Journal of Hydrogen Energy*, *47*(45), 19865-19875.

Talbi, E.G. (2009). *Metaheuristics: from design to implementation.* John Wiley & Sons.

Tian, Z., Zeng, W., Gu, B., Zhang, Y., & Yuan, X. (2021). Energy, exergy, and economic (3E) analysis of an organic Rankine cycle using zeotropic mixtures based on marine engine waste heat and LNG cold energy. *Energy Conversion and Management*, *228*, 113657.

Tronstad, T, Høgmoen, ÅH, Haugom, GP & Langfeldt, L. (2023, April 04). *Study on the use of fuel cells in shipping.* European Maritime Safety Agency (EMSA). https://www.emsa.europa.eu/newsroom/latest-news/download/4545/2921/23.html

Turgut, O. E., & Coban, MT. (2016). Optimal proton exchange membrane fuel cell modelling based on hybrid Teaching Learning Based Optimization – Differential Evolution algorithm. *Ain Shams Engineering Journal*, *7*(1), 347–360.

Turton, R., Shaeiwitz, J. A., Bhattacharyya, D., & Whiting, W. B. (2018). *Analysis, Synthesis and Design of Chemical Processes*. New York: Pearson PTG.

Tzeng, G. H., & Huang, J.J. (2011). *Multiple attribute decision making: methods and applications*. CRC press.

van Biert, L., Godjevac, M., Visser, K., & Aravind, P. V. (2016). A review of fuel cell systems for maritime applications. *Journal of Power Sources*, *327*, 345-364.

Veziroglu, T. N., Sherif, S. A., & Barbir, F. (2005). Hydrogen energy solutions. In F. J. Agardy, N. L. Nemerow. *Environmental Solutions* (pp. 143-180). Academic Press.

Walter, M. G., Warren, E. L., McKone, J. R., Boettcher, S. W., Mi, Q., Santori, E. A., & Lewis, N. S. (2010). Solar water splitting cells. *Chemical Reviews*, *110*(11), 6446-6473.

Wilailak, S., Yang, J. H., Heo, C. G., Kim, K. S., Bang, S. K., Seo, I. H., ... & Lee, C. J. (2021). Thermo-economic analysis of phosphoric acid fuel-cell (PAFC) integrated with organic ranking cycle (ORC). *Energy*, *220*, 119744.

Winkler, W. (2009). Ships: fuel cells. *Encyclopedia of Electrochemical Power Sources*, *1*, 338-358.

World Trade Organization. (2022, February 22). *Evolution of trade under the WTO: handy statistics.* https://www.wto.org/english/res_e/statis_e/trade_evolution_e/evolution_trade_wto_e.htm#fnt-1.

Xing, H., Stuart, C., Spence, S., & Chen, H. (2021). Fuel cell power systems for maritime applications: Progress and perspectives. *Sustainability*, *13*(3), 1213.

Xu, S., Wang, Y., & Wang, Z. (2019). Parameter estimation of proton exchange membrane fuel cells using eagle strategy based on JAYA algorithm and Nelder-Mead simplex method. *Energy*, *173*, 457-467.

Yang, M. H., & Yeh, R. H. (2018). The effects of composition ratios and pressure drops of R245fa/R236fa mixtures on the performance of an organic Rankine cycle system for waste heat recovery. *Energy Conversion and Management*, *175*, 313-326.

Yang, X. S., & Deb, S. (2009, December). Cuckoo search via Lévy flights. In *2009 World Congress on Nature & Biologically Inspired Computing (NaBIC)* (pp. 210-214). IEEE.

Yang, S., Chellali, R., Lu, X., Li, L., & Bo, C. (2016). Modeling and optimization for proton exchange membrane fuel cell stack using aging and challenging P systems based optimization algorithm. *Energy*, *109*, 569-577.

Yuksel, O., & Koseoglu, B. (2022). Numerical simulation of the hybrid ship power distribution system and an analysis of its emission reduction potential. *Ships and Offshore Structures*, 1-17.

Zhang, G., & Jiao, K. (2018). Multi-phase models for water and thermal management of proton exchange membrane fuel cell: A review. *Journal of Power Sources*, *391*, 120-133.

Zhang, L., & Wang, N. (2013). An adaptive RNA genetic algorithm for modeling of proton exchange membrane fuel cells. *International Journal of Hydrogen Energy*, *38*(1), 219-228.

Zhang, L., Yu, Y., Luo, Y., & Zhang, S. (2020). Improved cuckoo search algorithm and its application to permutation flow shop scheduling problem. *Journal of Algorithms & Computational Technology*, *14*, 1748302620962403.

Zhou, Y., Searle, S., & Baldino, C. (2022, February 1). Cost of renewable hydrogen produced onsite at hydrogen refueling stations in Europe. The International Council on Clean Transportation. https://theicct.org/wp-content/uploads/2022/02/fuels-eu-cost-renew-H-produced-onsite-H-refueling-stations-europe-feb22.pdf

Zitar, R. A., Al-Betar, M. A., Awadallah, M. A., Doush, I. A., & Assaleh, K. (2022). An intensive and comprehensive overview of JAYA algorithm, its versions and applications. *Archives of Computational Methods in Engineering*, *29*(2), 763-792.